Exploring Transcriptional Heterogeneity in the Postnatal SVZ

Stefan Zweifel

N°d'ordre NNT:
2018LYSE1047

THESE de DOCTORAT DE L'UNIVERSITE DE LYON
opérée au sein de
l'Université Claude Bernard Lyon 1

Ecole Doctorale N° ED 340
Biologie Moléculaire Intégrative et Cellulaire

Spécialité de doctorat: **Biology**
Discipline: **Neurosciences**

Soutenue publiquement le 29/03/2018, par:
Stefan ZWEIFEL

Exploring Transcriptional Heterogeneity in the Postnatal SVZ

Devant le jury composé de :

Bénédicte Durand	Professeur	Université Lyon 1	Présidente
Nathalie Spassky	Directrice de recherche	Université Paris VI	Rapporteure
Antoine De Chevigny	Chercheur	Université Aix-Marseille	Rapporteur
Olivier Raineteau	Directeur de recherche	Université Lyon 1	Directeur de thèse

UNIVERSITE CLAUDE BERNARD - LYON 1

Président de l'Université	M. le Professeur Frédéric FLEURY
Président du Conseil Académique	M. le Professeur Hamda BEN HADID
Vice-président du Conseil d'Administration	M. le Professeur Didier REVEL
Vice-président du Conseil Formation et Vie Universitaire	M. le Professeur Philippe CHEVALIER
Vice-président de la Commission Recherche	M. Fabrice VALLÉE
Directrice Générale des Services	Mme Dominique MARCHAND

COMPOSANTES SANTE

Faculté de Médecine Lyon Est – Claude Bernard	Directeur : M. le Professeur G.RODE
Faculté de Médecine et de Maïeutique Lyon Sud – Charles Mérieux	Directrice : Mme la Professeure C. BURILLON
Faculté d'Odontologie	Directeur : M. le Professeur D. BOURGEOIS
Institut des Sciences Pharmaceutiques et Biologiques	Directrice : Mme la Professeure C. VINCIGUERRA
Institut des Sciences et Techniques de la Réadaptation	Directeur : M. X. PERROT
Département de formation et Centre de Recherche en Biologie Humaine	Directrice : Mme la Professeure A-M. SCHOTT

COMPOSANTES ET DEPARTEMENTS DE SCIENCES ET TECHNOLOGIE

Faculté des Sciences et Technologies	Directeur : M. F. DE MARCHI
Département Biologie	Directeur : M. le Professeur F. THEVENARD
Département Chimie Biochimie	Directrice : Mme C. FELIX
Département GEP	Directeur : M. Hassan HAMMOURI
Département Informatique	Directeur : M. le Professeur S. AKKOUCHE
Département Mathématiques	Directeur : M. le Professeur G. TOMANOV
Département Mécanique	Directeur : M. le Professeur H. BEN HADID
Département Physique	Directeur : M. le Professeur J-C PLENET
UFR Sciences et Techniques des Activités Physiques et Sportives	Directeur : M. Y.VANPOULLE
Observatoire des Sciences de l'Univers de Lyon	Directeur : M. B. GUIDERDONI
Polytech Lyon	Directeur : M. le Professeur E.PERRIN
Ecole Supérieure de Chimie Physique Electronique	Directeur : M. G. PIGNAULT
Institut Universitaire de Technologie de Lyon 1	Directeur : M. le Professeur C. VITON
Ecole Supérieure du Professorat et de l'Education	Directeur : M. le Professeur A. MOUGNIOTTE
Institut de Science Financière et d'Assurances	Directeur : M. N. LEBOISNE

“Life is a Sisyphean race, run ever faster toward a finish line that is merely the start of the next race”

Matt Ridley, The Red Queen: Sex and the Evolution of Human Nature

“Success is peace of mind, which is a direct result of self-satisfaction in knowing you made the effort to become the best of which you are capable.”

John Robert Wooden, 10 times NCAA Basketball Champion Coach

Für mini Elterä

Abstract

Germinal activity persists in the postnatal mammalian brain in specialized niches, namely the dentate gyrus of the hippocampus and the subventricular zone (SVZ) surrounding the lateral ventricle. Neural stem cells (NSCs) of the postnatal SVZ differentiate into transient amplifying progenitors that will generate neuroblasts migrating through the rostral migratory stream, into the olfactory bulb, where they differentiate into neurons. The SVZ additionally generates glial progenitors that invade the nearby parenchyma. Recent work to which I have participated, highlights the heterogeneous nature of the postnatal SVZ in respect to different microdomains generating distinct neural lineages.

The objectives of my PhD work were twice: 1) to develop new means to explore the heterogeneity of the SVZ; and 2) to identify transcription factors expressed by subpopulations of NSCs of the SVZ and acting in their differential specification.

Objective 1: The SVZ is a highly complex and irregular region of ongoing postnatal germinal activity. The heterogeneous character of the SVZ is evident and recent studies generated enormous datasets of transcripts, which are differentially expressed between divergent microdomains. However, an appropriate tool for fast analysis of the protein level along the full rostro-caudal and dorso-ventral extend of the SVZ is still missing. Therefore, I developed "FlashMap", a semi-automatic software that allows rapid analysis of protein levels in the full SVZ, based on optical density measurements after immunohistochemistry. "FlashMap" generates easy readable heatmaps in two dimensions, which can be accurately superimposed on three-dimensional reconstructions of the ventricular system for rapid spatial visualization and analysis. This new approach will fasten research onto SVZ regionalization, by guiding the identification of markers, such as transcription factors expressed in specific SVZ microdomains.

Objective 2: I used transcriptomic as well as fate mapping approaches to investigate the relation between regional expression of transcription factors by NSCs and their acquisition of distinct neural lineage fates. Our results support an early priming of NSCs to produce defined

cell types depending of their spatial location in the SVZ and identify Hopx as a marker of a subpopulation biased to generate astrocytes. Interestingly, manipulation of Hopx expression showed minor effects on astrogenesis, but resulted in marked changes in the number of NSCs and of their progenies. Taken together, our results highlight transcriptional and spatial heterogeneity of postnatal NSCs, as well as their early priming toward specific lineages and suggest a role for Hopx in the evolution of SVZ germinal activity.

Résumé

Une activité activité germinale persiste après la naissance dans des niches spécialisées du cerveau des mammifères, à savoir le gyrus denté de l'hippocampe et la zone sous-ventriculaire (SVZ) bordant le ventricule latéral. Les cellules souches neurales (NSC) de la SVZ postnatale se différencient en progéniteurs transitoires qui vont générer des neuroblastes migrant à travers la voie de migration rostrale vers le bulbe olfactif, où ils se différencient en neurones. La SVZ génère également des progéniteurs gliaux qui se dispersent dans le parenchyme voisin. Les travaux récents auxquels j'ai participé soulignent la nature hétérogène de la SVZ postnatale, composée de différents microdomaines générant des lignées neurales distinctes.

Les objectifs de mon travail de thèse ont permis de : 1) développer de nouveaux moyens pour explorer l'hétérogénéité de la SVZ; et 2) d'identifier et d'étudier le rôle d'un facteur de transcription exprimé par une sous population des NSCs de la SVZ.

Objectif 1: La SVZ est une région hautement complexe et irrégulière dans laquelle une forte activité germinale persiste après la naissance. Le caractère hétérogène de la SVZ est évident et des études récentes ont généré une très grande base de données de transcrits, qui sont différentiellement exprimés entre les microdomaines. Cependant, un outil approprié pour l'analyse rapide du niveau d'expression d'une protéine d'intérêt, le long des axes rostro-caudal et dorso-ventral de la SVZ est toujours manquant et nécessaire. Par conséquent, j'ai développé "FlashMap", un logiciel semi-automatique qui permet une analyse rapide des niveaux d'expression de protéines dans le SVZ, basé sur des mesures de densité optique après immunohistochimie. "FlashMap" génère des cartes thermiques facilement lisibles en deux dimensions, qui peuvent être superposées avec précision aux reconstructions tridimensionnelles du système ventriculaire pour une visualisation spatiale fine et rapide. Cette nouvelle approche accélérera la recherche sur la régionalisation de la SVZ, en permettant l'identification de marqueurs (e.g. facteurs de transcription) exprimés dans des régions discrètes de la SVZ.

Objectif 2: J’ai utilisé des approches de transcriptomique et de « fate mapping » des NSCs pour étudier la relation entre l'expression régionale de facteurs de transcription et leur différenciation dans des lignées neurales distinctes. Mes résultats supportent un amorçage précoce des NSCs à produire différents types cellulaires en fonction de leur localisation spatiale dans la SVZ. Nos données identifient Hopx comme un marqueur d'une sous population de NSCs qui génère principalement des astrocytes. De façon intéressante, la manipulation de l'expression de Hopx montre des effets mineurs sur l'astrogénèse, mais entraîne des changements marqués quant au nombre de NSCs et de leur descendance. Dans son ensemble, Mes résultats mettent en évidence à la fois une hétérogénéité spatiale des NSCs postnatales ainsi que leur amorçage précoce à produire des types cellulaires distincts.

List of Abbreviations (Abbr.)

2D	2-dimensional
3D	3-dimensional
Aldh1l1	aldehyde dehydrogenase 1 family member L1
BF1	brain factor 1
BrdU	5-bromo-2'-deoxyuridin
CalB	calbindin
CalR	calretinin
CC	corpus callosum
cKO	conditional knock-out
CLoNE	clonal labeling of neural progenies
CNS	central nervous system
CSF	cerebrospinal fluid
Ctrl.	control
Cx	cortex
DCX	doublecortin
dEPO	dorsal electroporation
DG	dentate gyrus
DL	dorso-lateral corner
dlEPO	dorso-lateral electroporation
dlNSC	dorso-lateral neural stem cell
dlSVZ	dorso-lateral subventricular zone microdomain
DM	dorso-medial corner
dmEPO	dorso-medial electroporation
dmNSC	dorso-medial neural stem cell
dmSVZ	dorso-medial subventricular zone microdomain
dNSC	dorsal neural stem cell
dpe	days post electroporation
dSVZ	dorsal subventricular zone microdomain
E11	embryonic day 11
EPO	electroporation
FACS	fluorescence activated cell sorting
GCL	granule cell layer
GFAP	glial fibrillary acidic protein
GFP	green fluoresent protein
GL	glomerular layer
GoF	gain of function
Hopx	Homeodomain-only protein
hpe	hours post electroporation
JS_{div}	Jensen-Shannon divergence
KI	knock-in
KO	knock-out

LGE	lateral ganglionic eminence
lNSC	lateral neural stem cell
LoF	loss of function
lSVZ	lateral subventricular zone microdomain
LV	lateral ventricle
MADM	mosaic analysis with double markers
MAGIC	multiaddressable genome-integrative color
MAP2	microtubule-associated protein-2
MCL	mitral cell layer
MGE	medial ganglionic eminence
mSVZ	medial subventricular zone microdomain
NeuN	neuronal nuclei
NSC	neural stem cell
NSCs	Neural stem cells
NSE	neuron specific enolase
OB	olfactory bulb
OD	optical density
Olig1/2	oligodendrocyte transcription factor 1/2
OPC	oligodendrocyte precursor cell
oRG	outre radial glia
P3	postnatal day 3
PSA-NCAM	polysialylated-neural cell adhesion molecule
qPCR	quantitative polymerase chain reaction
RG	radial glia
RMS	rostral migratory stream
ROI	region of interest
S100β	s100 calcium-binding protein B
SGZ	subgranular zone
St	striatum
SVZ	subventricular zone
Tam	tamoxifen
TAP	transient amplifying progenitor
Tbr2	T-box brain protein 2
TF	transcription factor
TH	tyrosine hydroxylase
TOAD-64	Turned-On-After-Division 64-kDA
YFP	yellow fluorescent protein

Contents

1. Introduction – Technique Dependent Progression in the Field of Neuroscience

The central nervous system (CNS) is a very complex, highly organized structure. It is composed of three major cell types, the neurons and the glia cells (i.e. astrocytes and the oligodendrocytes). It was originally proposed by Rudolf Virchow (1846) that glia had a mesenchymal origin, like other supporter cells in the body. This hypothesis was later dismissed by Wilhelm, who demonstrated a CNS origin for glial cells (summarized in Jacobson, 1991). It is now well accepted that both neurons and glial cells originate from so called "neural stem cells" (NSCs). It also became apparent that their production does not stop at birth, but that a germinal activity persists in the postnatal CNS.

1.1. Nucleoside Analogs Shaped our Understanding of Germinal Regions

In this first part of my introduction, I would like to focus on how the use of nucleoside analogs shaped our current understanding of a persistent germinal activity in the postnatal brain. Prior to the "nucleoside analog age", the identification of mitotic activity relied on pure observations of cell morphology using ancient staining techniques (e.g. by the use of thionin followed by eosin or erythrosin). Using these approaches, mitotic features in the CNS of rats, were reported as early as in 1912, by Ezra Allen (Allen, 1912). While many of those early observations have greatly influenced the emerging field of neurosciences, the introduction of nucleoside analogs to study proliferation represents a major step forward. Indeed, these new techniques allowed proving or rejecting early made hypotheses in a convincing manner and opened the era towards modern neuroscience.

Nucleoside analogs shaped our understanding of niches with postnatally persisting germinal activity. In addition, because they allow fate mapping of cells that have proliferated at the time of nucleoside administration, they can give insights into embryonal and postnatal migration patterns. Further, they helped to make conclusions about the subventricular zone (SVZ) architecture when combined with immunohistochemistry and electron microscopy. While (especially in the 90's) many researchers added significant knowledge to the field using more

advanced techniques (e.g. virus approaches), this part of my thesis introduction focuses mainly on results achieved using nucleoside analogs in combination with cell specific markers. Most of the results discussed below are achieved using the radiolabeled nucleoside analog [H^3]thymidine and the halogen-based nucleoside analog 5-bromo-2'-deoxyuridin (BrdU). These nucleosides respectively can be visualized by autoradiography or immunohistochemistry using specific antibodies.

1.1.1. Nucleoside Analogs

A key challenge in the development of nucleoside analogs was to develop a detectable component, which is incorporated into DNA, but not into RNA. While the bases adenine, guanine and cytosine are found in DNA and RNA, thymine is only found in DNA and was therefore chosen. Thymine joins with deoxyribose to create the nucleoside deoxythymidine, which is also named thymidine (**Figure 1A**). Initial trials were made with N^{15} radiolabeled thymidine. [N^{15}]thymidine was shown to be efficiently incorporated into the DNA in rat tissue and was confirmed to be absent from RNA (Reichard and Estborn, 1951). Later studies used radioactive C^{14} to confirm its efficient uptake into synthesized DNA of proliferating cells (Friedkin et al., 1956), as well as in bacteria (Downing and Schweigert, 1956). However, the microscopic visualization by autoradiography (Pelc, 1956; Quastler and Sherman, 1959) appeared rather poor for [N^{15}]thymidine and [C^{14}]thymidine. This technical limitation was rapidly overcome by the use of [H^3]thymidine. Tritium-labeled thymidine ([H^3]thymidine) was used for the first time as a nucleoside analog in 1957 by Taylor, Woods and Hughes in broad beans. Briefly, root tips of the plant were placed into an [H^3]thymidine containing medium, transferred into a nonradioactive colchicine containing medium (to prevent anaphase) and stained by the Feulgen reaction. Then radioactive versus native sister-chromatids could be quantified following autoradiographic visualization (Taylor et al., 1957) (**Figure 1B**). This innovative approach allowed them to make important conclusions about the fundamental rules of mitosis, and was therefore later used in other organisms. It should however be noted that although [H^3]thymidine leaded to many hallmark findings, it is a time-consuming procedure and lacks spatial resolution due to its revelation by autoradiography. This is a particular issue in the central nervous system, where cells are densely organized. A later developed thymidine

analog, BrdU, had the potential to close this gap. It allows detection of newly synthetized DNA by immunohistochemistry.

Figure 1. Nucleoside analogs as a tool to detect germinal activity in the central nervous system
(A): Thymidine is identified as the nucleoside of choice for detection of DNA synthesis.
(B): Tritiated thymidine harbors radioactive hydrogen isotopes. Cells incorporate it efficiently into their DNA during cell division and it can be readily detected by autoradiography.
(C): BrdU is a halogen-based nucleoside analog harboring a bromine atom (blue) at the place of the methyl group. After incorporation into DNA it can be detected by immunohistochemistry using specific antibodies. Other halogen-based nucleoside analogs are IdU and CldU with iodine (orange) or chlorine (green) atoms replacing the methyl group.
(D): EdU has an alkyne group replacing the methyl. After incorporation into the DNA the azide group of the dye (N_3-dye) binds to it by "click it" chemistry catalyzed by Cu (I). ⟶

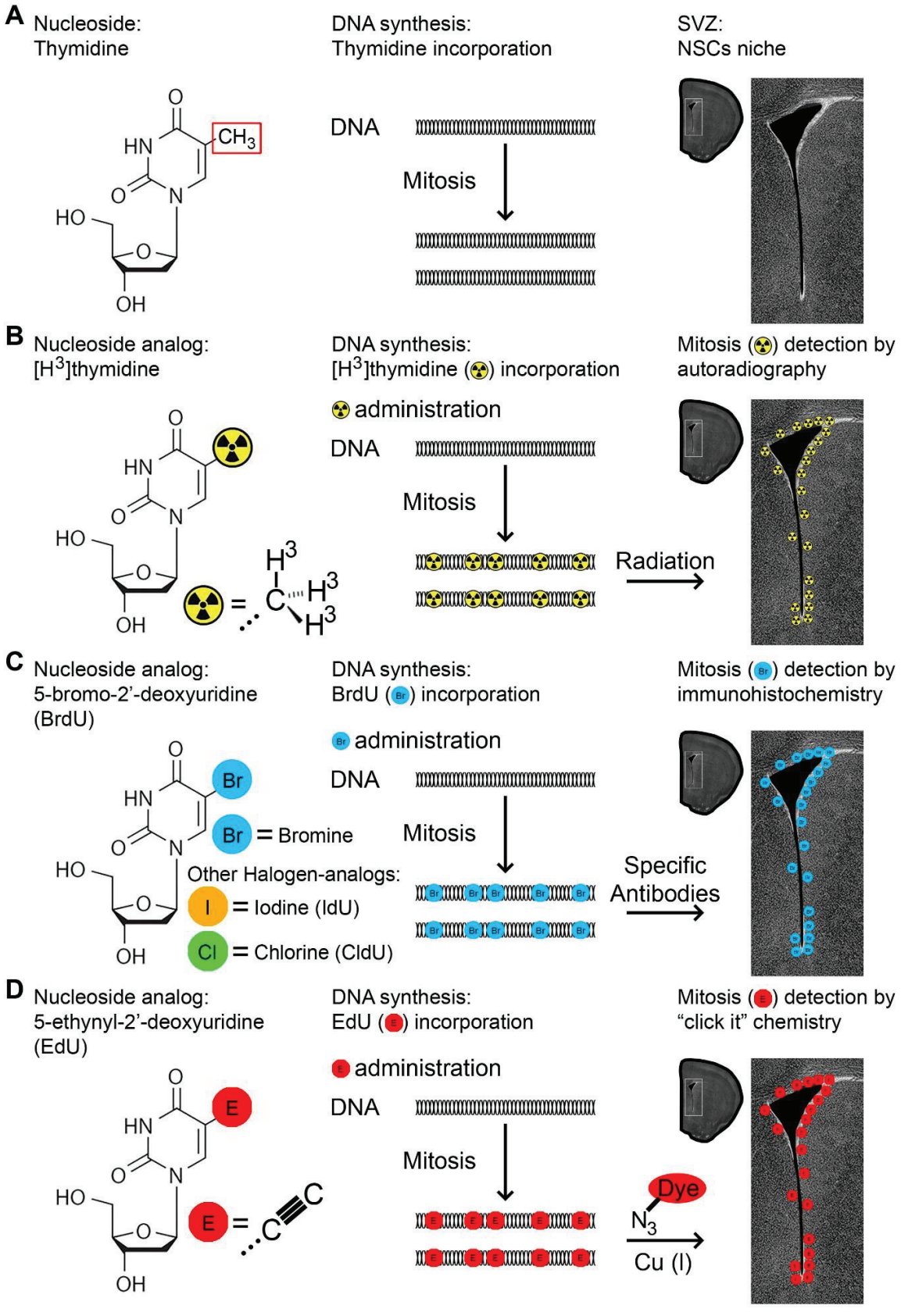
A
Nucleoside:
Thymidine
DNA synthesis:
Thymidine incorporation
SVZ:
NSCs niche
DNA
Mitosis
B
Nucleoside analog:
[H3]thymidine
DNA synthesis:
[H3]thymidine incorporation
Mitosis detection by
autoradiography
administration
DNA
Mitosis
Radiation
C
Nucleoside analog:
5-bromo-2'-deoxyuridine
(BrdU)
DNA synthesis:
BrdU incorporation
Mitosis detection by
immunohistochemistry
administration
DNA
Mitosis
Specific
Antibodies
Br = Bromine
Other Halogen-analogs:
I = Iodine (IdU)
Cl = Chlorine (CldU)
D
Nucleoside analog:
5-ethynyl-2'-deoxyuridine
(EdU)
DNA synthesis:
EdU incorporation
Mitosis detection by
"click it" chemistry
administration
DNA
Mitosis
Dye
N3
Cu (I)

BrdU became popular by the development of antibodies having both high affinity and specificity. It overcomes the time-consuming procedure of autoradiography necessary for [H^3]thymidine detection (Gratzner et al., 1975; Gratzner, 1982; **Figure 1C**). Finally, it allows concomitant immunodetection of cell type specific markers, allowing solid conclusions to be made regarding the identity and fate of $BrdU^+$ cells. The increasing popularity of BrdU is reflected by the huge amount of scientific articles referenced on PubMed (24375 by end of 2017; **Figure 2**).

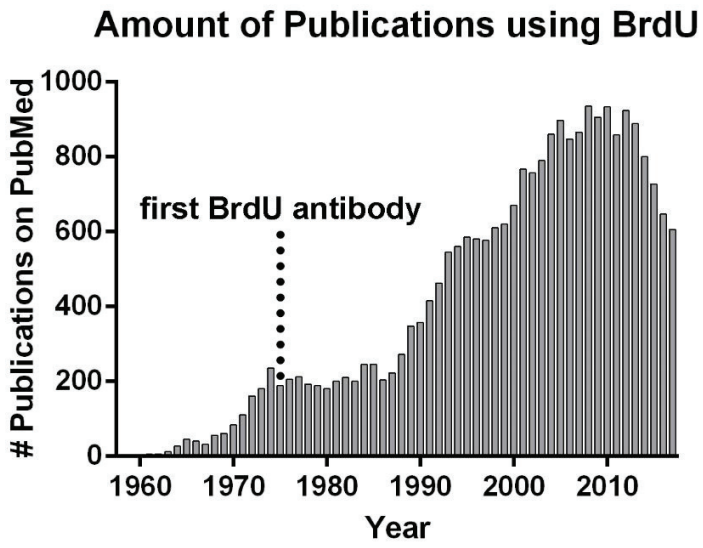

Figure 2. Timeline of BrdU publications
The first scientific article concerning BrdU was published in 1958. After the development of the first specific BrdU antibody in 1975 it became increasingly used for observations of diverse aspects of DNA synthesis and mitosis. By the end of 2017, 24375 research articles had been published by the scientific community.

Other halogen-based nucleoside analogs have appeared more lately, namely CldU and IdU (**Figure 1C**), as well as the "new generation" nucleoside analog EdU (**Figure 1D**), which can be chemically detected by the more advanced "click it" chemistry (for review Cavanagh et al., 2011). Those can be administrated at different time points. Their detections allow to address the long-term proliferative behavior of a cell, i.e. if it reenter cell cycle and therefore incorporate the second administrated nucleoside. Although they allow multiplex administration, the antibodies used to detect them need to be carefully chosen. Indeed, IdU and CldU have been shown to be specifically detected by two separate antibodies initially

generated for BrdU detection (Yokochi and Gilbert, 2007). The development of EdU circumvent the use of an antibody and allows a faster detection of DNA synthesis by "click it" chemistry, which can be accomplished within a few hours. In addition, the reaction component (fluorescent azides) have a high penetration capacity allowing efficient labeling of thick sections and even whole-mount tissues or organisms (Salic and Mitchison, 2008; **Figure 1D**).

A drawback of nucleoside analogs are their potential toxic effects, which have been widely analyzed and discussed. Administration of BrdU in neonates has been reported to shorten their life span in a dose dependent manner (Craddock, 1981). It induces mutations (Kaufman, 1988) resulting in alterations in differentiation (Tapscott et al., 1989) and proliferation (Weghorst et al., 1991). This adverse effects are explained by the preferential pairing of BrdU with guanine instead of adenine (Kaufman, 1988), which can cause problems in subsequent divisions. Thus, doses superior to 60 mg/kg have been suggested to induce such cytotoxic effects (for review Cavanagh et al., 2011). Similarly, EdU administration leads to long-term toxic effects, while no significant alterations in cell proliferation and survival were observed for short survival times (Ponti et al., 2013).

1.1.2. Nucleoside Analogs Give Insight into Embryonic Germinal Activity by Interkinetic Nuclear Migration

An important step in using [H^3]thymidine for studies in neurosciences, was the finding that radioactivity can be found in the brain as early as 15 minutes after intravenous injection into the young adult mouse (Hughes et al., 1958). Although this study focused on the gastrointestinal tract and did not make a thoughtful analysis of the brain, it demonstrated that [H^3]thymidine rapidly distributes throughout the mouse body, including the brain, following intravenous injection. It therefore opened the way to study proliferation in this tissue. Thus, [H^3]thymidine administration in mouse at embryonic day 11 (E11) revealed that the external half of the primitive ependymal layer of the cerebral vesicles is a region of intense DNA synthesis (**Figures 3A and 3B**). A time course analysis further revealed that [H^3]thymidine can be detected in the ventricular (inner) half of the primitive ependymal layer, 6 hours after its injection (**Figure 3C**). At 48 hours, some labeled cells were observed in regions located away from the ependymal layer (**Figure 3D**). Taken together, these observations demonstrate

that regions of DNA synthesis and cell division are distinct. They also suggest that newly generated cells migrate away from its region of origin (Sidman et al., 1959). Using the same method in the early chick neural tube, the cell cycle dependent movement of the cell body was described in more details and referred as interkinetic nuclear migration (Sauer and Walker, 1959). Injections into pregnant female mice at different gestational time points (E11-E17) identified the primitive ependyma of the lateral ventricles (LV) as source of cortical cells along the entire embryonal period. This experiment also revealed the inside-out formation of the cortex, as described in more details below (Angevine and Sidman, 1961).

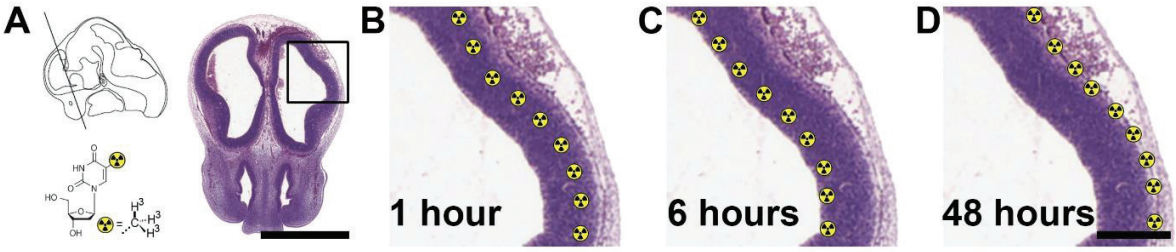

Figure 3. Embryonic NSCs undergo interkinetic nuclear migration.
(A): Representative coronal section from an early embryonal brain section (© 2008 Springer Science+Business Media, LLC) illustrates [H^3]thymidine administration.
(B-D): Micrographs highlight the position of labeled cells (☢) in the pallium at different time points after [H^3]thymidine administration. One hour after administration the labeled cells were found in the external half of the primitive ependymal layer (B). After 6 hours they were located in the inner half (C) and after 48 hours in the surrounding parenchyma.
Scale bars: A = 1 mm; D = 200 µm.

1.1.3. Nucleoside Analogs reveal Two Sites of persisting Postnatal Germinal Activity

[H^3]thymidine experiments confirmed the original observations made years before by Ezra Allen (Allen, 1912). Indeed, proliferation was shown to persist postnatally in the SVZ at postnatal day 3 (P3), as well as in young adult and adult mice (Messier et al., 1958; Smart, 1961; Smart and Leblond, 1961). This demonstrates that the potential to produce new cells does not abruptly stop after birth or after completing the development. Therefore, the SVZ is a niche of ongoing postnatal proliferation (**Figures 4A and 4B**). Subsequent [H^3]thymidine studies identified the dentate gyrus (DG) of the hippocampus as a second niche of ongoing

postnatal proliferation in the mammalian forebrain (**Figures 4A and 4C**). Importantly, the germinal potential of both the DG and SVZ was shown to decrease substantially during aging (Altman, 1963; Altman and Das, 1965). Major observations were made by Altman and Das from 1965 on. While already proposed earlier (e.g. Smart, 1961), their studies suggested the persistence of neurogenesis in the postnatal brain. They indeed observed germinal activity in the DG and SVZ of postnatal rats and guinea pigs, and presented data suggesting that it contributed to the generation of new neurons (Altman and Das, 1965; Altman and Das, 1967). Their claims were however examined by the scientific community with skepticism. In particular, technical limitations prevented them to unambiguously demonstrate the neuronal nature of newborn cells. Therefore Kaplan and Hinds reassessed their conclusions by combining [H^3]thymidine labeling and electron microscopy of ultrathin (1 μm) sections. The existence of neurogenesis in those two regions was confirmed in the adult rat brain, by identifying labeled cells for neuron specific traits like long microtubule filled processes and a smooth contoured cell body (Kaplan and Hinds, 1977). Evidences for postnatal neurogenesis in mammals accumulated rapidly. Beside adult mice (Smart, 1961) and rats, germinal activity was demonstrated in adult cats (Altman, 1963), guinea pigs (Altman and Das, 1967), and dogs up to an age of 17 years (Fischer, 1967).

While those findings became widely accepted, postnatal mitotic activity in the primate brain remained controversial, and a number of conflicting findings were published. Noetzel and Rox analyzed adult mice and rhesus monkey brains in parallel. While they succeeded in detecting [H^3]thymidine mitotic profiles in the mouse SVZ, they obtained negative results in rhesus monkeys. They concluded that the mitotic SVZ in mice is a leftover from the embryonic development and that "the absence of a SVZ" in rhesus monkeys is a sign of a higher developmental level and increased differentiation of the ape forebrain (Noetzel and Rox, 1964). Meanwhile others reported mitotic activity in the young and adult primate SVZ by revealing mitotic features (Lewis, 1968) or by [H^3]thymidine administration (Kaplan, 1983). The number of proliferative cells described by Kaplan appeared however anecdotic, as only 14 labeled cells were observed within 48 analyzed sections. Pasko Rakic undertook a large-scale experiment to address this unresolved issue as well as of a possible postnatal cortical neurogenesis. His study included twelve rhesus monkeys of different ages treated with different doses of [H^3]thymidine. While proliferation and some degree of neurogenesis was

confirmed in the DG during the first few postnatal months, [H^3]thymidine$^+$ cells in the cortex were identified as astrocytes and oligodendrocytes. Evidences for postnatal generated neurons in the cortex were not found (Rakic, 1985). Subsequent experiments by the Gould laboratory, confirmed germinal activity in the DG of old world monkeys (*Macaca fascicularis* and *Macaca mulatta*). They confirmed persisting granule cell neurogenesis by using mature and immature neuronal markers. They found a substantial number of cells being positive for NSE (neuron specific enolase), NeuN (neuronal nuclei), TOAD-64 (Turned-On-After-Division 64-kDa) and CalB (calbindin) in individuals of all ages with an age dependent reduction in neurogenesis (Gould et al., 1999). Another report from this group was far more controversial. They found evidences of neurogenesis in the adult SVZ (*Macaca fasciculari*), but also described migration of newborn neurons into the neocortex (prefrontal, inferior temporal and parietal cortex). While 2 hours after BrdU injection positive cells were located in the SVZ, they observed at longer time points cells with elongated nuclei in the white matter, classified as migrating cells, and in the neocortex. A fraction of these cells was confirmed to express the neuronal markers TOAD-64, NeuN, NSE and MAP2 (microtubule-associated protein-2), while others express the astrocytic marker GFAP (glial fibrillary acidic protein). Interestingly, survival of these adult born cells was found to decrease with age (Gould et al., 2001).

In parallel to these studies in old world monkeys, germinal activity and neurogenesis was also investigated in new world monkeys. Studies in the common marmoset *C.jacchus* demonstrated substantial mitotic activity in the postnatal SVZ using both [H^3]thymidine and BrdU labeling. A high labeling index was observed at early postnatal time points, which dropped remarkably with progressing age to be very low by two years of age. The fate of the postnatal born cells was not analyzed (McDermott and Lantos, 1990). Similar observations were made in the dentate gyrus, were new born neurons acquired the morphological characteristics of granule neurons and expressed the neuronal marker NSE 3 weeks after BrdU injection (Gould et al., 1998). I confirmed these findings in common marmosets during my master thesis project, by using the proliferation marker Ki67. We found a similar age-dependent decrease in proliferation. We observed a large number of doublecortin (DCX) expressing neuroblasts, supporting a persistent neurogenesis. Finally, we demonstrated the presence of progenitors of defined neuronal subtypes by immunodetection of the early GABAergic marker Dlx2 and the glutamatergic marker Tbr2. While Dlx2$^+$ progenitors persisted until adulthood, the pool of

Tbr2 expressing glutamatergic progenitors in the SVZ was found to be depleted early after birth (Azim et al., 2013).

A much-awaited study concerned the demonstration of such germinal activity and neurogenesis in humans. Eriksson et al., were the first to present evidences for neurogenesis in the aged human DG. They made use of postmortem brain biopsies from aged human patients that suffered from squamous cell carcinoma. These patients had been treated with BrdU at different time points during the course of their cancer for diagnostic purposes. Eriksson et al. described a persisting germinal activity in the human DG, as well as SVZ. First, they demonstrated a substantial germinal activity in the DG in all patients, although a large inter-individual variability was observed for the number of $BrdU^+$ cells in both the subgranular zone (SGZ) and the granule cell layer (GCL). This variability can be explained by the different ages of the patients, as well as by differences in the time span between BrdU treatment and death. Therefore, although not quantitative, these results concluded for a significant germinal activity in humans. They also provided evidence for neurogenesis, based on BrdU co-expression with the neuronal markers NeuN, CalB and NSE in the DG (Eriksson et al., 1998). Due to the sparsity of tissues from BrdU treated patients, other approaches had to be developed in order to more systematically quantify neurogenesis in humans. Thus, an elegant study introduced the method of radiolabeled C^{14} for retrospective birth dating of human cells. Analysis of biopsies issued from individuals of different ages confirmed the occurrence of an extensive hippocampal neurogenesis and neuronal turnover throughout life. Thus, every day, 700 new neurons are generated per hippocampus resulting in an impressive yearly turnover of ~2% of the dentate granule cells. An age dependent decline was observed, but was estimated to be less dramatic compared to mice (Spalding et al., 2013). Using the same method persistence of germinal activity in the adult human SVZ was confirmed (Ernst et al., 2014). Parallel histological studies revealed persistent neurogenesis during infancy (Sanai et al., 2011) but also adulthood (Ernst et al., 2014).

Taken together nucleoside analogs reveal that germinal activity and neurogenesis is a landmark of the mammalian brain, including humans. These studies however highlight that variation in the intensity of this process, as well as in the fate and distribution of newborn neurons may exist.

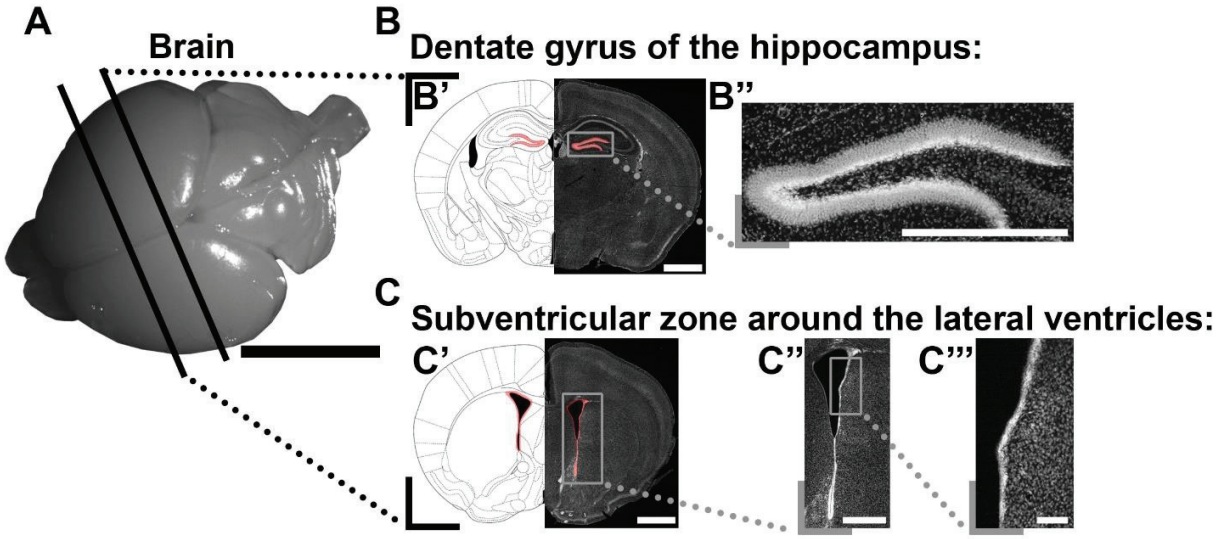

Figure 4. Nucleoside analogs reveal two sites of persistent postnatal germinal activity.
(A): Representative picture of a P10 mouse brain illustrates virtual cuts at the level of the DG and SVZ.
(B): The DG (highlighted in red) of the hippocampus is a niche of ongoing postnatal activity (B'). Higher magnification micrograph shows the shape of the DG (B'').
(C): The SVZ (highlighted in red) surrounds the LVs (C'). The micrograph illustrates that it consists of 3 regionally distinct microdomains (lateral, dorsal, medial; C''). The lateral microdomain is shown in higher magnification (C''').
Scale bars: A = 5 mm; B', C' = 1 mm; B'', C'' = 500 µm; C''' = 100 µm. Abbreviations: DG, dentate gyrus; SVZ, subventricular zone; LV, lateral ventricle.

1.1.4. Nucleoside Analogs Give Insights into the Migration Patterns of Cells Generated at Embryonic and Postnatal Times

Cells generated at proximity of the ventricular system rapidly migrate away to invade the surrounding parenchyma. Their pattern of migration however substantially differs at embryonic and postnatal time points. Analysis of cell distribution 10 days after birth, following [H^3]thymidine administration at various gestational days (E11, E13, E15 and E17), revealed migration of embryonal born cells into the cortex. Interestingly, they found evidences for an inside-out development, challenging the prevailing view that newborn cells peripherally displace older cells (Tilney, 1934). Thus, cells born at E11 reside in the deepest layer of the cortex. Cells born two days later (E13) were found in the middle third and cells born 4 days later (E15) in the outer third of the cortex. Finally, cells born at E17 were located in the most superficial cell layer at P10 (Angevine and Sidman, 1961; **Figures 5A and 5B**).

The mode of migration and therefore the final destination of newborn cells of the SVZ changes fundamentally during the transition from embryonal to postnatal development. Temporal analysis of newborn cells migration in the postnatal forebrain was first investigated by injecting a group of rats of the same age (P30) and sacrificing them from 1 hour to 180 days after injection. Systematic analysis of cell distribution, allowed to identify the olfactory bulb (OB) as the major final destination of cells originating from the postnatal SVZ. Up to 24 hours [H^3]thymidine labeled cells were found close to the LVs, while the OB was largely free of positive cells at this early time point. After 3 days, labeled cells were observed in the middle caudo-rostral portion of the rostral migratory stream (RMS) and after 6 days they arrived in the OB, where they distributed into both the granule cell and glomerular layers (GCL and GL, respectively) thereafter (Altman, 1969; **Figure 5A and 5C**).

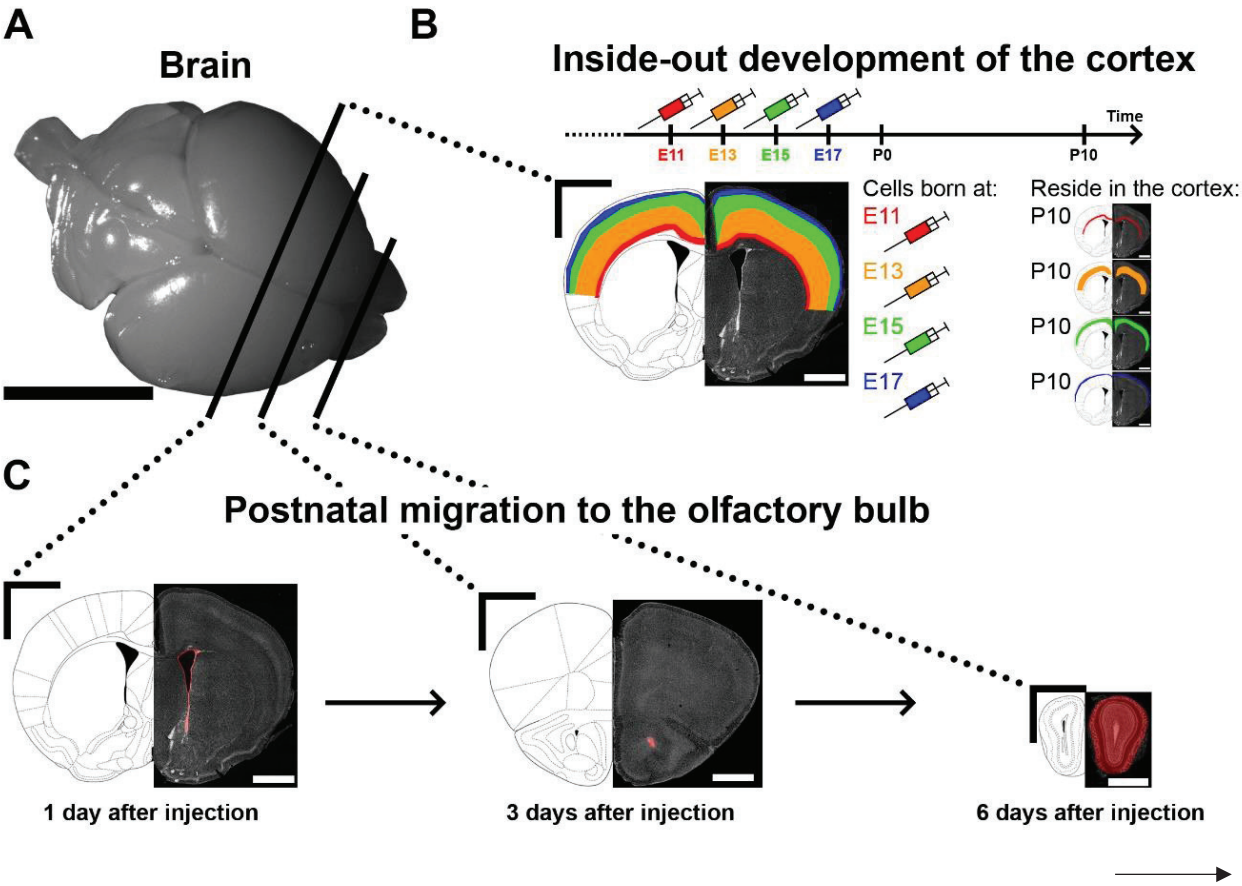

Figure 5. Migration pattern in the prenatal and postnatal rodent forebrain.
(A): Representative picture of a P10 mouse brain illustrates virtual cuts at the level of the SVZ, RMS and OB.
(B): The cortex develops in an inside-out fashion. Colored syringes in the timeline represent different [H^3]thymidine injection time points into pregnant females at E11 (red), E13 (orange), E15 (green) or E17 (blue).
Radiolabeled cells born at E11 reside in the deepest layer at P10. Cells born at E13 and E15 were found in the middle and outer third of the cortex, respectively. Cells that were generated at E17 were located in the most superficial layer.
(C): Postnatally born cells were found in the SVZ 1 day after injection, from where they invade the RMS after 3 days and arrive in the OB after 6 days.
Scale bars: A = 5 mm; B, C = 1 mm. Abbreviations: OB, olfactory bulb; RMS, rostral migratory stream; SVZ, subventricular zone.

In humans the migration pattern is suggested to be remarkably different from rodents and obtained results are subject of controversial discussions. While in young individuals (up to 6 months) the RMS can be recognized by "broad streams" or chains of DCX and frequently co-expressing PSA-NCAM cells (Sanai et al., 2011), there are also extensive arc shaped migration features in the frontal lobe of infants (Paredes et al., 2016; **Figure 6A**). This situation changes dramatically in older individuals (from 2 years on). At these later stages, chains of migrating cells are not observed. Rather, rare single (or pairs of) migrating neuroblasts can be detected (Sanai et al., 2004; Sanai et al., 2011). A subsequent study, using retrospective C^{14} birth dating, supports these findings by concluding that neurogenesis in the adult human OB is negligible. On the other hand, the neuronal turnover in the adult hippocampus is evident (Bergmann et al., 2012; **Figure 6B**). Interestingly, histological and C^{14} birth dating experiments rather suggest a dispersion of newborn neurons at proximity of their site of origin, i.e. they may participate to the cellular turnover in the striatum (Ernst et al., 2014; **Figure 6C**). The analysis of neurogenesis in the adult marmoset, which I performed during my Master, support these conclusions. I could indeed observe many DCX^+ cells in the striatum, which increase proportionally with age. Thus, as much as 30% of DCX^+ cells were found in the striatum of a 56 months old marmoset (Azim et al., 2013). Together, these observations suggest a progressive disappearance of cues required for rostral neuroblast migration, which progressively disperse to nearest regions.

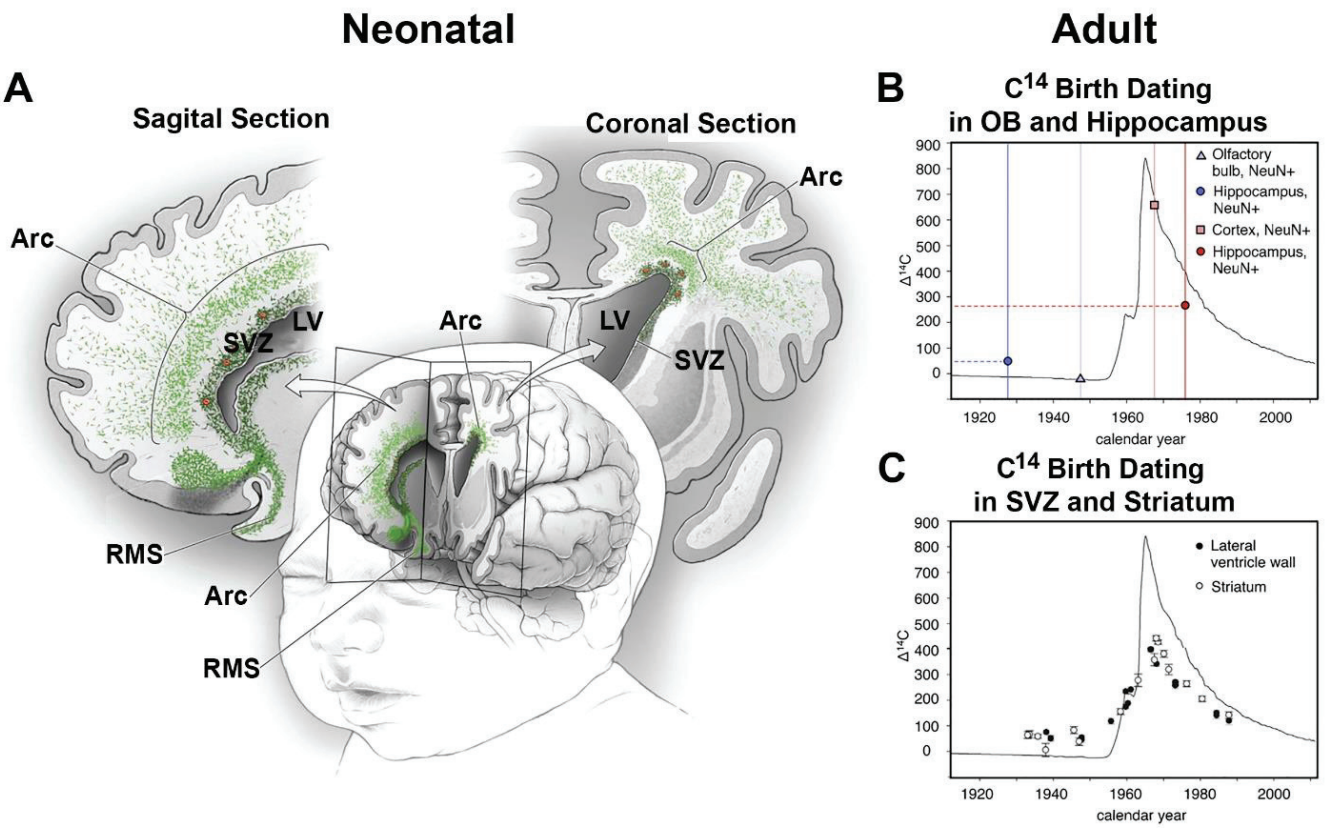

Figure 6. Migration pattern in the neonatal and adult human forebrain.
(A): Illustration of the migration pattern in a neonatal human brain in 3D, as well as in a sagittal and a coronal section. Chains of migrating neuroblasts (green) leave the SVZ ventrally and enter the RMS. Dorsally of the SVZ there is an additional arc shaped region of extensive migration towards the cortex (modified from Paredes et al., 2016).
(B+C): Graphs showing the measured C^{14} concentration as a function of the calendar year. Y-axis represents the difference of the C^{14} concentration in the air compared to the natural level. The solid black line shows the concentration before, during and after the majority of the nuclear bomb tests. Represented data of hippocampus and OB illustrate and summarize the results from different studies (Bhardwaj et al., 2006; Bergmann et al., 2012; Spalding et al., 2013). Circles illustrate C^{14} values of hippocampal neurons obtained from individuals born before (blue) and after (red) the peak of nuclear bomb tests. C^{14} values at death of the individuals were increased and decreased compared to their concentration at birth, respectively. This suggests a postnatal neuronal turnover in the hippocampus. For neurons of the OB (triangle and square) no such correlation was observed (B). Post mortem C^{14} measurements in cells of the SVZ (black circle) and the striatum (white circle) show substantial differences to the C^{14} concentrations compared to the date of birth of the individuals (C; both graphs were obtained from Ernst et al., 2014).
Abbreviations: LV, lateral ventricle; OB, olfactory bulb; RMS, rostral migratory stream; SVZ, subventricular zone.

1.1.5. The SVZ Has a Complex Cytoarchitecture and Consists of Different Cell Types with Distinct Cycling Behaviors

The cytoarchitecture of the SVZ, as well as the identity of neural stem cells it harbors, remained elusive for several decades. This was changed in the 90s with a series of landmark publications from the group of Arturo Alvarez-Buylla at the Rockefeller University in New York. The SVZ is not a homogeneous pool of cells, it is rather a heterogeneous mix of different cell types and cells at different levels in their maturation process, which differ in their morphology, function and cycling behavior. NSCs in the SVZ of the postnatal and adult brain originate from radial glia (RG) cells of the embryonal and perinatal brain (for review Kriegstein and Alvarez-Buylla, 2009). NSCs give sequentially rise to distinct cell types of divergent cycling behavior (Doetsch et al., 1997; Ponti et al., 2013). Doetsch and collaborators proposed in 1997 (Doetsch et al., 1997) a revolutionary view on the cellular architecture of the SVZ. They were able to distinguish a number of unique cell types, as well as to provide a detailed description of their organization in the SVZ. They proposed a nomenclature, which is still in use (i.e. type A, B and C cells; see below for more details) as well as the term "neurogenic niche" to define their peculiar 3D organization. Further, they demonstrated the presence of an abundant population of ependymal cells in the SVZ (type E cells), which are ciliated, aligned to the ventricular lumen and non-cycling. These different cell types are readily distinguishable by electron microscopy, based on their diverse ultrastructural morphologies and marker expression. Type A cells express PSA-NCAM and correspond to chains of migrating neuroblasts previously described in the RMS (Rousselot et al., 1995; Lois et al., 1996). They cluster in the SVZ to form a complex network of chains before engaging rostral migration toward the OB (Doetsch and Alvarez-Buylla, 1996). Type B cells exhibit ultrastructural traits (Peters et al., 1991) and expression signature (GFAP, vimentin) of astrocytes (Bignami and Dahl, 1974; Schiffer et al., 1986; Cohen et al., 1994). B cells can be further subdivided into two distinct subtypes, which are distinguishable by their ultrastructure and their position within the SVZ (B1: close to the ependymal layer; B2: at the SVZ-striatum border) and their proliferative behavior (B1 cells were not found to incorporate [H^3]thymidine). Type C cells represent the transition between type B and type A cells. They appear in clusters, which are closely associated to type A chains. They contribute to half of the proliferating population, while being negative for type A and type B markers, which also incorporate [H^3]thymidine, although to lesser extent.

[H^3]thymidine positive type B and C cells are distributed along the entire dorso-ventral axis of the lateral SVZ, while cycling type A cells appear to be largely located in the dorsal and ventral aspects only (Doetsch et al., 1997; **Figure 7**). A more recent study investigated the cycling behaviors of type A, B and C cells in more details. They made use of dual labeling techniques using the nucleoside analogs CldU and EdU. This method revealed that the cell cycle length (T_C) in adult mice progressively increases throughout differentiation (B1 cells: 17 hrs; C cells: 18-25 hrs). Further, the time for DNA synthesis (T_S) was found to be surprisingly short for type B1 cells compared to type C cells (B1 cells: 4.5 hrs; C cells: 12-17 hrs). When interpreting these data it needs to be considered that only actively cycling B1 cells, but not the quiescent fraction of the population, were included into the analysis (Ponti et al., 2013). Interestingly, the T_C and T_S of actively cycling NSCs appear almost identical to the one reported for RG cells during embryonic development at E16 (Takahashi et al., 1995). Further analysis showed that type B1 and type C cells cycle 3 times before generating type A cells, which make one or two additional divisions in the SVZ before entering the RMS (Ponti et al., 2013). Cells with a similar ultrastructure like the described type B cells can also be found in the RMS, where they enwrap the chains of migrating type A cells and separate them from the surrounding parenchyma (Lois et al., 1996). Similarly, type B1 and B2 cells appear to isolate migrating neuroblasts in the SVZ from the ependymal layer and the striatal parenchyma. Whereas neurogenesis has been the focus of most studies, it should however be mentioned that SVZ NSCs do not only generate neurons, but also produce astrocytes (Reynolds and Weiss, 1992) and oligodendrocytes (Kirschenbaum and Goldman, 1995) *in vitro.* The *in vivo* evidence for the generation of glia by the postnatal SVZ was given by retrovirus approaches (Levison et al., 1993).

Taken together, the SVZ harbors stem cells showing astrocytic traits (type B cells), which have the capacity to produce a glial and neuronal progeny. Type B cells can be further subdivided into an actively cycling and a quiescent subpopulation (Levison et al., 1993; Doetsch et al., 1997; Doetsch et al., 1999). Recent findings, using more advanced technical approaches, which will be discussed in the general discussion of this thesis manuscript, suggest that most adult NSCs arise from a pool of radial glial cells, which enter quiescence between E13.5 and E15.5 (Furutachi et al., 2015; Fuentealba et al., 2015) and gradually reactivates after birth.

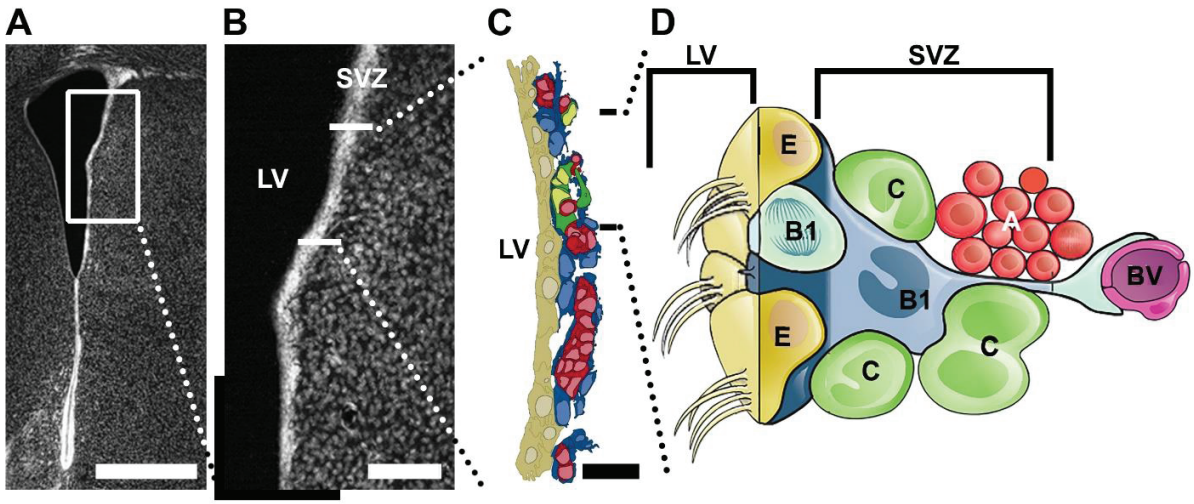

Figure 7. The cytoarchitecture of the adult SVZ.
(A+B): Representative micrographs of the SVZ (A) and the higher magnification of the lateral microdomain (B) show the zone of interest to illustrate the SVZ cytoarchitecture.
(C+D): Ciliated ependymal cells (E; yellow) align the LV and isolate the lumen from the proliferative SVZ. NSC (type B1; blue) give rise to type C cells (green) which generate migrating neuroblasts (type A; red) (schemes were modified from Doetsch et al., 1997 and Tong and Alvarez-Buylla, 2014).
Scale bars: A = 500 µm; B = 100 µm; C = 20 µm. Abbreviations: BV, blood vessel; LV, lateral ventricle; SVZ, subventricular zone.

1.2. Transgenesis Revealed Early Regionalization of Germinal Regions

Although nucleotide analogs represent a technical breakthrough in the study of germinal activity and have led to major advances in its understanding, they also present limitations. Indeed, they are incorporated in all cycling cells, thereby preventing the study of subpopulations of NSCs. Also, they don't provide any information on the molecular mechanisms involved in NSCs biology. The emergence of advanced transgenic approaches have allowed circumventing these limitations, to shape our current understanding of postnatal germinal regions. These regions appear now highly heterogeneous, with NSCs located in different location generating distinct progenies. Here I will summarize the key methodological developments, which have led to these conclusions.

1.2.1. The Development of Transgenesis Approaches Represents a Further Milestone in the History of Neuroscience

Domestication of animals and plants by selecting certain individuals for breeding, while excluding others from the line, can in the broader sense be defined as the slowest transgenic approach. The gene pool of a population gets artificially changed over many generations and new strains arise from the ancestor population. Spontaneous mutations might be kept in the population or rejected by excluding them from breeding. Approaches have been developed which allow direct genome editing. The first transgenic animals (fruit flys) were gained by random mutagenesis of the genome using different mutagens, e.g. by exposure to X-ray irradiation (Herman Joseph Muller, 20s) or mustard gas (Charlotte Auerbach, Alfred Joseph Clark, John Michael Robson, 40s). As insects have a segmental organized body plan (Lawrence, 1992), mutated larvae and flies were screened and those presenting identifiable phenotypes , such as the absence of certain segments, body parts or the poor development of them, were selected (for review McGinnis and Krumlauf, 1992). This method was used for early identification of key developmental regulator genes. Because it first identifies mutated phenotypes (induced or spontaneous), then the mutated gene, it is called forward genetic (for review St Johnston, 2002; **Figure 8A**). In *Drosophila,* segmental identity was found to depend on the segment position along the anterior-posterior axis. It led to the identification of homeobox genes, which expression follows a strict segmental code (for review McGinnis and Krumlauf, 1992). Many of the region specific transcription factors (homeobox and others) were discovered in *Drosophila* by spontaneous and induced mutagenesis approaches (forward genetic). Subsequently, their presence in mammals was confirmed by histological methods and their function resolved by transgenesis.

Later, reverse genetic approaches opened a new era in the field of neuroscience. They allowed to target specific genes to perform loss and gain of function experiments. The development of these refined transgenic strategies represents a milestone in the history of neurosciences. The capability to precisely target specific genes and loci in the genome allowed a wide range of powerful transgenic approaches (**Figure 8B**). This “transgenic era” in neurodevelopmental research began with the creation of null mutants for regionalized transcription factors (TF), for loss of function approaches.

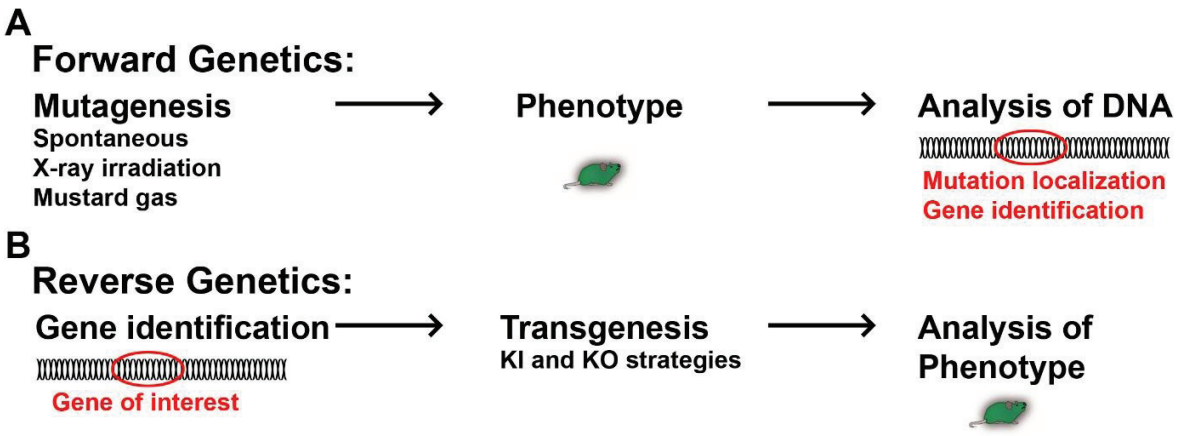

Figure 8. Illustration of the principles of forward and reverse genetics.
(A): In forward genetic approaches mutations are induce or occur spontaneously. If a phenotype was observed, the DNA was analyzed to identify the mutated gene.
(B): Reverse genetic approaches identify first the gene of interest. Targeted mutations/modifications are induced by diverse transgenic approaches and the phenotype analyzed thereafter.

However, as many of these TFs are essential for the proper development, complete knock-out (KO) often leads to perinatal death (Qiu et al., 1995; Yoshida et al., 1997). Therefore, it is frequently not possible to investigate the function of these factors in a postnatal or adult context. The discovery of the Cre-Lox systems in combination with targeted knock-in (KI) strategies allowed to overcome this limitation. The Cre-Lox system can be defined as a technology for site-specific DNA recombination. Briefly, the gene of interest is flanked by Lox sites, which are recognized by a Cre-recombinase. This Cre-recombinase can be expressed by any cell type, based on its insertion into the genome, under the control of a well-chosen promoter. This allows controlling its spatial, and to a certain degree also its temporal expression (Sauer, 1998; **Figure 9A**). Newer generations of Cre-recombinases ensure a more advanced temporal control of recombination activity. By fusing genes coding for the Cre-recombinase and a fragment of the estrogen receptor, researcher have engineered several generations of Cre-recombinase (i.e. Cre^{ERT}; Cre^{ERT2}) that are sequestered into the cell cytoplasm. Administration of the chemical tamoxifen allows the nuclear translocation of the fusion protein, and therefore its activation (Feil et al., 1996; **Figure 9B**).

Taken together, the Cre-Lox systems allows conditional KO (cKO) experiments, which are crucial for investigating the function of certain genes at a given time of development and/or of

postnatal life. In addition, it allows the conditional expression of reporter genes for lineage fate mapping. In this context, several transgenic mouse lines have been generated over the years, which varies in the detectable marker they express (e.g. LacZ, GFP, tdTomato; Madisen et al., 2010). These new developments offered a powerful tool box to advance our understanding of SVZ heterogeneity and regionalized populations greatly.

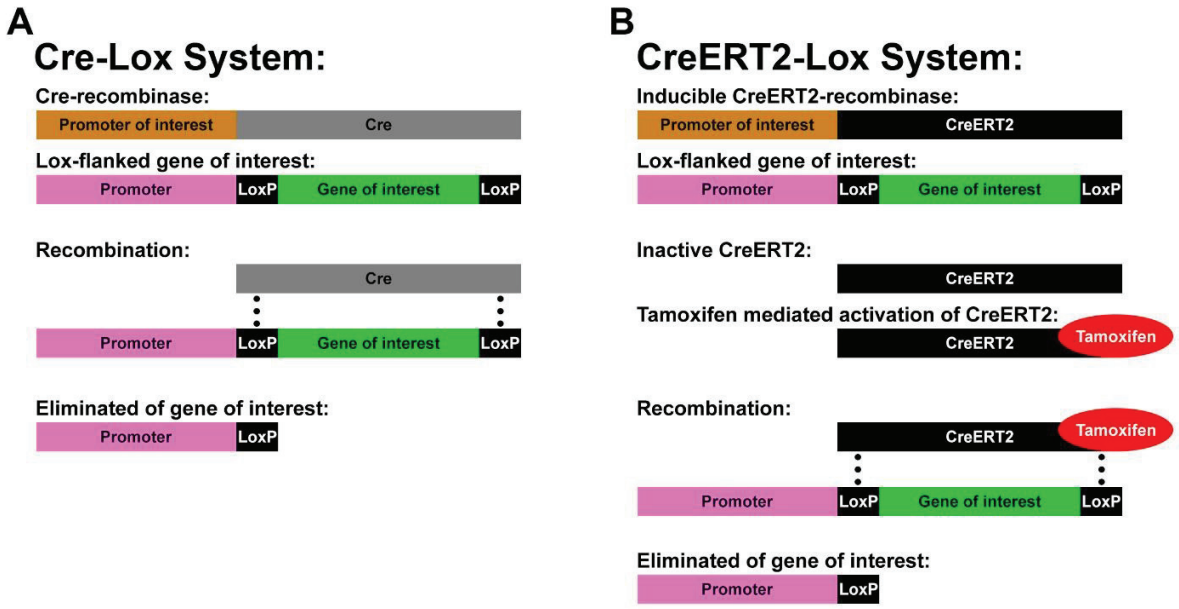

Figure 9. Temporal and spatial genetic manipulations using the Cre-Lox system.
(A): The Cre-recombinase (gray) is under the control of a promoter of interest to ensure the spatial and to a certain degree also temporal restricted expression. The gene of interest (green) is flanked by Lox sites (here LoxP; black), which are recognized by the Cre-recombinase. Expression of the Cre-recombinase leads automatically to recombination of the Lox sites and elimination of the gene of interest.
(B): Additional temporal control can be achieved by fusion of the Cre-recombinase with a fragment of the estrogen receptor (here ERT2). Cre^{ERT2}-recombinases (black) remain in the cytoplasm and therefore inactive until they are activated by tamoxifen (red) administration. Recombination of the Lox sites and elimination of the target gene occurs subsequently.

1.2.2. Expression Analyses and Fate Mapping Approaches Highlight the Regionalized Organization of the VZ/SVZ

One of the most important feature of multicellular organisms is the existence of a clearly defined rostro-caudal and dorso-ventral axis. This organization arises during early embryonic development and depends greatly on the regional expression of combinations of genes. In general, all cells are identical during the first embryonic days. However, cell fates start to diverge from each other already during blastocyst formation around E3.5, long before organogenesis (for review Saiz and Plusa, 2013; Kojima et al., 2014). Heterogeneous expressed cues are major players during embryogenesis and into adulthood. Much of the knowledge we have about these early patterning of the body plan originates from studies in insects, which have a segmental organized body (Lawrence, 1992). Like in *Drosophila*, the development of the mouse central nervous system is orchestrated by regionally expressed genes. Further, the developing forebrain, hindbrain and spinal cord resemble such segmental structures (reviewed in Rubenstein et al., 1994; Philippidou and Dasen, 2013). Focusing on the developing forebrain, we gained insight in these processes by discovering differentially expressed genes by initial immunohistochemistry. Such genes were closer investigated regarding their functional importance in fate decision of regionalized populations by transgenic approaches.

Regionalization is Observed During the Period of Neurogenesis

Several transcription factors have a clear regionalized expression pattern during early forebrain development. This is particularly apparent for markers of the pallium and the subpallium (i.e. lateral and medial ganglionic eminences, LGE, MGE; septum), some regions which contribute to the formation of specific SVZ microdomains at postnatal stages (reviewed in Fiorelli et al., 2015).

Many markers of the ganglionic eminences, belong to the ANTP class of the homeobox genes, which is the largest class of homeobox genes (Zhong et al., 2008; Zhong and Holland, 2011). This includes members of the Dlx family (Distal-less), namely Dlx1, Dlx2 (Bulfone et al., 1993), Dlx5 and Dlx6 (Simeone et al., 1994), which start to be highly expressed as early as E10. They are enriched in the ganglionic eminences and consistently absent from the pallial

domain. Other ventrally enriched genes of the homeobox familly are Nkx2.1 (also called TTF1), Nkx6.2, Gsx1 and Gsx2 (also called Gsh1 and Gsh2) of the Nk2.1, Nk6 and Gsx homeobox gene families (Zhong et al., 2008; Zhong and Holland, 2011). While Nkx2.1 was described to be partly overlapping to the Dlx genes (Price et al., 1992), Nkx6.2 was initially described as a ventral marker of the spinal cord and being largely absent of the developing forebrain (Qiu et al., 1998). However, later experiments revealed its restricted expression in a dorsal stripe of the MGE at E12.5 (Fogarty et al., 2007). Gsx1 and Gsx2 were both found to be expressed in the ganglionic eminences. While Gsx1 is restricted to the MGE (Valerius et al., 1995), Gsx2 is described to be expressed by both the LGE and MGE (Hsieh-Li et al., 1995; **Figure 10, green**). Lineage tracing approaches have shown that subpallial progenitors give rise to GABAergic interneurons. Different Cre reporter mouse lines were used to demonstrate that defined progenitor populations generate distinct lineages of interneurons, which invade the cortex tangentially (Fogarty et al., 2007).

Other homeobox genes show restricted expression to the dorsal forebrain regions, i.e. the pallium. The most studied ones are Emx1, Emx2 and Pax6 (Emx family of the ANTP class; Pax4/6 family of the PRD class; Zhong et al., 2008; Zhong and Holland, 2011). Emx1 and Emx2 start to be expressed in the mouse pallium at E9.5 and E8.5, respectively. While both genes are largely overlapping, Emx2 expression is more widespread than Emx1 (Simeone et al., 1992a). Similarly, the homeobox gene Pax6 is embryonal expressed in the pallium but absent from the ganglionic eminences (Stoykova and Gruss, 1994). Other transcription factors have been shown to act downstream of these homeobox genes, and as a result, keep a strict regional expression. Other highly specific pallial markers are the T-box transcription factors Tbr1 and Eomes (also referred as Tbr2; Bulfone et al., 1995; Bulfone et al., 1999), as well as the bHLH transcription factor Ngn2 (also referred as Neurog2; reviewed in Lee, 1997; **Figure 10, red**). Lineage tracing of the Tbr2 (Pimeisl et al., 2013) and Neurog2 (Berger et al., 2004; Donega et al., 2018) lineages revealed their participation in producing cortical projection neurons (Mihalas et al., 2016). Expression of these TFs antagonize a subpallial expression of the bHLH transcription factor Mash1 (Casarosa et al., 1999).

A third region of the developing forebrain known to participate to the formation of the postnatal SVZ, is the most medial part of the developing forebrain, the septum (for review Fiorelli et al., 2015). Examples of medially enriched markers in the embryonal forebrain belong to the Zic

family of transcription factors (Aruga et al., 1994; **Figure 10, blue**). Zinc-finger TFs control various processes of animal development (for review Grinberg and Millen, 2005). In mammals, there are five Zic- related genes that share highly conserved zinc finger domains. In terms of neural development, Zic2 is particularly important for forebrain development. Thus, mice homozygous for the Zic2 hypomorphic allele (Zic2 kd/kd) show holoprosencephaly (HPE), in which the medial part of the forebrain is defective (Nagai et al., 2000).

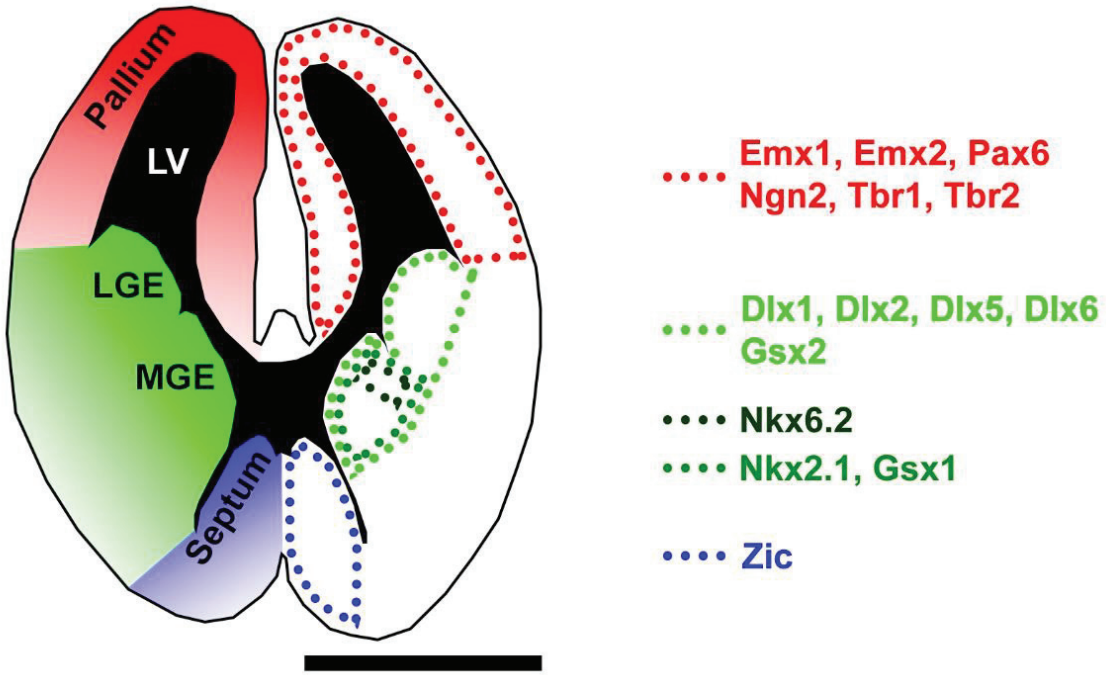

Figure 10. Illustration of regionalized TFs expression in the embryonic forebrain.
Scheme of an E14 coronal section illustrates restricted expression in the pallium (red), the LGE and MGE (green) and the septum (blue). Restricted dorsal markers are Emx1, Emx2, Pax6, Ngn2, Tbr1 and Tbr2. The ganglionic eminences harbor some markers, which are expressed by both subdivisions (Dlx1, Dlx2, Dlx5, Dlx6 and Gsx2) and others that are restricted to the MGE (Nkx2.1 and Gsx2) or parts of it (Nkx6.2). Finally, markers showing restriction to the septum belong to the Zic family.
Scale bar = 1 mm. Abbreviations: LV, lateral ventricle; LGE, lateral ganglionic eminence; MGE, medial ganglionic eminence; TF, transcription factor.

Regionalization is Observed During the Period of Gliogenesis

Astrocytes are known to be produced at the end of the period of neurogenesis. It is classically accepted that RG cells switch fate and start to produce astrocytes that migrate to the cortex and associate with previously generated neurons in so called cortical columns (Magavi et al., 2012; for review Tabata, 2015). Recent studies indicate that their production is highly regionalized and newborn astrocyte precursors migrate radially away from their region of origin (Tsai et al., 2012). It has been shown that the major source of the cortical astrocyte population are astrocytes that proliferate and differentiate in the parenchyma (Ge et al., 2012; **Figure 11A**). TFs associated with astrogenesis are rare. In the developing spinal cord the TF NFIA has been proposed to inhibit neurogenesis and to trigger gliogenesis. Within the glia population, NFIA expression leads to migration and differentiation of astrocyte precursors. This function was found to be antagonized by the expression of Olig2 in oligodendrocyte precursors (Deneen et al., 2006). Despite the description of diverse subtypes of astrocytes (for review Tabata, 2015) there are, to my best knowledge, no TFs described for its association with the specification to these subtypes.

The other macroglia lineage, oligodendrocytes, are described to be produced in 3 different temporal and spatial waves. The first wave originates from the MGE and the medial part of the ventral forebrain, while the second is more laterally generated by the LGE. The final third wave appears postnatally in the dorsal SVZ microdomain. Ablation of a specific line does not result in a phenotype, as the missing "temporal lineage" is replaced by the remaining waves. However under physiological conditions, progenies of the first wave disappear postnatally (Kessaris et al., 2006; **Figure 11B**). While Olig1 and Olig2 are identified as general oligodendrocyte TFs (Zhou and Anderson, 2002), TFs specifying or differentiating oligodendrocytes from these three waves are still missing.

All together, these observations indicate that a regionalization of neurogenesis appears early in the developing forebrain. This regionalization relies on the regional expression of defined TFs and translate into the generation of different neuron subtypes. Similar principles apply to gliogenesis, although the exact transcriptional mechanisms involved in their regional production and its functional importance remains to be fully explored.

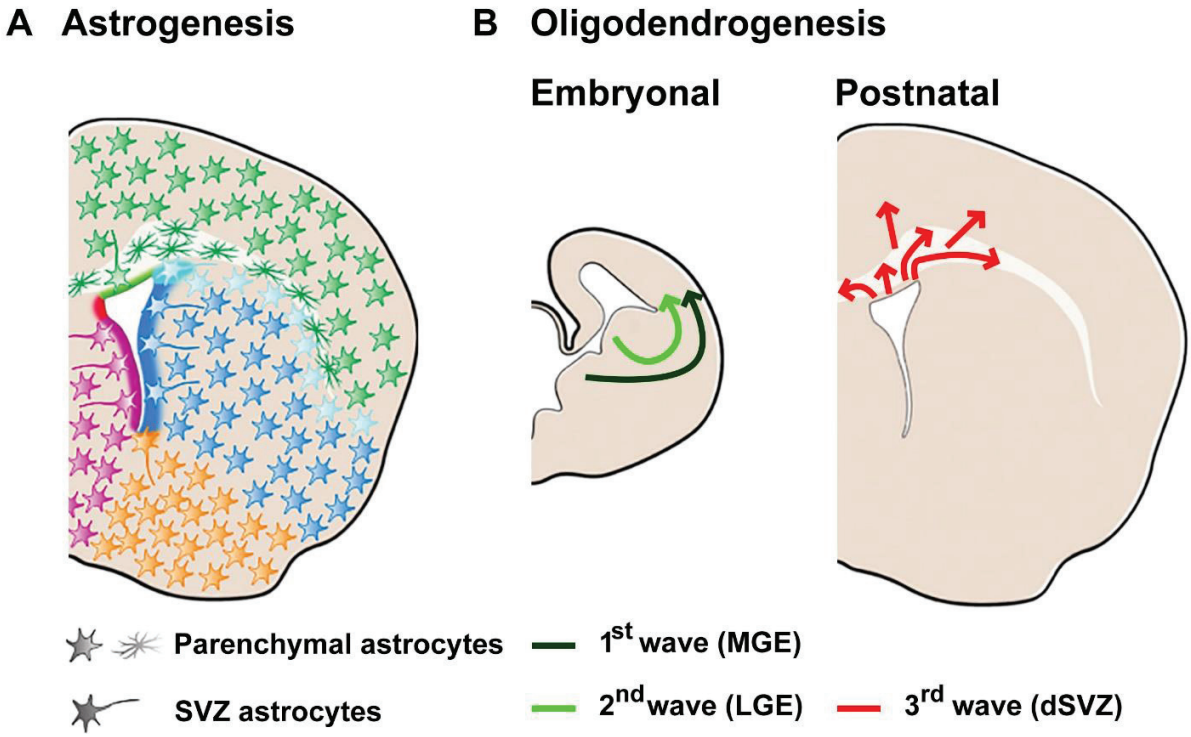

Figure 11. Illustration of astrogenesis and oligodendrogenesis.
(A): Astrocyte precursors that are generated in the SVZ, migrate radially away from their region of origin and amplify subsequently. Cortical and white matter astrocytes (green) originate in the dorsal SVZ (dSVZ; modified from Bayraktar et al., 2015).
(B): Oligodendrogenesis occurs in 3 waves. The first wave (dark green) and the second wave (light green) originate from the MGE and LGE, respectively, and invade the cortex tangentially. The postnatal third wave (red) of oligodendrogenesis occurs in the dSVZ and invades the CC and cortex radially (template used from Bayraktar et al., 2015).
Abbreviations: CC, corpus callosum; SVZ, subventricular zone; dSVZ, dorsal subventricular zone ; LGE, lateral ganglionic eminence ; MGE, medial ganglionic eminence.

Regionalization of the SVZ is Retained After Birth

Both neurogenesis and gliogenesis persist in the postnatal SVZ (Levison and Goldman, 1993). Interestingly, the transcriptional regionalization of the developing forebrain is retained postnatally. This is reflected by the restricted expression of the same TFs within defined microdomains of the postnatal SVZ (for review Fiorelli et al., 2015). As described above, these distinct embryonic regions (pallial vs. ganglionic eminences vs. septal domains) are all contributing to the generation of the postnatal SVZ (dorsal vs. lateral vs. medial SVZ microdomains; **Figure 12**). The transcriptional analogies of the embryonic and postnatal/adult

VZ/SVZ, also translate into similarities in the regional generation of defined cell lineages (for review Fiorelli et al., 2015). During my Master, we made use of the Mash1$^{BAC\text{-}EGFP}$ mouse line, to label postnatal forebrain progenitors. Interestingly, we could show that both Dlx2 and Tbr2 are expressed by Mash1^{+} progenitor populations in the postnatal and adult SVZ. These two distinct populations of progenitors were non-overlapping, but also enriched in distinct SVZ microdomains. While Dlx2 positive progenitors were mainly restricted to the lateral SVZ, Tbr2 expressing glutamatergic progenitors were exclusively located in the dorsal SVZ (Azim et al., 2012a). Other studies demonstrated that these two populations give rise to different neuronal lineages. Studies using genetic fate mapping (Neurog2$^{+/GFP}$; Neurog2iCreERT2) approaches showed sequential expression of Pax6, Ngn2, Tbr2 and Tbr1 by the cells in the dorsal SVZ at embryonal and perinatal ages (**Figures 10, 12A and 12B**). This lineage was demonstrated to generate glutamatergic OB neurons until adulthood (Brill et al., 2009; Winpenny et al., 2011).

In line with the regional expression of Dlx2 (Azim et al., 2012a; Kohwi et al., 2007), Gsx1 and Gsx2 appear to be enriched in the adult lateral SVZ (López-Juárez et al., 2013). Interestingly, Gsx1 was expressed more ventrally, while Gsx2 was rather dorsally in the lateral SVZ (López-Juárez et al., 2013). This highlights the developmental origin of postnatal lateral SVZ from the embryonic ganglionic eminences, where Gsx1 is restricted to the MGE (Valerius et al., 1995), while Gsx2 is more broadly expressed in the ganglionic eminences (Hsieh-Li et al., 1995). Similarly, Nkx6.2 is expressed by the ventral most region of the adult lateral SVZ, as well as by its medial aspect (Merkle et al., 2014). Interestingly Nkx2.1 is the only TF to date to not show such a strong correlation in its expression pattern, before and after birth (**Figures 10 and 12C**). While it overlaps with Dlx genes in both the LGE and MGE (Price et al., 1992), it is restricted to the ventral tip of the SVZ at postnatal stages (Merkle et al., 2014). Lateral NSCs have been identified, by lineage tracing, to generate interneurons of the OB, in line with their contribution to cortical interneuron generation during development (Fogarty et al., 2007). Inducible fate mapping experiments revealed that Dlx1/Dlx2 expressing progenitors give rise to different OB interneuron subtypes at different embryonal and postnatal ages. These interneuron subtypes diverge in their destination in the OB and in the expression of specific subtype markers (Batista-Brito et al., 2008).

Finally, TFs of the Zic family, which are expressed in the septum during embryonic development, appear to keep their regional expression postnatally. Thus, Zic TFs can be

observed in the septum of the adult forebrain (Aruga et al., 1994), including the medial microdomain of the adult SVZ (**Figures 10 and 12C**). Zic expressing progenitors have been shown to generate mainly calretinin (CalR) interneurons of the GL layer in the OB (Merkle et al., 2014; Tiveron et al., 2017).

Taken together, the embryonic VZ as well as the postnatal SVZ, are highly regionalized germinal regions. This regionalization, which is reflected by the differential expression of defined transcription factors, is observed at both pre- and postnatal ages. This suggest that these embryonic and postnatal NSC niches are developmentally related. This was indeed directly demonstrated by using fate mapping approaches (Young et al., 2007).

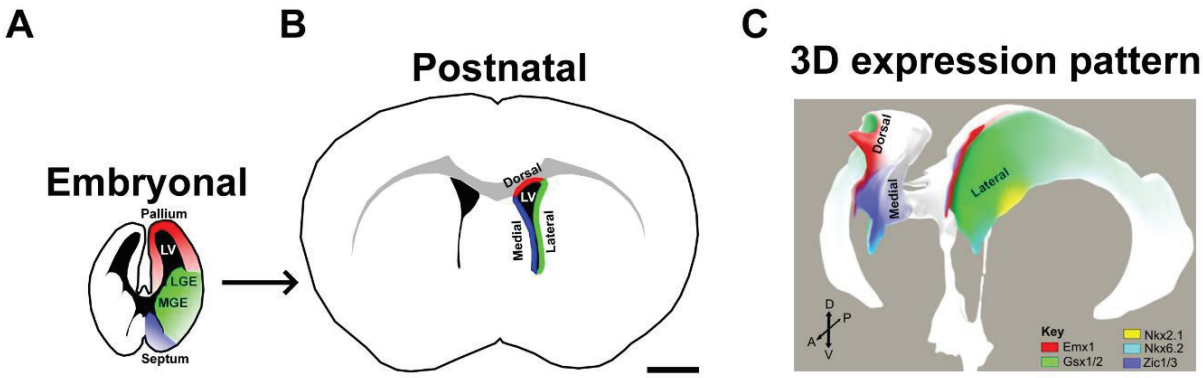

Figure 12. Embryonic regionalization is retained postnatally.
(A+B): Illustrations of embryonal established transcriptional domains (pallium, ganglionic eminences and septum; A), which are retained into postnatal ages. This domains are transcriptionally correlated to their postnatal analogs in the SVZ (lateral, dorsal and medial SVZ; B).
(C): 3D representation of the ventricular system highlights the postnatal expression pattern of some regionalized markers of the SVZ (modified from Fiorelli et al., 2015).
Scale bar: B = 1mm. Abbreviations: LGE, lateral ganglionic eminence; MGE, medial ganglionic eminence; LV, lateral ventricle.

1.2.3. Function of Regionally Enriched TFs in Lineage Specification

Null Mutants Reveal the Importance of Single Regionalized Genes in Forebrain Development

Deletion of widely expressed TFs have a dramatic impact onto brain development, demonstrating the importance of single genes in brain formation. The brain factor 1 (BF1) is a global telencephalon marker (Shimamura et al., 1995). Null mutations of BF1 demonstrated the importance of single genes in maturation. While heterozygous animals appear normal, homozygous mutants suffer from severe developmental defects and die within 20 minutes after birth (**Figure 13A**). The cerebral hemispheres of these animals were found extremely reduced in size (by 95%), with subpallial regions appearing more affected than pallial ones. These defect results from a marked reduction of RG cells proliferation, as demonstrated by BrdU administration (Xuan et al., 1995). Even more severe are mutations of another widely expressed TF, i.e. Otx2 (Simeone et al., 1992b). Otx2 KO mice die embryonically and lack anterior regions of the neural tube. Beside severe abnormalities in gastrulation they fail to develop forebrain and midbrain regions (Acampora et al., 1995; Ang et al., 1996; **Figure 13B**).

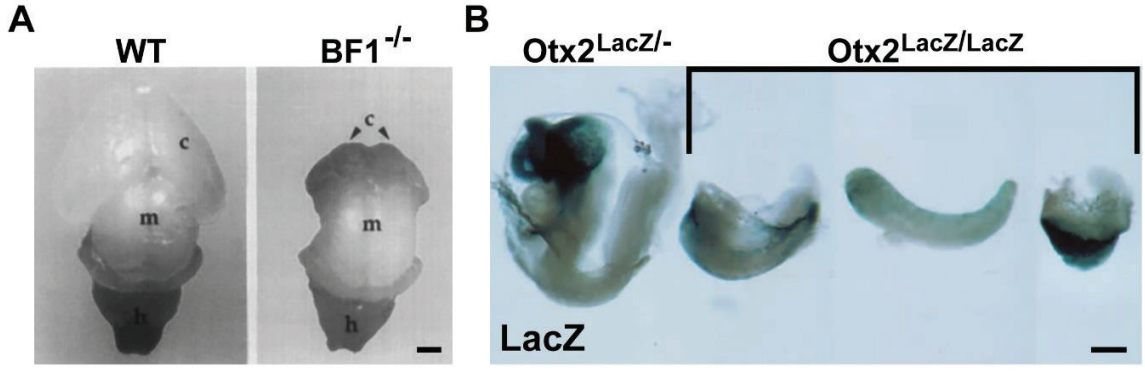

Figure 13. Severe developmental defects after deletion of widespread telencephalon factors.
(A): Brains from P0 BF1 null mutants have markedly reduced cerebral hemispheres compared to WT controls (modified from Xuan et al., 1995).
(B): KO of Otx2 leads to severe developmental malformations and a lack of the anterior regions of the neural tube (modified from Acampora et al., 1995).
Scale bar: A = 1 mm; B = 100 µm. Abbreviations: KO, knock out; WT, wild type.

Ablation of ventral and dorsal markers usually have less severe consequences, due to their more restricted expression pattern, although they often result in death at birth. For example ablation of Dlx1 or Dlx2, which show uniform expression in the ganglionic eminences (Bulfone et al., 1993), leads to death before the age of one month or immediately at birth, respectively. However, neither Dlx1 nor Dlx2 mutants show any obvious morphological changes (**Figure 14A**). Closer investigation of Dlx2 null mutants exhibited no changes of regionalized expression of ventral (Dlx1, Dlx5, Nkx2.1; Price et al., 1992; Bulfone et al., 1993; Simeone et al., 1994) or dorsal (Emx1; Simeone et al., 1992a) markers. Only the absence of TH^+ periglomerular interneurons in the OB was observed. In contrast, simultaneous ablations of both markers leaded to severe abnormalities, such as impaired expression of other ventral markers (Dlx5, Dlx6; Simeone et al., 1994), accumulation of neurons in the LGE, while the striatum is poorly developed (Qiu et al., 1995; Anderson et al., 1997b; **Figure 14A**). Further, the generation of ventral GABAergic interneurons ($CalB^+$) destined for the cortex (**Figure 14B**) and OB was severely disrupted (Anderson et al., 1997a; Bulfone et al., 1998). This results suggest that Dlx1 and Dlx2 seem to be able to compensate the lack of each other to some degree but not completely.

Figure 14. Severe developmental defects by Dlx1 Dlx2 double KO.
(A): Representative micrographs of P0 animals illustrate the compensatory roles of Dlx1 and Dlx2. Individuals with ablations of single Dlx genes show no obvious morphological changes. However, double mutants exhibit sever subpallial abnormalities. Cells accumulate in a LGE like area (LGE*) and the striatum is only poorly developed (St*; modified from Anderson et al., 1997b).
(B): Representative micrographs of E14.5 show that double KO animals lack tangentially migrating $CalB^+$ cells from the subpallium into the pallium (white arrow; modified from Anderson et al., 1997a).
Scale bar: A = 500 µm; B = 100 µm. Abbreviations: LGE, lateral ganglionic eminence; St, striatum; WT, wild type.

In contrast, the pallial markers Emx1 and Emx2 (Simeone et al., 1992a) were shown to play more divergent roles. Viability seems to depend greatly of the background. While for Emx1 null mutants different studies found normal viability to 50% neonatal death, lack of Emx2 leads to death within hours after birth. Morphologically, Emx1 ablation exhibits a lack of the CC connection between the two hemispheres (**Figure 15A**). Some degree of this defect appears also in Emx2 KO animals, besides the missing of a DG and a poorly developed hippocampus. Further, they reported a significant smaller cortex (poorly developed lateral and lacking of medial cortex; **Figure 15B**) and OB with a disorganized mitral cell layer (MCL; Qiu et al., 1996; Yoshida et al., 1997). Also Tbr1, another dorsal marker (Bulfone et al., 1995), was found to be important in the development of the MCL. Animals lacking Tbr1 fail to generate most projection neurons and do not develop a MCL at all (Bulfone et al., 1998).

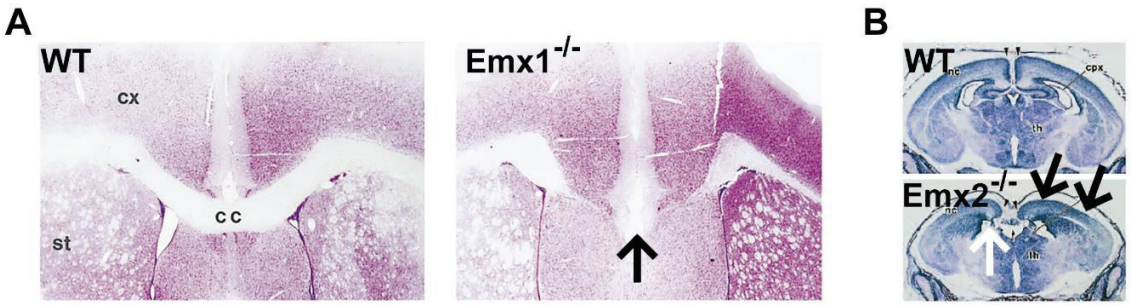

Figure 15. Severe dorsal defects following Emx1 and Emx2 ablation.
(A): Representative micrographs show the lack the CC connection (arrow) between the two hemispheres in young adult Emx1 null mutants (modified from Qiu et al., 1996**)**
(B): Ablation of Emx2 leads to severe morphological changes and neonatal death. Representative micrographs of E19.5 animals show a reduced hippocampus and a lack of the DG (white arrow). Further, the lateral cortex is only poorly developed and the medial part is completely missing (black arrows; modified from Yoshida et al., 1997).
Abbreviations: CC, corpus callosum; cx, cortex; st, striatum.

Taken together, complete KO of single genes results often in reduced viabilities and in different degrees of developmental defects. These defects correlate to the regional appearance of the marker and the lineage-specific expression. However, cKO approaches might be necessary for investigations of their function postnatally.

Advanced Transgenic Approaches Allow more Specific Gene Manipulations

As described above, many null mutations are lethal and results might be influenced by potential bystander effects. Therefore, it is hard to make conclusions of the proper function of a certain factor in one particular population, especially if focusing on postnatal processes. Advanced transgenic mouse lines, making use of the Cre-Lox system, allow spatial and temporal restricted loss of function experiments for more specific investigations.

For example, early cKO of Tbr2 from the CNS, using Nestin-Cre and Sox1-Cre animals, leads to substantial defects in the OB morphogenesis (Kahoud et al., 2014), microcephaly and severe behavioral defects (Arnold et al., 2008). These cKO animals allow to confirm postnatally the results gained by null mutations. Mutant animals have a reduced number of SVZ progenitors and a disturbed upper cortical layer. While neurogenesis in the newborn DG is not affected, it is extremely reduced in adult animals. Otherwise, neurogenesis of the adult SVZ is reported to be not affected (Arnold et al., 2008). However, the OB appears generally disorganized and lack the MCL, including the virtual absence of Tbx21, a mitral cell marker (Faedo et al., 2002), from the OB. In addition, lack of Tbr2 leads to an abnormal enlargement of the SVZ-RMS system. Regarding Tbr1, a general marker of the glutamatergic lineage (Brill et al., 2009; Winpenny et al., 2011), it has been shown that migrating neuroblasts of the glutamatergic lineage (DCX^{+}; $Tbr1^{+}$) accumulate in the perinatal RMS. However, while Tbr2 seems to be nonessential for embryonic glutmatergic neuroblast generation (regardless their accumulation), adult ablation of Tbr2 leaded to a substantial decrease of Tbr1 positive cells (Kahoud et al., 2014).

During embryonic development, Ngn2 is a marker of the pallium, while Mash1 is enriched in subpallial regions. It has been shown that Ngn2 is necessary for the existence of these two transcriptional regions, as the ventral marker Mash1 ectopically invades dorsal regions after Ngn2 KO (Fode et al., 2000). In elegant KI approaches KO mouse lines for Ngn2 and Mash1 were generated by replacing Ngn2 with Mash1 ($Ngn2^{KIMash1}$; Fode et al., 2000) or Mash1 with Ngn2 ($Mash1^{KINgn2}$; Parras et al., 2002). It has been demonstrated that the $Ngn2^{KIMash1}$ mutation leads to a ventralization of the pallium, by expression of ventral markers, similarly to Ngn2 mutants (Fode et al., 2000). On the other hand, the forced ventral expression of Ngn2

(Mash1^{KINgn2}) did not result in any obvious dorsalization of the subpallium (Parras et al., 2002). This suggests that Mash1 and Ngn2 have different functions in neuronal specification. While Ngn2 is necessary to develop a dorsal fate, Mash1 seems to be less important for the acquisition of a ventral fate.

1.3. Advanced Approaches to Explore the Transcriptional Correlates of Postnatal Heterogeneity

1.3.1. Electroporation Allows Efficient Targeting of Different SVZ Microdomains

Beside the use transgenic modified animals, postnatal SVZ stem cells can also be manipulated using viruses and electroporation (EPO) approaches (for review Lacar et al., 2010). While the generation of transgenic animals is time-consuming, the two later approaches allow studying gene functions in a rather fast and straight forward way. The big advantage of EPO compared to viral approaches is the possibility to target specific SVZ microdomains. Indeed, injected plasmids move unidirectionaly towards the anode and therefore can be efficiently targeted to a chosen region of the brain (Saito and Nakatsuji, 2001). EPOs have been successfully performed in bacteria (Calvin and Hanawalt, 1988), cultured animal and plant cells (Neumann et al., 1982; Fromm et al., 1985), as well as in mouse embryos following their *in vitro* isolation (Itasaki et al., 1999). Subsequent studies have demonstrated its efficiency *in vivo*, into mouse muscle cells (Aihara and Miyazaki, 1998) and in the chick (Muramatsu et al., 1997). Finally, this method has been applied to *in vivo* approaches of the embryonic mouse brain (Saito and Nakatsuji, 2001) and spinal cord (Saba et al., 2003).

Postnatally, EPO of RG cells, i.e. the NSCs of the early postnatal forebrain, can be done during a restricted time window, i.e. from P0 to P4. Transfected RGs keep proliferating and generate progenies harboring and expressing the electroporated gene (e.g. GFP; **Figure 16**). Their neuronal progenies can be detected along the whole RMS 4 days post EPO (dpe) migrating tangentially towards the OB. In the OB they start to migrate radially into the GL and GCL, where they develop characteristic neuronal morphologies (Boutin et al., 2008). Manipulation

of single genes by EPO has been shown to be sufficient to induce changes in the cell cycle and differentiation behaviors of postnatal NSCs (Boutin et al., 2008; Boutin et al., 2010; Azim et al., 2014a; Fischer et al., 2014). However, the real beauty of the EPO approach is the possibility to efficiently target specific, distinct regions of the postnatal SVZ. Therefore it allows to study SVZ heterogeneity between NSCs residing in defined microdomains. For instance, our team demonstrated that neuronal lineages generated in distinct microdomains differ remarkably in their fate and final destination in the OB. While lateral NSCs generate predominantly cells for the GCL, medial EPO targets NSCs producing progenies mainly destined for the GL. The dorsal originated population scatters from the outer part of the GCL, through the MCL and to the GL of the OB (Fernández et al., 2011). The majority of the interneurons residing in the GL can be subdivided into three non-overlapping populations by their expression of tyrosine hydroxylase (TH) or the calcium binding proteins CalR or CalB (Panzanelli et al., 2007). We showed that in the GL TH expressing interneurons preferentially originate from the dorsal microdomain, followed by the lateral microdomain. CR positive interneurons are generated by the medial and to a lesser extend the dorsal microdomain. The largest proportion of the CB lineage comes from the lateral microdomain. Similarly, a comparable fraction of the CR expressing interneurons in the GCL have a dorsal and medial origin, while just few are generated by lateral NSCs (Fernández et al., 2011).

One major drawback of plasmid electroporation is the transient expression of the transgene. Indeed, because it does not integrate into the genome, it gets progressively diluted by successive cell cycles (for review Lacar et al., 2010; Mamber et al., 2010). Advances in plasmid engineering allow to overcome this limitation. For instance, Cre plasmids (constitutive or inducible) can be used in Cre reporter mice, such as the Rosa-EYFP mouse line (Srinivas et al., 2001; **see Chapter 2**). In the same way conditional gain and loss of function experiments of a gene of interest can be performed using an appropriate mouse line if already available. Another possibility of permanent labeling or genetic manipulation is the use of transposon systems (Akhtar et al., 2015). There is a number of transposon systems known including *PiggyBac* and *Sleeping Beauty*. Mammalian cell culture comparisons have demonstrated that the *PiggyBac* system is far the most efficient among them (Wu et al., 2006).

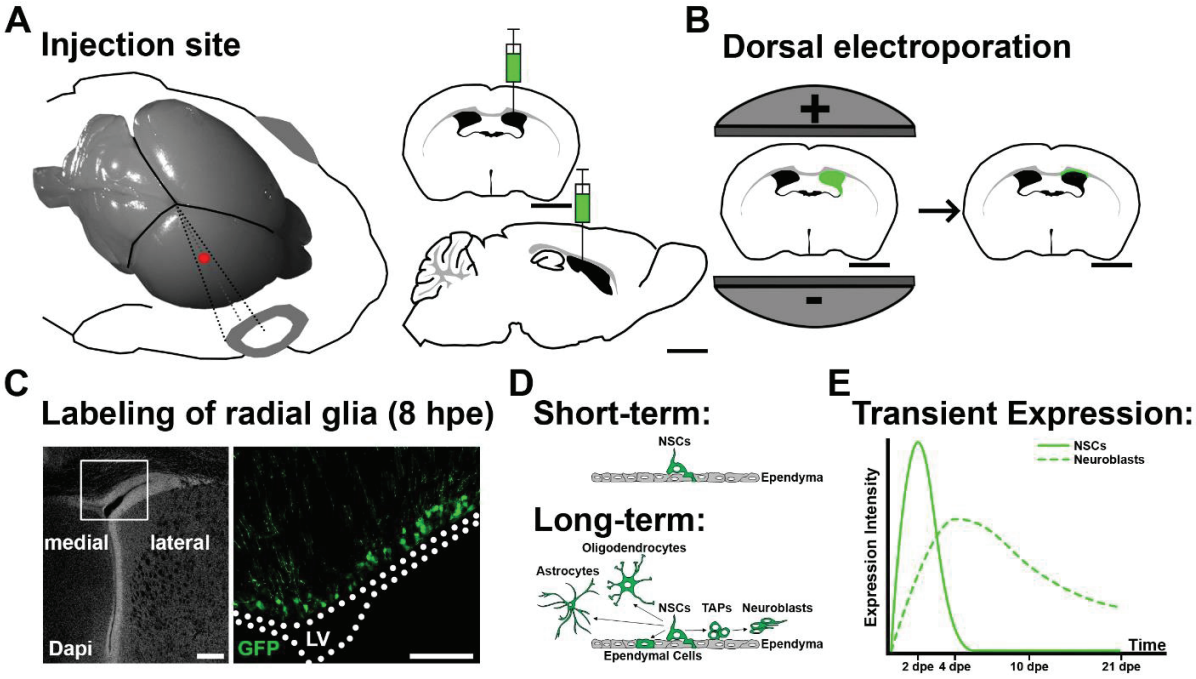

Figure 16. Illustration of the postnatal EPO approach.
(A): Schematic illustration of the injection site for the plasmids in postnatal EPO. The injection site (red point) in P1-P2 mouse pubs lies on a virtual connectional line between lambda and the caudal half of the eye. The optimal location for injection depends on the age/size of the pup and is a little closer to lambda than to the eye. Additionally, schemes of a coronal and a sagittal section illustrate the injection site. The optimal injection depth varies as a function of the age/size of the pup. Highest success rate can be achieved by moving the Hamilton 34G syringe 2 mm down and 0.5 mm up for small animals and 2.25 mm down and 0.75 mm up for larger animals, respectively.
(B): For targeted electroporation the anode of the tweezer electrodes needs to be placed next to the region of interest (here the dorsal SVZ microdomain). Targeted transfection of NSCs is driven by 5 pulses of 95 V for 50 ms in 950 ms intervals.
(C): Representative micrographs demonstrate efficient transfection of NSCs 8 hours after dorsal EPO. Note that the NSCs are exclusively located in the dorsal SVZ microdomain and have a RG like morphology.
(D): Short-term EPO can be efficiently used to label NSCs (see **Chapter 2**). Long-term approaches can be used to investigate the fates of the progenies from the transfected NSCs.
(E): A major drawback of this approach is the transient labeling, which is mainly due to plasmid dilution. NSCs lose their labeling within 4 dpe and also in neuroblasts the intensity of the labeling decreases over time.
Scale bars: A, B = 2 mm; C (overview) = 200 µm; C (crop) = 100 µm. Abbreviations: EPO, electroporation; dpe, days post electroporation; hpe, hours post eletroporation; LV, lateral ventricle; NSC, neural stem cell; TAP, transient amplifying progenitor.

1.3.2. Large Scale Transcriptional Profiling Reveals the Full Extent of Postnatal SVZ Heterogeneity

During my Master, we initiated a large scale study to explore further the transcriptional specificities of NSCs residing in defined domains of the postnatal SVZ. In order to probe heterogeneity of the postnatal SVZ, we microdissected its dorsal and lateral walls at different postnatal ages and isolated NSCs and their immediate progeny based on their expression of Hes5-EGFP/Prominin1 and Ascl1-EGFP, respectively. Whole genome comparative transcriptome analysis revealed transcriptional regulators as major hallmarks that sustain postnatal SVZ regionalization. We found an unexpected high amount of genes being differentially expressed between the dorsal and lateral SVZ (1948), NSCs (1224) and TAPs (1215). Interestingly, many of these genes were not just differentially expressed between those two regions, but also specific for SVZ (1461), NSCs (533) and TAPs (577) (Azim et al., 2015). This suggests a highly complex and specific transcriptional regulation of regionalized NSCs niches, the NSCs and the TAPs, their immediate progenies. These results leaded directly to my PhD project.

1.4. Objectives of the PhD Thesis

Objective 1: The SVZ is a highly complex and irregular region of ongoing postnatal germinal activity. The heterogeneous character of the SVZ is evident and recent studies generated enormous datasets of transcripts, which are differentially expressed between divergent microdomains. However, an appropriate tool for fast analysis of the protein level along the full rostro-caudal and dorso-ventral extend of the SVZ is still missing. Therefore, I developed "FlashMap", a semi-automatic software that allows rapid analysis of protein levels in the full SVZ, based on optical density measurements after immunohistochemistry. "FlashMap" generates easy readable heatmaps in two dimensions, which can be accurately superimposed on three-dimensional reconstructions of the ventricular system for rapid spatial visualization and analysis. This new approach will fasten research onto SVZ regionalization, by guiding the identification of markers, such as TFs expressed in specific SVZ microdomains (**Chapter 1**).

Objective 2: I used transcriptomic as well as fate mapping approaches to investigate the relation between regional expression of transcription factors by NSCs and their acquisition of distinct neural lineage fates. Our results support an early priming of NSCs to produce defined cell types depending of their spatial location in the SVZ and identify Hopx as a marker of a subpopulation biased to generate astrocytes. Interestingly, manipulation of Hopx expression showed minor effects on astrogenesis, but resulted in marked changes in the number of NSCs and of their progenies. Taken together, our results highlight transcriptional and spatial heterogeneity of postnatal NSCs, as well as their early priming toward specific lineages and suggest a role for Hopx in the evolution of SVZ germinal activity (**Chapter 2**).

2. Chapter 1: "FlashMap" - A Fast and Semi-Automatic Tool for Accurate Spatial Analysis of Protein Expression in the Subventricular Zone

Stefan Zweifel[1], Julie Buquet[1,2], David Rousseau[3,2], Olivier Raineteau[1]

[1]Univ Lyon, Université Claude Bernard Lyon 1, Inserm, Stem Cell and Brain Research Institute U1208, 69500 Bron, France
[2]CREATIS CNRS UMR5220 & INSERM U1044, Université de Lyon, Université Claude Bernard-Lyon 1, INSA-Lyon, Villeurbanne, France
[3]LARIS, IRHS UMR INRA, Université d'Angers, 62 avenue Notre Dame du Lac, 49000, Angers, France

In preparation for submission

In this chapter, I designed the study, performed all experiments and analyses and wrote the manuscript. Further, I supervised the coding from "FlashMap", which was performed by Julie Buquet.

2.1. Abstract

The subventricular zone (SVZ) is a region of ongoing postnatal germinal activity that shows complex spatial heterogeneity. Thus, distinct SVZ microdomains contain neural stem cells (NSCs) that express distinct transcription factors and accordingly generate different glial and neuronal progenies. These unique characteristics call for the development of new methods to integrate a spatial dimension to analyses performed in the SVZ.

We developed "FlashMap", a semi-automatic software that allows the segmentation and rapid measurement of optical densities (ODs) throughout the SVZ rostro-caudal extent. "FlashMap" generates easily readable two-dimensional (2D) heatmaps that can be superimposed onto three-dimensional (3D) reconstructions of the ventricular system for optimal spatial exploration. Accurate heatmaps can be obtained even following serial section subsampling thereby reducing the amount of tissue and time required for analysis. We illustrate the potential of this new tool by exploring the correlation of SVZ thickness and cellular density with the germinal activity observed along its full rostro-caudal extend. We finally used 'FlashMap" to analyze the spatial expression of the transcription factors Dlx2, Tbr2 and Hopx, as well as of the

neuroblast marker DCX, to demonstrate the suitability of this approach to explore the regional production of cells of distinct lineages by defined SVZ microdomains.

This newly developed approach, which is easily adaptable to the study of other germinal regions, will considerably fasten the spatial analysis of germinal activity and of the generation of neural lineage diversity.

Key words: subventricular zone, germinal activity; spatial heterogeneity; segmentation; optical density measurements

2.2. Introduction

The SVZ is a germinal region surrounding the opened lateral ventricles (LV) along its full rostro-caudal extend. It is one of only two niches of the mammalian forebrain, where germinal activity persists throughout postnatal life (Smart, 1961; Altman and Das, 1965; McDermott and Lantos, 1990). At its apical border it lines the lateral ventricle and is restricted at its basal borders by defined brain regions: i.e. the corpus callosum (dorsal border), the striatum (lateral border), the septum and hippocampus (medial border). NSCs harbored by the postnatal SVZ generate neuroblasts, that migrate along the rostral migratory stream (RMS) into the olfactory bulb (OB), where they differentiate into various types of neurons and integrate into the pre-existing network (Lois and Alvarez-Buylla, 1993; Lois and Alvarez-Buylla, 1994; Carleton et al., 2003). Further, NSCs of the postnatal mammalian SVZ give rise to astrocytes and oligodendrocytes (Levison and Goldman, 1993). Accumulating evidences highlight the heterogeneous nature of the SVZ. Thus, the SVZ appears to be populated by regionalized populations of NSCs that are biased to generate diverse neuronal subtypes (Merkle et al., 2007). For instance, most GABAergic (inhibitory) interneurons originate from the lateral microdomain of the SVZ (lSVZ), while glutamatergic (excitatory) projection neurons are exclusively generated by its dorsal counterpart (Brill et al., 2008; Brill et al., 2009; Azim et al., 2012a). Oligodendrocytes are described to be produced in three separated waves. The third and last wave is produced postnatally and originates from the dorsal SVZ (dSVZ; Kessaris et al., 2006). Similarly to these findings in rodents, dorsal restriction of glutamatergic progenitors and lateral enrichment of GABAergic progenitors was found in newborn marmosets (Azim et

al., 2013). This suggests that a certain degree of heterogeneity might be evolutionary conserved.

Recent research, driven by the development of new technologies, led to an accumulation of a large amount of transcriptional datasets of various SVZ cell types. For instance, we recently described an unexpected level of transcriptional heterogeneity between the dSVZ and lSVZ, but also between NSCs and transient-amplifying progenitors of those two microdomains (Azim et al., 2015). While the list of regionally expressed genes continuously increases, an appropriate tool for rapid analysis of their expression in the SVZ is still missing. As accurate 3-dimensional quantifications are very time-consuming in the SVZ, we aimed to develop a tool that allows rapid expression analysis along the full rostro-caudal and dorso-ventral extend of this germinal region. “FlashMap” is a software for semi-automatic protein expression measurements in the SVZ in the fastest possible way, based on OD measurements. “FlashMap” allows subsampling of serial sections, in order to further reduce the time for analysis. Data are exported as heatmaps that can be superimposed onto volumetric reconstructions of the lateral ventricle for optimal and intuitive visualization. “FlashMap” has the potential to be applied to a wide range of semi-automated analyses. The software is therefore of substantial interest for the field.

2.3. Experimental Procedures

2.3.1. Animals and Ethics

All animal experimentation procedures were performed according to European requirements 2010/63/UE and have been approved by the Animal Care and Use Committee CELYNE (APAFIS #187 & 188). OF1 mice (Charles River, France; n=3 for all markers) were sacrificed at postnatal day 10 (P10) by an intraperitoneal overdose of pentobarbital followed by transcardial perfusion with Ringer Lactate solution and 4% paraformaldehyde (PFA) dissolved in 0.1 M phosphate buffer (PB; pH 7.4). Tissues were postfixed for 48 hrs in 4% PFA at 4° C.

2.3.2. Tissue Processing and Immunohistochemistry

Brains (**Figure 1A**) were cut into 50 µm thick sections using a vibratome (VT1000 S; Leica; Wetzlar; Germany) and LV containing sections were serially collected in series of 6. When necessary, antigen retrieval was performed by incubating sections for 20 minutes in citrate buffer (pH 6) at 80° C, cooling for 20 minutes at room temperature, followed by extensive washings in 0.1 M PB. Blocking was performed for 2 hrs in TNB buffer (0.05% Casein; 0.25% Bovine Serum Albumin; 0.25% TopBlock in 0.1 M PB) with 0.4% triton-X (TNB-Tx). Incubation with primary antibodies in TNB-Tx was done overnight at 4° C. The following primary antibodies were used: Rabbit anti-Ki67 (1:500; MM France Microm Microtech; RM-9106-S1); Rabbit anti-Tbr2 (1:1000; Abcam; ab23345); Guinea pig anti-Dlx2 (1:5000; kind gift of Kazuaki Yoshikawa; Kuwajima et al., 2006); Rabbit anti-Hopx (1:400; Santa Cruz; sc-30216); Goat anti-DCX (1:500; Santa Cruz; sc8066). Sections were extensively washed in 0.1 M PB with 0.4% triton-X (PB-Tx) and incubated for 2 hrs at room temperature with suitable secondary antibodies (Alexafluor 488, 555 or 647; 1:500; Life Technologies). After washing (0.1 M PB) sections were counterstained with Dapi (1:500; Life Technologies; D1306) for 30 minutes for optimal detection of SVZ borders by "FlashMap". Ki67 staining was performed on a complete series of sections, while a subsampling of 1/3 was used for Tbr2, Dlx2, Hopx and DCX stainings, as well as for generating the 3D brain and ventricular system models.

2.3.3. Image Acquisition and 3D Reconstruction

Acquisition of images was performed with a Leica DM5500 epifluorescent microscope (Leica Microsystems GmbH, Wetzlar, Germany). Whole brain mosaics were acquired at 4x (HC PL FLUOTAR; N.A. 0.13) for representative overview pictures and 3D reconstruction, at 10x (HCX PL FLUOTAR; N.A. 0.30) for OD analysis and assembled using the LAS X software (Leica Microsystems GmbH, Wetzlar, Germany). For accurate OD analysis, settings were carefully chosen to avoid signal saturation and were maintained throughout the acquisition. Image mosaics were exported in TIFF format (.tif) for further analysis.

A Dapi series of 1/3 sections was used for generating the 3D brain and ventricular system models. Acquired mosaics were orientated using Photoshop (CS4). Contours of the brain and the ventricular system were drawn on individual sections (series of 1/3) using Neurolucida 360

(MBF Bioscience) to generate a 3D mesh. Meshes were saved in "obj" format and exported to the open-source 3D computer graphics software Blender (www.blender.org) for further editing. For optimal superimposition of 2D heatmaps onto the 3D ventricular system model, the three SVZ walls (medial, dorsal, lateral) were defined for UV unwrapping. Individual heatmaps were then superimposed to the corresponding 2D UV projection to generate accurate 3D representations (see **Figure 2** for the workflow of the experimental design).

2.3.4. Software Generation and Analysis

"FlashMap" was coded using the commercial coding software MATLAB (R2017a; The MathWorks) and a stand-alone version was generated to facilitate distribution and use by other researchers. Description of the workflow for a complete "FlashMap" analysis is described in the current manuscript (see **Figure 3** for a step by step walkthrough of the software).

2.4. Results

2.4.1. The Subventricular Zone is a Poorly Defined Region of the Postnatal Forebrain

The SVZ of the mouse brain is a highly complex and irregular structure, well known for its persisting germinal activity after birth (Smart, 1961; Lois and Alvarez-Buylla, 1993; Doetsch et al., 1997). It surrounds the lateral ventricles, which extend at P10 approximately 2.5 mm along the rostro-caudal axis. The SVZ is defined by its dense cellular organization compared to the surrounding tissue, i.e. striatum; corpus callosum, that respectively line its lateral, dorsal and medial aspects (**Figures 1A to 1B**).

We first aimed at defining the SVZ from its rostral most aspect corresponding to the appearance of the LV (coordinate 0 in **Figure 1C**) to its more caudal aspect. Classically, the SVZ is subdivided into 3 microdomains (lateral, dorsal, medial) according to their location around the LV. While these 3 microdomains are well defined in the rostral most SVZ regions, their definition becomes more ambiguous in regions caudal to the 3rd ventricle. This applies particularly to the dSVZ which is not present in caudal sections. There, only the lateral and

medial walls were identified based on a dense Dapi counterstaining (**Figure 1D**), as well as the presence of numerous Ki67^{+} cells (see below). It is noticeable that the density of cells (detectable by Dapi) declines from rostral to caudal sections. This is particularly apparent in the more caudal sections, where the ventricular walls develop into a thicker cell layer of lower cell density (**Figure 1B**). Those caudal sections were however included in our analysis in order to directly assess the presence of proliferative and/or progenitor markers (see below).

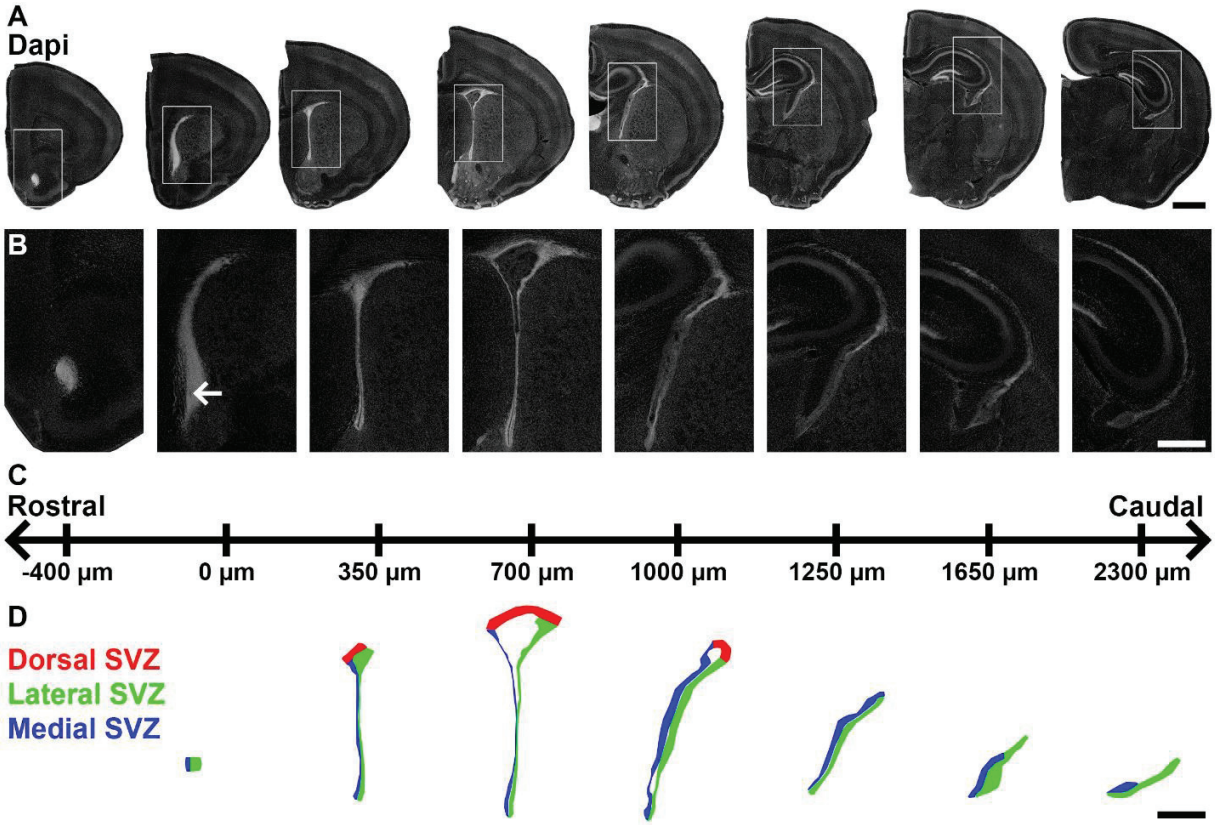

Figure 1. Definition of SVZ microdomains.
(A): Representative mosaics of P10 coronal sections counterstained with Dapi at various rostro-caudal coordinates (indicated in C).
(B): Higher magnification micrographs showing the rostro-caudal extension of the open lateral ventricle from its first rostral appearance (arrow) to its more caudal coordinates.
(C): Coordinates used in this study. The coordinate "0" is defined as the first appearance of the opened lateral ventricle.
(D): Schematic representation of the opened lateral ventricle at various rostro-caudal coordinates. The dorsal (red), lateral (green) and medial (blue) microdomains are indicated.
Scale bars: (A) = 1 mm; (B+C) = 500 µm. Abbreviations: SVZ, subventricular zone; LV, lateral ventricle.

2.4.2. "FlashMap" Allows Rapid Investigation of Gene Expression along the Full Extent of the SVZ

We developed "FlashMap" to perform a rapid analysis of marker expression in the SVZ along its full rostro-caudal as well as dorso-ventral extents. "FlashMap" allows the generation of 2D heatmaps of relative OD in the least time and tissue-consuming way. The workflow of "FlashMap" is illustrated in **Figure 2** and a more detailed, step by step description given in **Figure 3**. Brains of the species and age of interest (here, mouse and P10) are sectioned and collected in series. For 3D analysis of gene and protein expression in the SVZ, coronal sections are preferred. Sections are immunostained for markers of interest (**Figures 2A and 2B**). To reduce time and tissue consumption, series may be subsampled. The subsampling factor will depend on the abundance of the marker of interest, as well as of its distribution. Abundant markers showing a "widespread distribution" will allow higher frequency subsampling, as illustrated below. After definition of the region of interest (ROI; here lSVZ in green; **Figure 2D**), "FlashMap" defines automatically the thickness of the SVZ based on the OD of the Dapi counterstaining (as described later in more detail). The software automatically distributes probes of a defined width and adapt their height (thickness of the SVZ at the corresponding position). The OD of the markers of interest is then measured within each probe (**Figure 2D**). These ODs are then represented in a color code of relative OD (from 0 (0 OD = blue) to 1 (highest value = red)). A 2D heatmap is generated, which represents the marker distribution along the region of interest. Analysis of multiple sections allows representing the full rostro-caudal extend of the region of interest (**Figure 2F**). For 3D representation, the contours of a series of sections (**Figure 2C**) are used to generate a 3D mesh of the LV (**Figure 2E**) using Neurolucida 360 (MBF Bioscience). 2D heatmaps are then superimposed onto these 3D volumes by using the open access software Blender (www.blender.org; **Figure 2G**).

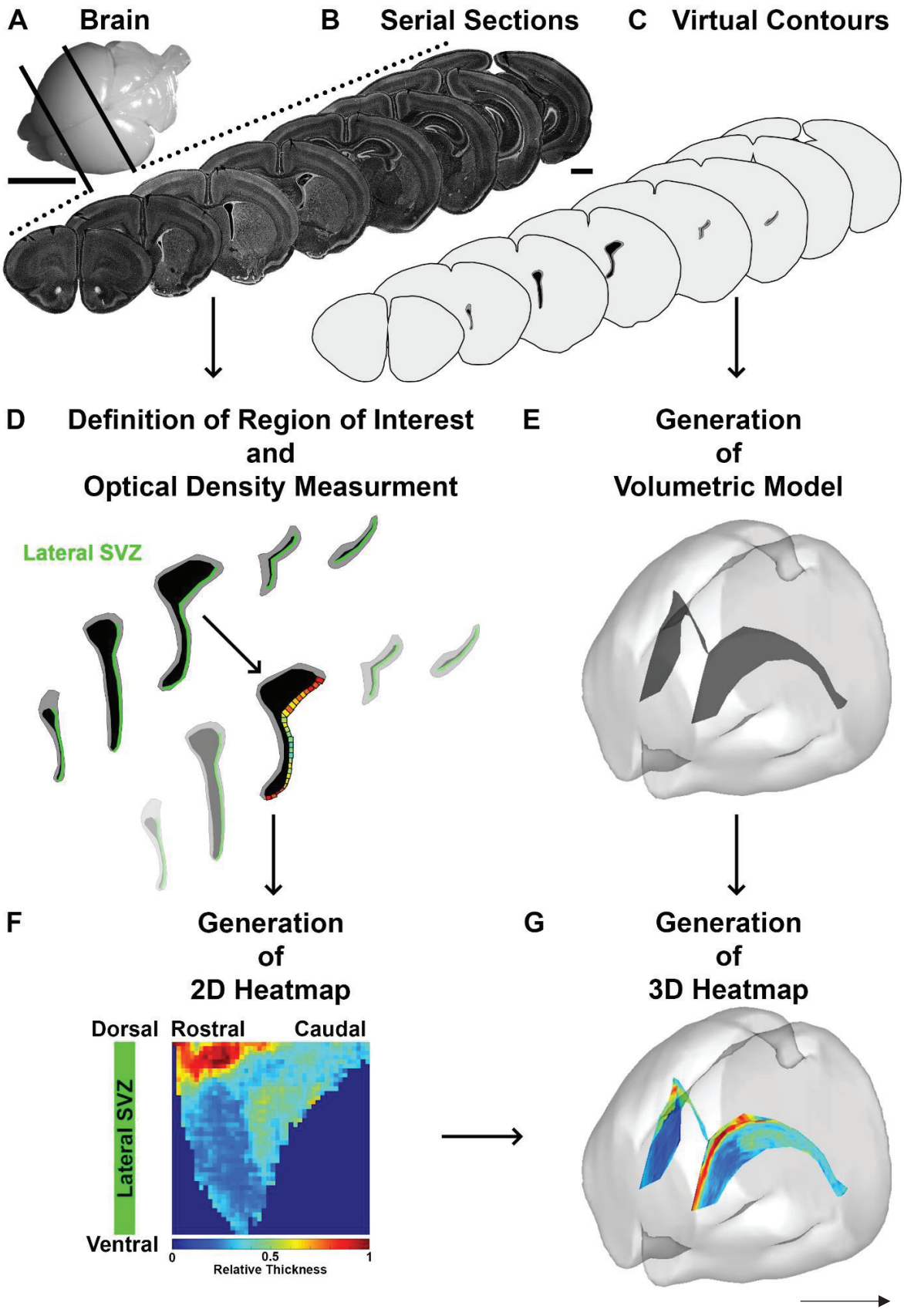
A Brain
B Serial Sections
C Virtual Contours
D Definition of Region of Interest and Optical Density Measurment
E Generation of Volumetric Model
Lateral SVZ
F Generation of 2D Heatmap
G Generation of 3D Heatmap
Dorsal
Rostral
Caudal
Lateral SVZ
Ventral
0
0.5
1
Relative Thickness

Figure 2. Schematic illustration of the workflow for sampling and analysis of the SVZ.
(A): Picture of a P10 mouse brain prior to cutting.
(B): Representative micrographs show a subsampled series of counterstained brain sections (Dapi) covering the full rostro-caudal extent of the LV. Sections are collected/subsampled in series according to the experimental question (here an example of series of 1 out of 12).
(C+E): Schematic illustration of virtual contours of serial brain sections (C), which are used for generation of 3D reconstructions of the brain (bright gray) and ventricular system (black) (E). In the virtual contours the thickness of the SVZ is represented in dark gray (C).
(D): Schematic illustration of the definition of the region of interest (here lSVZ in green) and the automatic calculation of the thickness of the SVZ and measurement and color coding of the OD of the investigated marker. The region of interest is subsampled into probes of a defined size.
(F): The software generates automatically 2D heatmaps of the region of interest (here lSVZ) along the rostro-caudal axis of the marker of interest (here thickness of the SVZ). The values of the thickness are represented by a color code of the relative thickness (0 to 1).
(G): Heatmaps can be presented in 3D, by superimposing them onto a 3D reconstruction of the ventricular system.
Scale bars: (A) = 5 mm; (B+C) = 1 mm. Abbreviations: SVZ, subventricular zone; 2D, two-dimensional; 3D, three-dimensional; OD, optical density.

2.4.3. Step by Step Walkthrough for an Optimal Use of "FlashMap"

After installing the software, a shortcut to "FlashMap" should be placed on the desktop (**Figure 3A1**), as well as all the images which will be analyzed. After starting "FlashMap", a window appears to define the settings of the analysis to be performed. For illustrative purposes, we chose to analyze one microdomain in one section (number of sections: 1; frequency of sections: 1). The thickness of the sections (here 50 µm) and the µm/pixel ratio also need to be given (here 0.64 µm/pixel; **Figure 3A2**). Thereafter, images are loaded by selecting the "Load" button (**Figure 3A3**). The dimension of the probes (width) can be chosen, as well as the hemisphere (left; right) and the ROI (medial; lateral; dorsal) to be analyzed (here 50 µm; right; lateral; **Figure 3B**). The beginning and end of the ROI are defined by accepting the invitation and right clicking on the image at the appropriate position (1 and 2, 3 and 4, respectively in **Figure 3C**). A left click allows zooming into the image for better accuracy. The internal side of the ROI is traced for automatic positioning of the probes (**Figure 3D**). A "reference region" is placed within the parenchyma, immediately adjacent to the SVZ (here in the striatum, **Figure 3E**), to enable "FlashMap" to automatically calculate the height of the probes. In order to define the optimal height of the probes, the Jensen-Shannon divergence (JS_{div}; Lin, 1991) was used to accurately define the drop in OD between the SVZ and adjacent tissue (gray values in

the “probe region” (*P*) and “reference region” (*R*); **Figures 3F1 and 3F2**). In the JS_{div} the normalized values P_i and R_i represent the intensity versus the frequency of gray values in the “probe region” and the “reference region” for the height N_i and JS_{div} measures the dissimilarity between the gray value distribution between them (**Figures 3F2 and 3F3**):

$$JS_{div} = \frac{1}{2}\sum_i P_i[\log(P_i) - \log(M_i)] + \frac{1}{2}\sum_i R_i[\log(R_i) - \log(M_i)]$$

$$\text{With } M = \frac{1}{2}(P + R)$$

N_0 and N_{max} are empirically fixed values and “FlashMap” automatically estimates the optimal height (N_{opt}) for every single probe. N_{opt} is defined as the height at which the JS_{div} value continuously drops as the gray value distributions of P_i and R_i become identical. Importantly, the estimation of N_{opt} starts at N_0 larger than the real apical end of the probe (0 pixel) at 30 pixels, as JS_{div} exhibits spurious variations for very small values (**Figures 3F4 and 3F5**). We further tested if the calculated height of the probes differ by selection of divergent “reference regions”. While the values JS_{div} were slightly different for divergent “reference regions”, the calculated positions N_i for N_{opt} turned out to be very consistent. Thus, a precise positioning of the “reference region” is not necessary, as it does not affect optimal detection of the SVZ thickness (**Figure S1**). Importantly, errors in estimations of probe heights can be corrected manually. First, the probe is selected by right-clicking close to its apical end. The new height is chosen by right-clicking at the right position in basal direction (**Figure 3G**). The analysis is finished by declining the invitation to analyze other SVZ walls (1) and other images (2). Measurements can then be exported as raw values in Excel files and/or as heatmaps (3). It is strongly recommended to always export raw values for accurate interpretation of heatmaps (**Figure 3H**). Indeed, heatmaps provide a spatial representation of marker expression, but does not give information on their level of expression (e.g. amplitude between high and low expression values). Heatmaps are exported in TIFF format by manually adding the “.tif” extension to the file name. The heatmaps we produced in this illustration are orientated with the dorsal end of the lSVZ at the top and the ventral end at the bottom (1). Here the thickness of the lSVZ is represented (2), as well as the density of cells along the lSVZ, based on OD measurements of Dapi (3). The heatmaps represent the relative thickness/OD, which are color

coded (here “jet”) from 0 (blue) to the maximal measured OD value (normalized to 1; red). Different options for color coding of OD values are available in “FlashMap” and can be chosen prior to the heatmap export (**Figure 3I**).

A similar procedure will be used to analyze multiple sections. The total number of sections is defined at the start (**step A2**), before loading the first image (here corresponding to 43 sections). Subsampling of the series could be done, as described below, and the degree of subsampling needs to be defined in the same window (“frequency of sections”; here 1; **Figure 3J**). The full SVZ of the series can be analyzed as illustrated in (**Figure 3K**). Multiple LV walls can be sampled on the same series of images by choosing “continue with another wall” (**Figure 3H1**). After defining all walls in a section, the option “continue on another image” is clicked (**Figure 3H2**), to load the next image. After analysis of all the sections the heatmaps can be generated as described previously (**Figure 3H3**). This results in complete heatmaps (here thickness and cellular density of the 3 walls of the SVZ; **Figure 3L**).

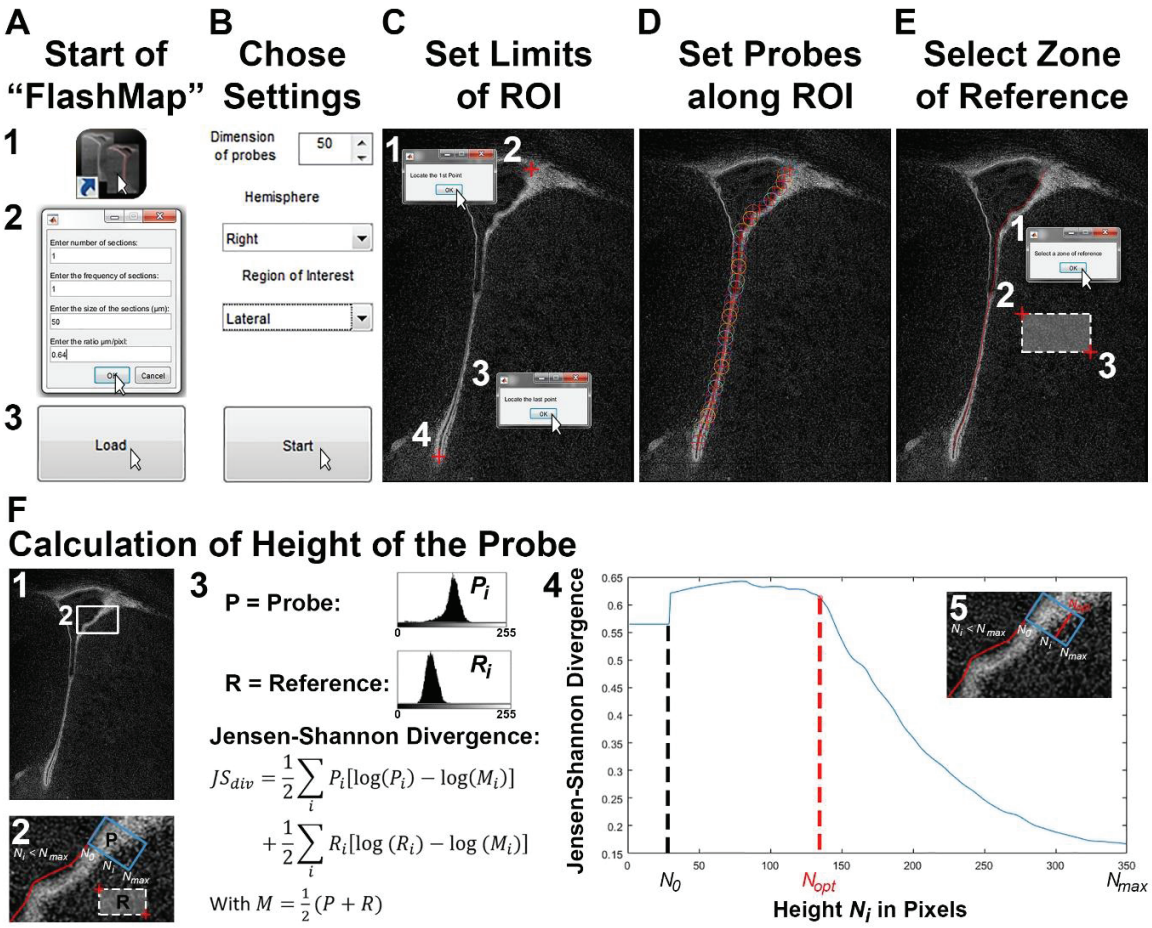
A
Start of "FlashMap"
B
Chose Settings
C
Set Limits of ROI
D
Set Probes along ROI
E
Select Zone of Reference
1
2
3
Enter number of sections:
Enter the frequency of sections:
Enter the size of the sections (µm):
Enter the ratio µm/pixl:
OK
Cancel
Load
Dimension of probes
50
Hemisphere
Right
Region of Interest
Lateral
Start
4
Locate the 1st Point
Locate the last point
Select a zone of reference
F
Calculation of Height of the Probe
P = Probe:
R = Reference:
Jensen-Shannon Divergence:
$JS_{div} = \frac{1}{2}\sum_i P_i[\log(P_i) - \log(M_i)]$
$+ \frac{1}{2}\sum_i R_i[\log(R_i) - \log(M_i)]$
With $M = \frac{1}{2}(P + R)$
Jensen-Shannon Divergence
Height N_i in Pixels
N_0
N_{opt}
N_{max}
G
Adjust Probes
H
Finish Analysis
I
Export Heatmaps
Would you like to adjust the samples ?
Would you like to continue on another image ?
Would you like to continue on another wall ?
Collect datas
What do you want to do with datas ?
Export to Excel
Create heatmaps
Both
Dorsal
Ventral
Lateral SVZ
Relative Thickness
Relative Optical Density
J
Full Analysis
K
Complete Series
L
Export Heatmaps
Thickness
Dapi OD
Medial
Dorsal
Lateral
Relative Thickness / Optical Density

Figure 3. Detailed "FlashMap" walkthrough.
(A): Start "FlashMap" and load images (1-3). For illustration, we chose to analyze a single microdomain in a single section. Define the thickness of the sections and the µm/pixels ratio (2).
(B): Define the dimension of the probes (in µm), the hemisphere (left; right) and the ROI (medial; dorsal; lateral), here: 50 µm; right; lateral.
(C): Define ROI by placing a "starting point" (1, 2) and an "end point" (3, 4).
(D): Draw the internal face of the ROI for automatic distribution of probes.
(E): Define a reference area in the adjacent tissue (here striatum) by selecting two points in that region (1-3).
(F): "FlashMap" calculates the height of the probes automatically using the Jensen-Shannon divergence (JS_{div}) to estimate the optimal basal height of the probe (N_{opt}) between N_0 and N_{max}.
(G): Probes can be adjusted manually.
(H): Complete the analysis by declining the offer to define another ROI (1) and another section (2). Export values (Excel file) and/or heatmaps in TIFF format (3).
(I): Heatmaps of the (single section) lSVZ analysis are orientated with its dorsal end at the top and ventral end at the bottom (1). Heatmaps of the SVZ thickness and cellular density (here Dapi) are color coded (here Jet-code) with a scale of relative height and OD, respectively (2, 3).
(J+K): Illustration of an analysis with a complete series of sections. The number of sections to be analyzed is defined at the start (step A2). Analysis of multiple walls is achieved by clicking "continue with another wall" (H1). Analysis of multiple sections is achieved by clicking "continue on another image" (H2) until the series is complete (K).
(L): Full heatmaps are gained as described in (H3) with the same scale bars as described in (I). Orientation of full heatmaps is described in **Figure 4B**.
Abbreviations: ROI, region of interest; JS_{div}, Jensen-Shannon divergence; SVZ, subventricular zone; OD, optical density.

2.4.4. "FlashMapping" of the Full SVZ Highlights Regions of Maximal Germinal Activity

To test "FlashMap", we first aimed at sampling the full extent of the SVZ for regions of maximal germinal activity. The thickness and cellular density, as well as the distribution of proliferative cells were mapped throughout the rostro-caudal extend of the three SVZ walls (**Figure 4A**). As a marker of proliferation, we chose Ki67, a marker of actively cycling cells (Gerdes et al., 1984) .

For optimal heatmap orientation, we virtually opened the LV at its ventral tip along the full rostro-caudal extent, in order to "unfold" the ventricle and represent the medial, dorsal and lateral walls on top of each other (**Figure 4B**). We first generated heatmaps for the relative thickness and cellular density throughout the SVZ, based on the Dapi counterstaining (**Figures**

4C and 4D). Analysis revealed the existence of a "hotspot" at the junction between the lSVZ and the dSVZ. This region corresponds to the accumulation of neuroblasts before they engage into rostral migration through the RMS. In this region, the increased SVZ thickness correlates with an increased cell density (**Figures 4C and 4D; gray dashed boxes**). Heatmaps also reveal a gradual increase in SVZ thickness in more caudal regions of both the lSVZ and medial SVZ (mSVZ). Interestingly, this increase was however correlated with a decrease in cell density, suggesting a gradual cell dispersion in these more caudal regions, which may correlate with a loss of germinal activity. We then generated a heatmap for the density of proliferative cells (i.e. $Ki67^+$ cells; **Figure 4E**). The highest germinal activity was detected in a "banana shaped area" along the rostro-caudal extent of the lSVZ, as well as in the most ventral and rostral regions of the mSVZ. Interestingly, comparison of the thickness of the walls and density of $Ki67^+$ cells revealed that the regions with highest germinal activity also appear to be the thinnest (**Figures 4C and 4E; white dashed boxes**). In contrast, regions of lowest germinal activity were thicker and presented a low cellular density (**Figures 4C and 4E; black dashed boxes**). For a more intuitive representation, heatmaps were superimposed on 3D templates of the LVs (**Figures 4F and 4H**).

Figure 4. FlashMap reveals major differences in SVZ thickness, cellular density and germinal activity throughout the SVZ.
(A): Representative micrographs of the proliferation marker Ki67 (green) at distinct rostro-caudal coordinates of the SVZ (Dapi, blue).
(B): Schematic representation of the orientation of sections and heatmaps. The LV is cut open (scissors) at its most ventral tip between the mSVZ (blue) and the lSVZ (green). This allows unfolding the three SVZ walls for 2D heatmap representations (see C-E).
(C-E): Heatmaps of the relative thickness of the SVZ (C) and of relative ODs of Dapi (D) and $Ki67^+$ cells (E) along the full rostro-caudal extent of the LV. White dashed boxes underline regions of maximal germinal activity, while black dashed boxes underline regions of minimal germinal activity. Note the differences existing between these regions in term of SVZ thickness and cellular density. The location of the RMS is highlighted with a gray dashed box. The heatmap color code goes from 0 (blue) to maximal detected thickness/OD 1 (red).
(F-H): Representations of 3D heatmaps of relative thickness (F) and relative ODs of Dapi (G) and $Ki67^+$ cells (H). Scale bars: (A+E) = 500 µm. Abbreviations: SVZ, subventricular zone; lSVZ, lateral subventricular zone; dSVZ, dorsal subventricular zone; mSVZ, medial subventricular zone; LV, lateral ventricle; DM corner, dorso-medial corner; DL corner, dorso-lateral corner. ⟶

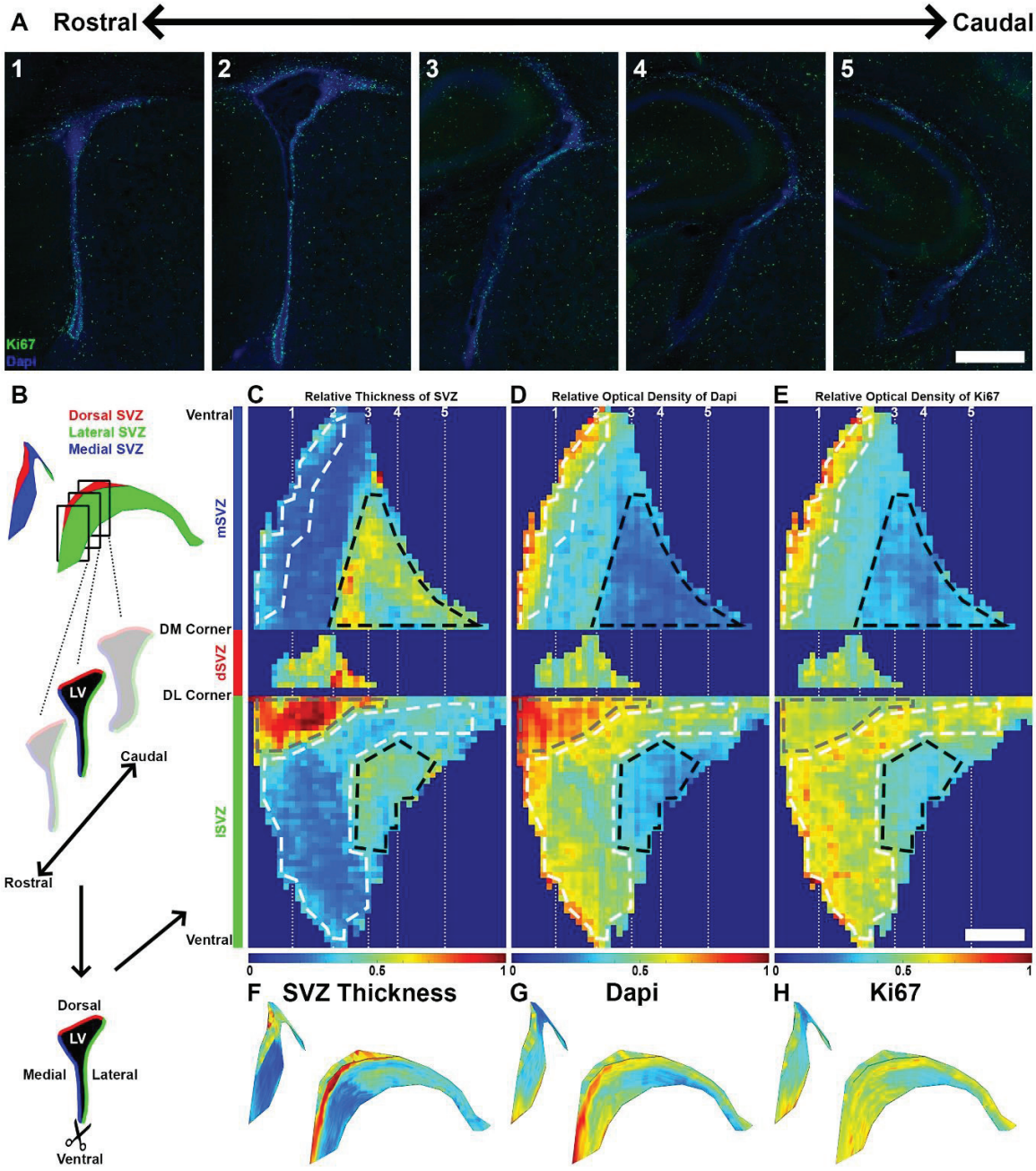
A
Rostral
Caudal
1
2
3
4
5
Ki67
Dapi
B
Dorsal SVZ
Lateral SVZ
Medial SVZ
Ventral
mSVZ
DM Corner
dSVZ
DL Corner
lSVZ
LV
Caudal
Rostral
Ventral
Dorsal
LV
Medial
Lateral
Ventral
C
Relative Thickness of SVZ
D
Relative Optical Density of Dapi
E
Relative Optical Density of Ki67
1
2
3
4
5
0
0.5
1
F
SVZ Thickness
G
Dapi
H
Ki67

2.4.5. Subsampling of the Region of Interest Results in a Minimal Loss of Spatial Information

In order to reduce time and the amount of tissue required to perform an analysis, we equipped "FlashMap" with the ability to process subsampled series of sections (1 section out of "n"). The applied calculations for interpolating missing values, follows the concept of linear interpolation. Values between two analyzed sections (X; Y) were calculated by using the following formula (**Figure 5A**):

$$v_n = \left(1 - \frac{n}{N}\right) * v_x + \frac{n}{N} * v_y$$

N stands for the degree of subsampling and *n* for the intersection number between section X at the rostral and Y at the caudal end:

$$N = degree\ of\ subsampling$$

$$n = \{1, 2, \dots, N-2, N-1\}$$

The smoothening of the values interpolation is applied row by row. First, "base values" (v_x; v_y) of the two adjacent sections are calculated for every row. This is achieved by averaging the real values (*X''*; *Y''*) with its neighbors (*X'*, *X'''*; *Y'*, *Y'''*) for every row and section separately:

$$v_x = \frac{X' + X'' + X'''}{3}$$

$$v_y = \frac{Y' + Y'' + Y'''}{3}$$

For probes located at the border of the ROI, a single adjacent measured value was available and therefore used:

$$v_x = \frac{X' \text{ or } X''' + X''}{2}$$

$$v_y = \frac{Y' \text{ or } Y''' + Y''}{2}$$

All the necessary steps of a full interpolation of the SVZ thickness in the lSVZ are illustrated in **Figures 5B to 5E**. For illustrative purposes, we generated a complete heatmap (**Figure 5B**) and one by analyzing every 5th section (**Figure 5C**). We then interpolated missing values in

two steps. For the first step, the "intersection-interpolation", the general formula is used as described above with:

$$N = 5$$

$$n = \{1, 2, 3, 4\}$$

Its integration into the general formula reads as follow:

$$v_{1,2,3,4} = \left(1 - \frac{n_{1,2,3,4}}{5}\right) * v_x + \frac{n_{1,2,3,4}}{5} * v_y$$

Weighting of the influence of adjacent sections in the series to calculate values for the four missing sections (v_1, v_2, v_3, v_4) reads as follow:

$$v_1 = 0.8 * v_x + 0.2 * v_y$$

$$v_2 = 0.6 * v_x + 0.4 * v_y$$

$$v_3 = 0.4 * v_x + 0.6 * v_y$$

$$v_4 = 0.2 * v_x + 0.8 * v_y$$

Comparison of the heatmaps generated following analysis of a complete series of sections or a subsampling of 1/5 (**compare Figures 5B and 5D**) highlight the accuracy of the "intersection-interpolation". A second step of "intrasection-interpolation" allows a further refinement of the heatmap (**Figure 5E**), while preserving the accuracy of the mapping.

Figure 5. Interpolation of heatmaps after subsampling by 5.
(A): Formula for intersection-interpolation.
(B): Heatmap representing the thickness of the lateral wall in a complete series of sections.
(C-E): Heatmaps representing values obtained for a subsampling of 1/5, without interpolation (C), following intersection-interpolation (D) and intrasection-interpolation (E). Formula are presented on the left, as well as a cropping of a region of reference for all heatmaps.
Scale bar: (B) = color coded relative thickness; (E) = 500 µm. ⟶

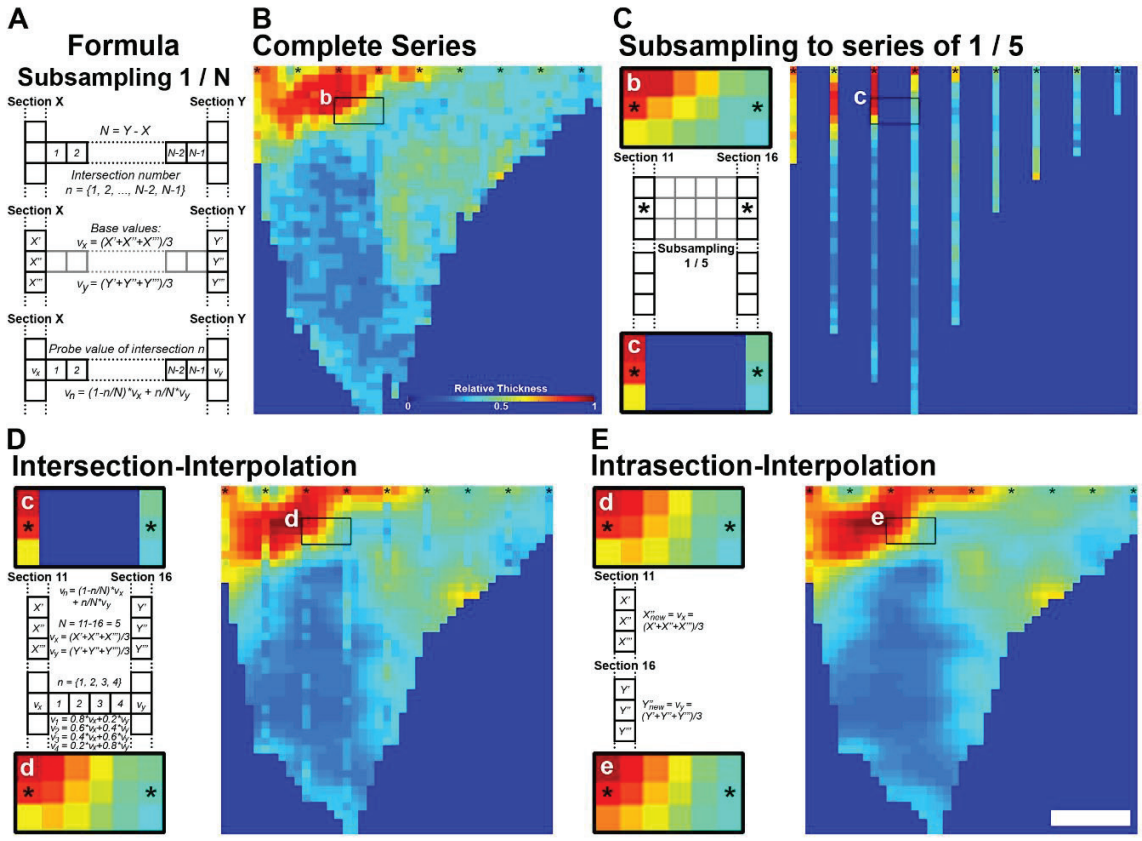

Next, we systematically assessed the maximal degree of subsampling allowing to produce a heatmap that accurate reflects the mapping obtained with a complete series of sections. We repeated all analysis with sub-samplings ranging from 1/2 to 1/6. Interestingly, all previously described regions (germinal regions, non-germinal regions, RMS; **Figures 4C to 4E**) could be identified in all heatmaps, regardless of the degree of subsampling or the section number with which the analyses were started (**Figures S2 to S4**).

2.4.6. "FlashMap" Allows a Rapid Analysis of SVZ Transcriptional Heterogeneity

Next, we used "FlashMap" to generate full heatmaps of selected markers known to be heterogeneous distributed. First, we choose the GABAergic and glutamatergic progenitor markers Dlx2 and Tbr2 (**Figure 6A**). Those two transcription factors show a preferential expression in the lSVZ and the dSVZ, respectively (Brill et al., 2008; Brill et al., 2009; Azim

et al., 2012a). Further, we analyzed the expression pattern of Hopx and DCX. Hopx is a heterogeneously distributed transcriptional regulator, which recently gains increasing attention as a marker for outer radial glia cells in humans (Pollen et al., 2015 ; Thomsen et al., 2016) and DCX, a marker for migrating neuroblasts, which is also described to be heterogeneously expressed in the SVZ (Yang et al., 2004) (**Figure 6B**).

Remarkably, Dlx2 was found in the lSVZ and the mSVZ in the regions we identified previously as zones of high germinal activity **(Figures 4C to 4E; white dashed boxes)**. Highest Dlx2 expression was detected in the rostral parts of the lSVZ, as well as in the dorsal aspect of the lSVZ corresponding to the emerging RMS. Further, the ventral tip of the mSVZ showed also some enrichment in rostral sections. In contrast, Dlx2 was consistently absent from the dSVZ and more caudal regions of the lSVZ and mSVZ (**Figures 6C and 6G**). This expression pattern contrasts to the one obtained for Tbr2, which showed an exclusive expression in the dSVZ and was consistently absent from the lSVZ and mSVZ (**Figures 6D and 6H**). Those findings are in line with previous reports (Brill et al., 2008; Brill et al., 2009; Azim et al., 2012a) and further validate "FlashMap" as an rapid but accurate mapping method.

"FlashMap" revealed a strikingly different pattern for Hopx expression. Hopx was found to be high in the dSVZ and in the caudal regions of the mSVZ. Some level of expression could also be detected in the caudal regions of the lSVZ, where only few $Ki67^{+}$ cells are observed (**Figures 6E and 6I**). It is noticeable that this pattern of expression is the opposite of the one obtained for DCX. As revealed by the "FlashMap" analysis, this migrating neuroblast marker is enriched in the dorsal part of the lSVZ, where the RMS is located. A second smaller hotspot was also observed in the ventral parts of the lSVZ in rostral sections (**Figures 6F and 6J**).

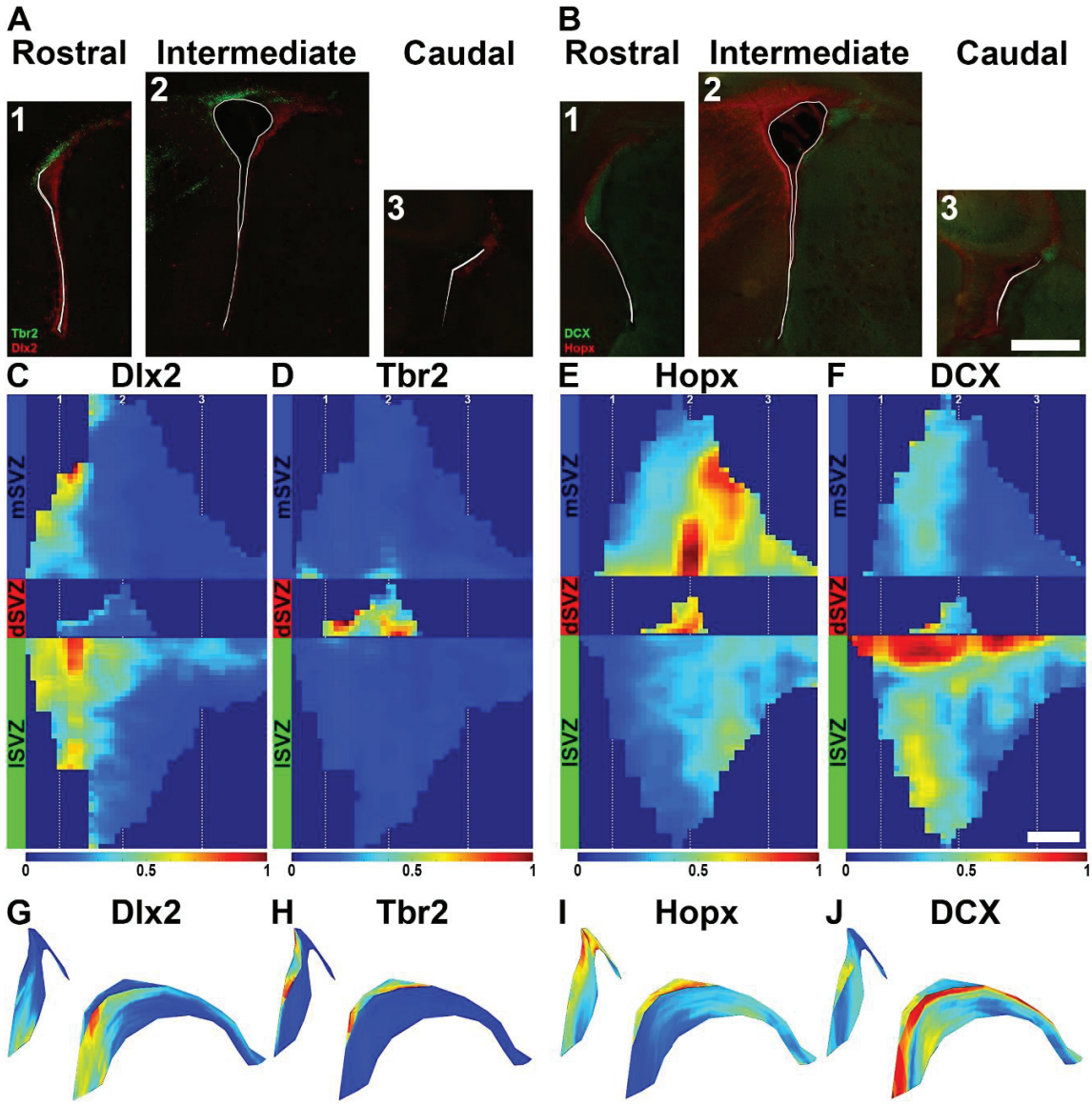

Figure 6. Illustration of "FlashMap" analysis with four regionally expressed markers.
(A+B): Representative micrographs of Dlx2, Tbr2 (A), Hopx and DCX (B) at a rostral (A1+B1), intermediate (A2+B2) and caudal level (A3+B3) along the rostro-caudal axis of the ventricular system.
(C-F): Expression heatmaps obtained for Dlx2 (C), Tbr2 (D), Hopx (E) and DCX (F) along the full extent of the SVZ are represented in a color code of relative OD.
(G-J): 2D heatmaps of Dlx2 (G), Tbr2 (H), Hopx (I) and DCX (J) are superimposed in 3D LVs.
Scale bars: (B3+F) = 500 µm; Abbreviations: lSVZ, lateral subventricular zone; dSVZ, dorsal subventricular zone; mSVZ, medial subventricular zone.

2.5. Discussion

Our results demonstrate, that "FlashMap" is a useful method to keep pace with the increasing amount of transcriptional datasets that reveal a regional marker expression in postnatal germinal regions of the forebrain (Azim et al., 2015). This semi-automatic mapping approach, allows a rapid screening of selected markers along both the rostro-caudal and dorso-ventral coordinates of the postnatal SVZ.

The SVZ is an ill-defined region of the postnatal mouse forebrain. The SVZ is particularly thin and tortious, and our study further demonstrates that the cellular density greatly varies along its dorso-ventral and rostro-caudal dimensions. To perform this study, we first defined the dorsal, lateral and medial walls of the opened lateral ventricle along its full rostro-caudal coordinates. A more accurate subdivision of the three walls may be achieved by using tissues from transgenic mice expressing permanent markers in various brain regions (pallium, ganglionic eminences, septum; Young et al., 2007). Although the approach used in the current study is more arbitrary, it allowed detecting significant differences in the thickness, cell density and proliferation occurring in different regions of the postnatal SVZ. Our results confirm previous results obtained for the distribution of proliferating cells ($Ki67^{+}$) in the lSVZ (Falcão et al., 2012), and refine them significantly by providing a more complete and precise map. Concerning the rostro-caudal distribution of proliferative cells they found the same rostral enrichment like we did here, as well as in an earlier study in 10 to 12 weeks old mice (Azim et al., 2012a). In addition, we found a low germinal activity in the dorsal part of the lSVZ, where the RMS is located. We also provide a more detailed mapping of the density of proliferative cells in more caudal regions, where a large region of low germinal activity is clearly visible. The differences existing between our maps and those generated by Falcao et al., may be at least partially explained by differences in species (mice vs. rats) and age of the animals (P10 vs. P70). A systematic mapping at different ages using "FlashMap" would be of interest to better describe potential spatial changes in germinal activity that occur over a lifetime. Such an analysis could also include embryonic time points to investigate in more details the spatial and temporal aspects of astrogenesis and oligodendrogenesis (reviewed by Reemst et al., 2016). This would be particularly interesting for oligodendrogenesis, as it occurs in different waves originating from different regions of the VZ and SVZ (Kessaris et al., 2006).

Interestingly, the regions of "lowest germinal activity" highlighted by "FlashMap" in the SVZ microdomains shared some key characteristics: i.e. a thick wall with a low cell density. These observations highlight the importance of the cellular microenvironment in the persistence of a germinal activity. This is in agreement with previous studies demonstrating the importance of a highly organized cellular niche (also named neurogenic niche) in the maintenance of both proliferation and neurogenesis (e.g. Ponti et al., 2010). Further, we demonstrated that the contribution of the ventral most part of the mSVZ might be underestimated in its participation to the germinal activity observed in the postnatal SVZ. While progenies from the dorsal proliferating cells most likely migrate through the RMS into the OB, some progenies of the ventral population of the lSVZ and mSVZ might migrate away in a more ventrally located stream as suggested elsewhere (Yang et al., 2004). This ventral migration might be a premise of the ventrally located RMS observed in primates, which we highlighted in an earlier study in common marmosets (Azim et al., 2013).

In the last part of our study we confirmed the value and reliability of "FlashMap", by analyzing markers known to be regionally expressed, i.e. the transcription factors Dlx2 and Tbr2. The produced heatmaps reflect accurately the prior description of their distribution (Brill et al., 2008; Brill et al., 2009; Azim et al., 2012a). In addition, comparison of Hopx and DCX highlights the existence of two domains: one presenting a high germinal activity in which neuroblasts are numerous, one presenting a low level of germinal activity that are devoid of neuroblasts. It would be interesting to investigate if the $Hopx^{+}$ regions preferentially give rise to non-neuronal cell types. This was the subject of the second project of my PhD.

Several aspects of "FlashMap" have been optimized to make it both user friendly, accurate and rapid. First, we used the Jensen-Shannon divergence (JS_{div}) to automatically adapt the probe to the height of the SVZ. JS_{div} has been extensively used for multiple types of image processing and analysis, such as the analysis of edge detection (Gómez-Lopera et al., 2000), the characterization of the compositional complexity (Rigau et al., 2005), the tracking of moving root sections in a stack for tracing out the 3D root architecture (Mairhofer et al., 2012) and others. Second, we performed extensive subsampling testing to demonstrate that accurate maps can be obtained with an incomplete (but homogeneous) series of sections. This allows a reduction of both the time and tissue required to generate an expression heatmap. A series of one section out of five reduces the time required for performing the staining, mounting and

imaging to 20%. In other words, subsampling allows the parallel analysis of several markers in approximately the same time than required for a single marker in a full series. Other future improvement might be applied. For example, “FlashMap” could facilitate the analysis of tissue organization, proliferation, and apoptosis in various physiological and pathological conditions. It could also be applied to other brain regions (germinal or non-germinal). For example, it could be used to measure cortical thickness in microcephaly or following hypoxia. For such approaches, some small modifications in the detection mechanism of the probes height would be necessary.

Altogether, this work underlines the need to develop new means to investigate the spatial organization of germinal region. It proposes “FlashMap” as an open source, user-friendly and flexible software to perform such, otherwise time-consuming analysis.

2.6. Acknowledgments

We are very grateful to Kazuaki Yoshikawa for providing us the guinea pig anti-Dlx2 antibody. This study was supported by a Grant from the “Programme Avenir Lyon Saint-Etienne” and S.Z. was further supported by a Doc.Mobility fellowship from the Swiss National Science Foundation (SNF; grant number P1SKP3_168418). Other support was received from a SNF project grant NRP63 to O.R. (grant number 406340_128291).

2.7. Supplementary Figures

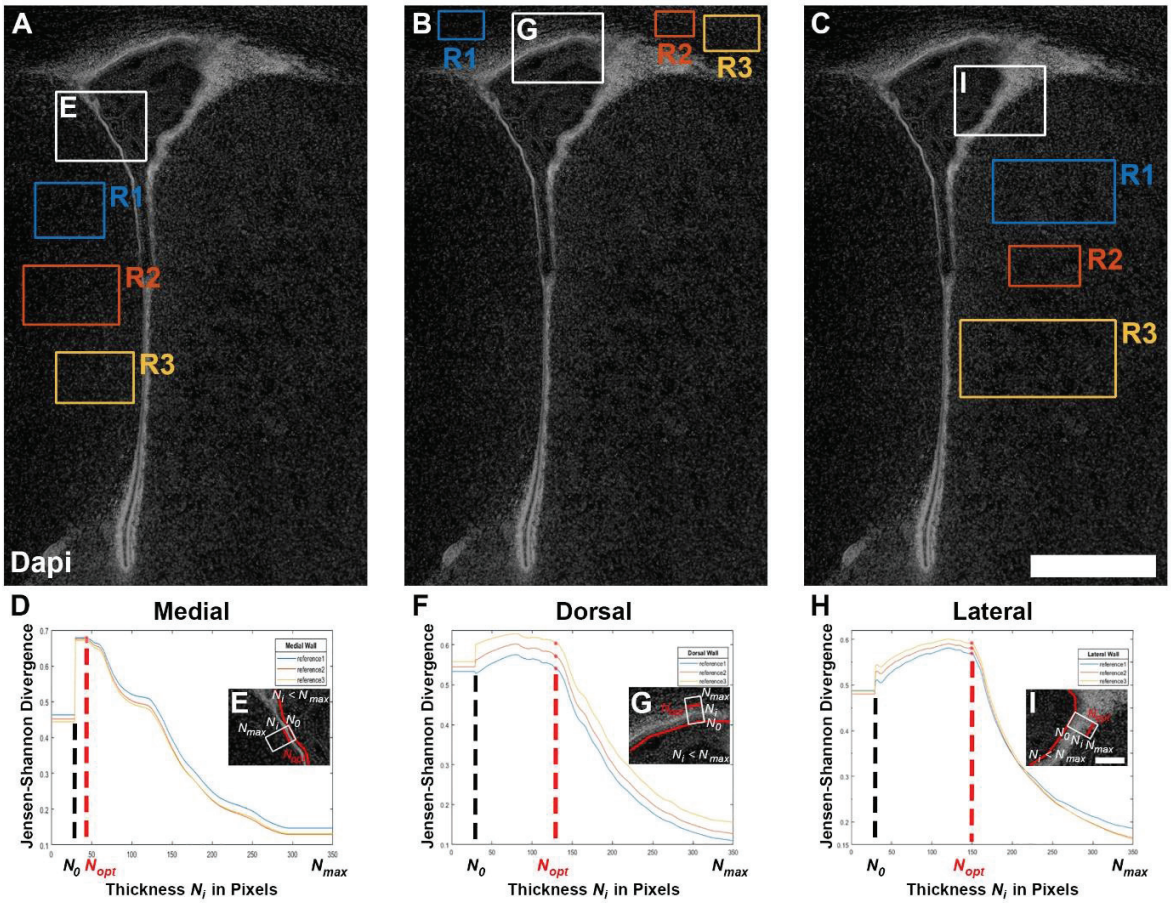

Figure S1. Optimal detection of the SVZ thickness with various "reference regions".
(A-C): Representative micrographs of Dapi staining for the three ROI: medial (A), dorsal (B), lateral walls (C). Colored boxes (R1, blue; R2, orange; R3, yellow) represent three different "reference regions".
(D, F, H): Graphs showing that the precision of the Jensen-Shannon divergence method to define the wall thickness and therefore the correct probe height is not affected by different "reference region" size and location.
(E, G, I): Representative micrographs illustrating the precision of N_{opt} calculation, reflected by the optimal positioning of the probe heights.
Scale bars: (C) = 500 µm; (I) = 100 µm. Abbreviations: ROI, region of interest; R1-3, "reference region" 1-3.

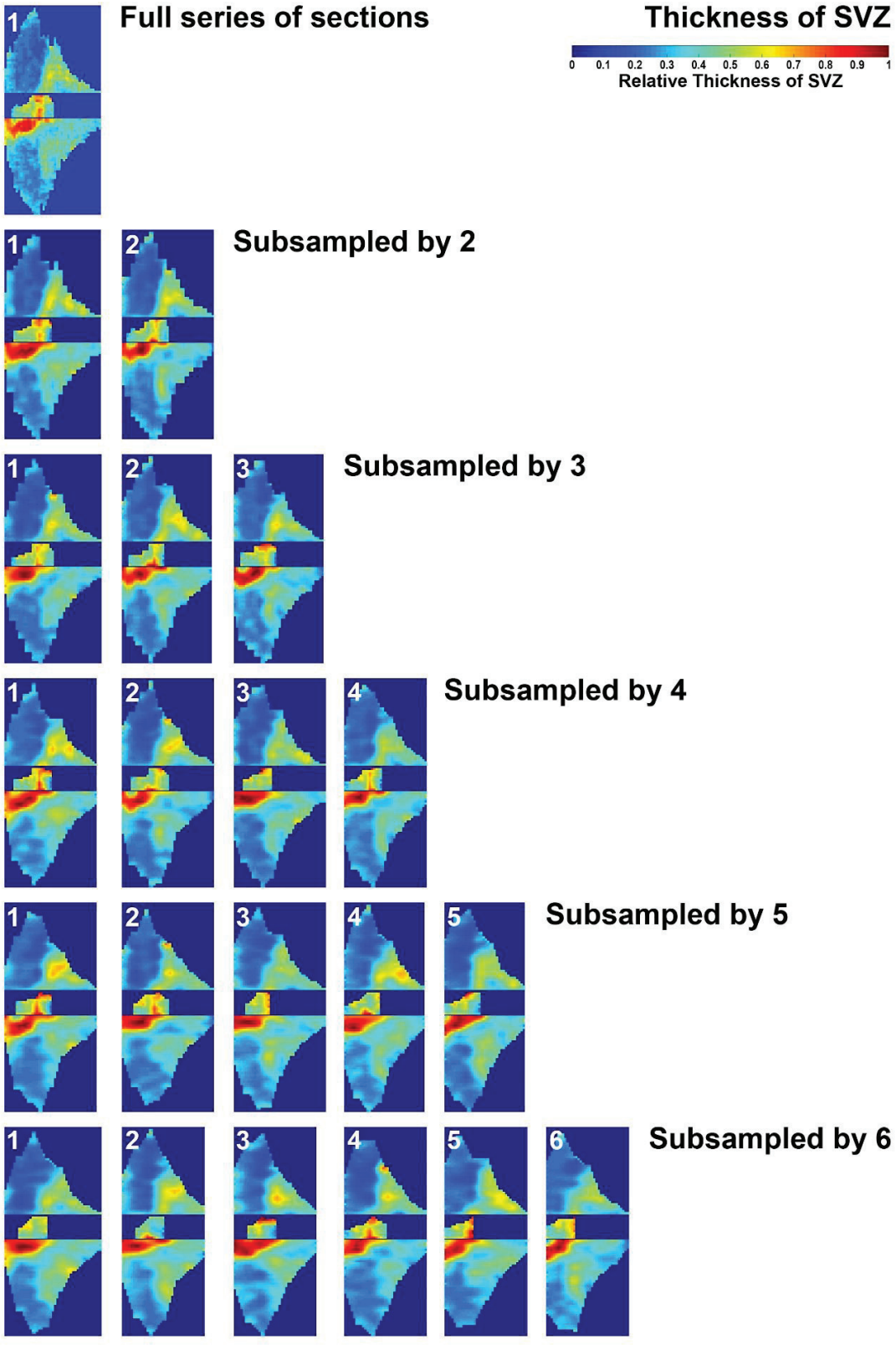
Full series of sections
Thickness of SVZ
0 0.1 0.2 0.3 0.4 0.5 0.6 0.7 0.8 0.9 1
Relative Thickness of SVZ
Subsampled by 2
Subsampled by 3
Subsampled by 4
Subsampled by 5
Subsampled by 6

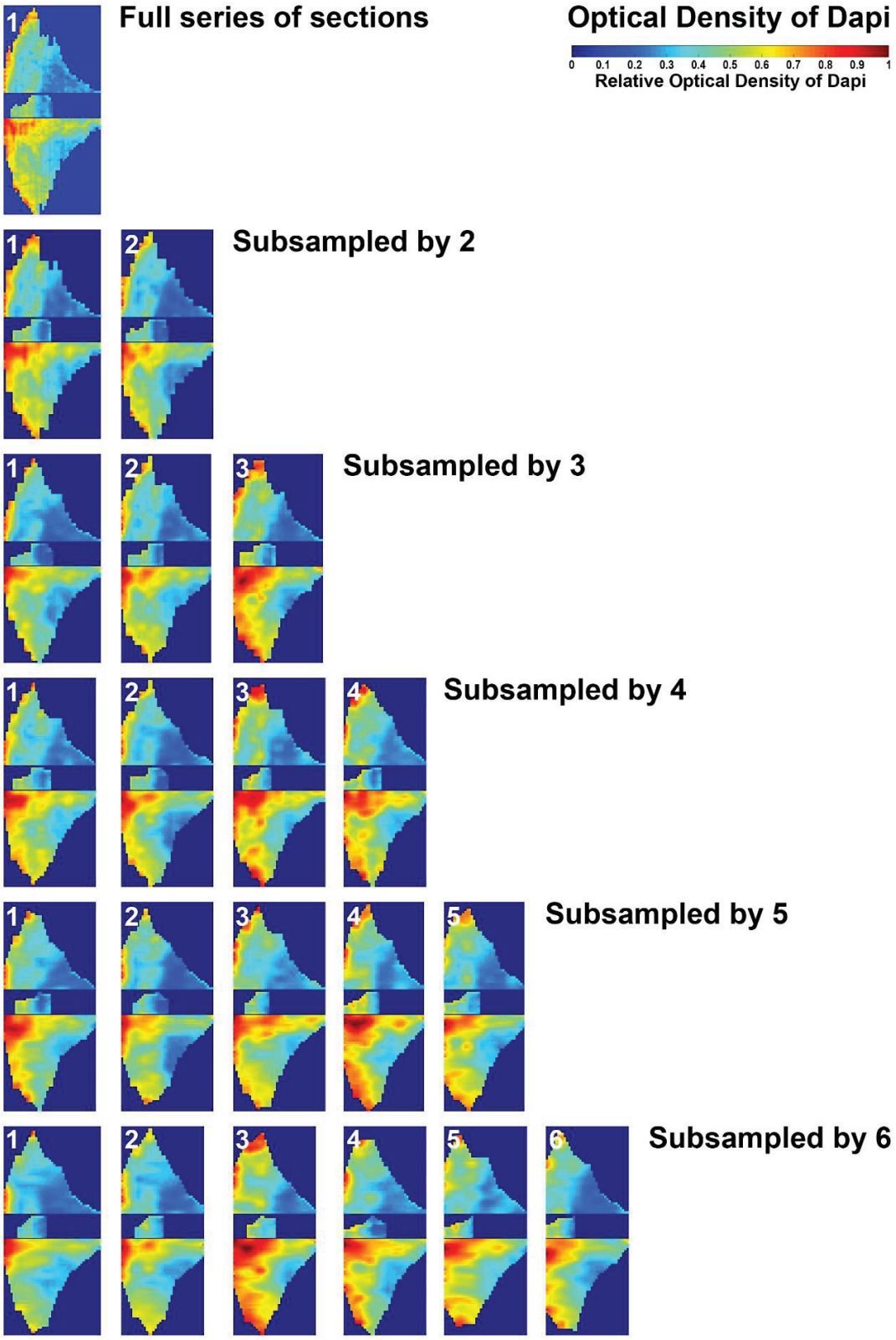
Full series of sections
Optical Density of Dapi
0 0.1 0.2 0.3 0.4 0.5 0.6 0.7 0.8 0.9 1
Relative Optical Density of Dapi
Subsampled by 2
Subsampled by 3
Subsampled by 4
Subsampled by 5
Subsampled by 6

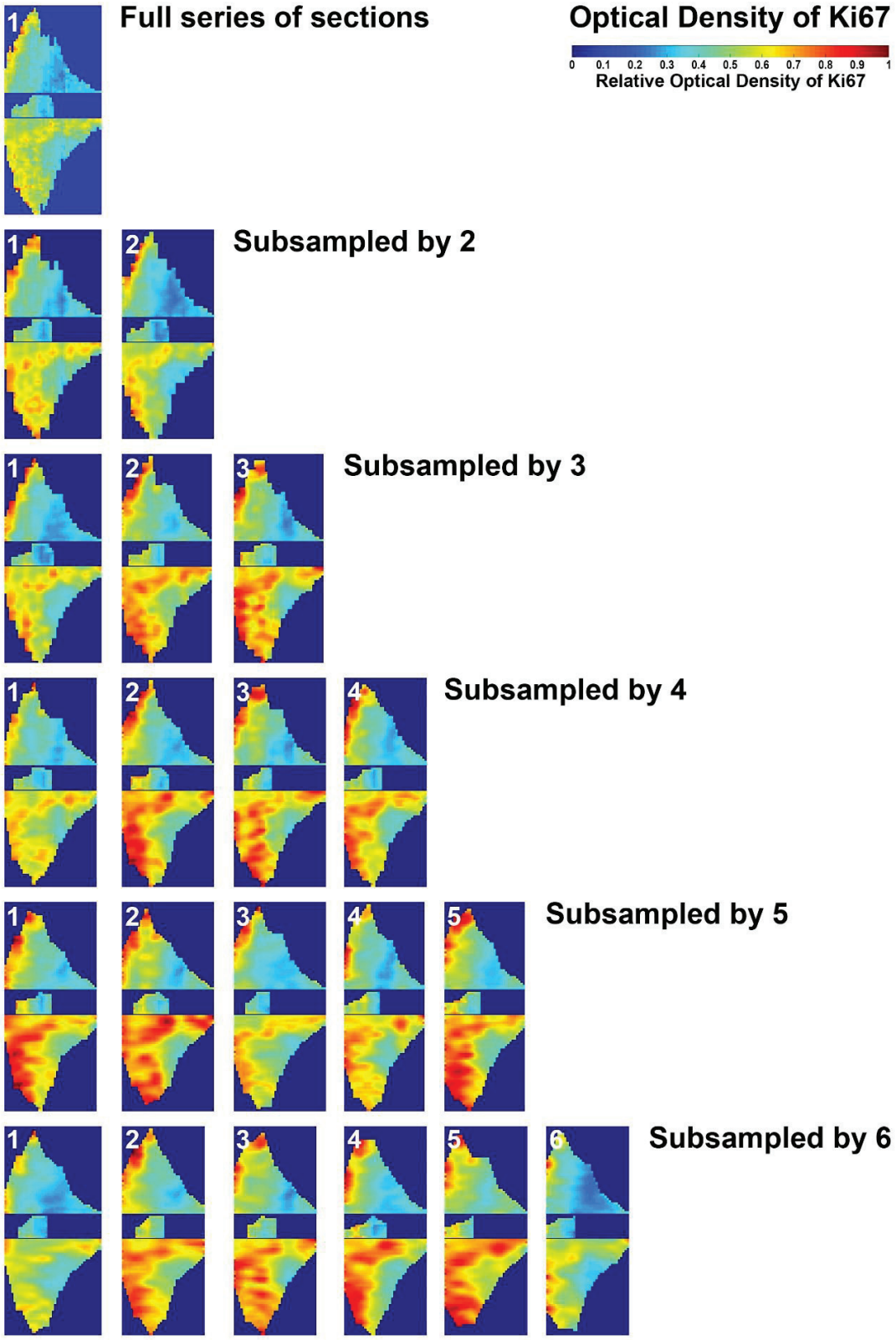
Full series of sections
Optical Density of Ki67
0 0.1 0.2 0.3 0.4 0.5 0.6 0.7 0.8 0.9 1
Relative Optical Density of Ki67
Subsampled by 2
Subsampled by 3
Subsampled by 4
Subsampled by 5
Subsampled by 6

Figures S2 to S4. Validation of the subsampling approach up to series of 6.
Heatmaps obtained with subsamplings ranging from 1/2 to 1/6 for analysis of SVZ thickness (**Figure S2**), cellular density (**Figure S3**) and $Ki67^+$ cells density (**Figure S4**). Heatmaps of the first line represent full analyses, 2^{nd} to 6^{th} line show the outcome when a subsampling of 1/2 to 1/6 is applied. Row numbers indicate with which section number the analysis was started.

3. Chapter 2: Hopx Defines Heterogeneity of Postnatal Subventricular Zone Neural Stem Cells

Stefan Zweifel[1], Kasum Azim[2], Guillaume Marcy[1,3], Quentin Lo Guidice[1], Deqiang Li[4], Olivier Raineteau[1]

[1]Univ Lyon, Université Claude Bernard Lyon 1, Inserm, Stem Cell and Brain Research Institute U1208, 69500 Bron, France
[2]Brain Research Institute, University of Zurich, 8057 Zurich, Switzerland
[3]Ecole Pratique des Hautes Etudes, PSL Research University, Neurogenetics Dpt, 75014, Paris
[4]Department of Cell and Developmental Biology, Cardiovascular Institute, Institute for Regenerative Medicine, Perelman School of Medicine at the University of Pennsylvania, Philadelphia, PA 19104, USA

Under revision: *Stem Cell Reports*

In this chapter, I designed the study, performed the experiments and analyses and wrote the manuscript. The development of the heatmap generator was achieved by Quentin Lo Guidice.

3.1. Abstract

The greatest diversity of neural lineages generated in the subventricular zone (SVZ) occurs early after birth, is regulated in a spatiotemporal manner and depends on the expression of specific transcriptional cues. We used transcriptomic as well as fate mapping approaches to investigate the relation between regional expression of transcription factors by neural stem cells (NSCs) and their acquisition of distinct neural lineage fates. Our results support an early priming of NSCs to produce defined cell types depending of their spatial location in the SVZ and identify Hopx as a marker of a subpopulation biased to generate astrocytes. Manipulation of Hopx expression showed however no effect on astrogenesis, but resulted in marked changes in the number of NSCs and of their progenies. Taken together, our results highlight transcriptional and spatial heterogeneity of postnatal NSCs as well as their early priming toward specific lineages and suggest a role for Hopx in the evolution of SVZ germinal activity.

Key words: astrogenesis; neurogenesis; subventricular zone; neural stem cell subpopulations; regionalization; Hopx.

3.2. Introduction

Germinal activity persists in the postnatal mammalian brain in specialized niches, namely the dentate gyrus (DG) of the hippocampus and the subventricular zone (SVZ) surrounding the lateral ventricle (LV). Neural stem cells (NSCs) of the postnatal SVZ differentiate into transient amplifying progenitors (TAPs) that will generate neuroblasts migrating through the rostral migratory stream (RMS), into the olfactory bulb (OB), where they differentiate into neurons (Lois and Alvarez-Buylla, 1994). The SVZ additionally generates glial progenitors that invade the nearby parenchyma (Reviewed in Azim et al., 2016; Bayraktar et al., 2015). Recently, accumulating evidences highlight the heterogeneous nature of the postnatal SVZ in respect to different microdomains generating distinct neural lineages. For example, progenitors of GABAergic neurons are predominantly generated along the lateral SVZ (lSVZ) wall, whilst the genesis of glutamatergic neuron progenitors are restricted to the dorsal SVZ (dSVZ; Brill et al., 2009; Azim et al., 2012a). Furthermore, postnatally-derived oligodendrocytes are generated from the dSVZ (Kessaris et al., 2006) under the control of different signaling mechanisms (Azim et al., 2012b; Azim et al., 2014a). This heterogeneity originates from early embryonic development (Fuentealba et al., 2015) and is intrinsically encoded by the expression of selected transcription factors (TFs). Therefore, TFs enriched in specific embryonic forebrain regions are persistent in their expression in corresponding domains of the postnatal SVZ. Examples of such TFs include Emx1 (pallium; dSVZ), Gsx1/2 (lateral and medial ganglionic eminence; lSVZ) and Zic1/3 (septum; medial SVZ; reviewed in Fiorelli et al., 2015). We recently resolved the transcriptional heterogeneities of different cell populations of the postnatal SVZ, in which an unexpected large number of transcripts (i.e. 1900) were differentially expressed in cells sorted from dorsal and lateral SVZ microdomains. Intriguingly, most of the transcriptional heterogeneity observed between the dorsal and lateral NSCs (dNSCs; lNSCs) populations were due to the expression of transcriptional cues. Notably, *Hopx* was identified with specific abundant expression to dNSCs, and its ectopic expression into lNSCs, revealed that it may have progliogenic functions (Azim et al. 2015). Hopx is a small (73 amino acids) atypical homeodomain protein that lacks DNA binding sites (Chen et al., 2002; Shin et al., 2002), and is relatively conserved within vertebrates (Asanoma et al., 2003). *Hopx* expression is minimal at embryonic day 14.5 (E14.5) and peaks around E16.5 with a rostro-medial to caudo-lateral gradient (Mühlfriedel et al., 2005). Presence of Hopx has been

found in radial astrocytes of the adult DG, while it is described to be consistently absent from the adult SVZ (De Toni et al., 2008). Moreover, expression of Hopx has recently received increasing attention due to its expression in quiescent NSCs, in mature astrocytes in the adult mouse DG (Li et al., 2015), as well as in outer radial glia cells (oRG) of the developing human brain (Pollen et al., 2015; Thomsen et al., 2016). Here, we used various approaches to further investigate the regionalization of the postnatal SVZ and of the NSCs it contains. We characterized the spatiotemporal and lineage-specific pattern of Hopx expression in the postnatal SVZ and investigated its potential function in postnatal SVZ germinal activity.

3.3. Experimental Procedures

3.3.1. Animals and Ethics

All animal experiments in Zurich were performed according to the Ethics Committee of the Veterinary Department of the Canton of Zurich (Approval ID 182/2011). Experiments in France were performed in accordance with European requirements 2010/63/UE and have been approved by the Animal Care and Use Committee CELYNE (APAFIS#187 & 188).

Animals used in this study were: OF1 wild-type animals from Charles Rivers (France), Hes5::EGFP animals (Basak and Taylor, 2007), $Hopx^{CreERT2}$ (Takeda et al., 2011), $Hopx^{LacZ/WT}$ knockin (Shin et al., 2002) and Rosa-EYFP mice (Srinivas et al., 2001).

3.3.2. Plasmids Preparation and Electroporation

The following plasmids were used in this study: pCX-GFP (kind gift of X Morin, ENS, Paris; France); pFloxpA-DsRed express (kind gift of Colette Dehay; INSERM U1208; Bron; France); pCAG-Cre (Addgene; 13775); pCMV-Hopx (Open Biosystems; MMM1013-202767606). Plasmids were purified using the EndoFree Plasmid Kit according to the manufacturer's protocol (Qiagen; 12362). Plasmids were re-suspended to a final concentration of 5 µg/µl. Dorsal electroporations were performed in P1 to P2 (postnatal day 1 to 2) pups as previously described (Boutin et al., 2008, Fernández et al., 2011). In $Hopx^{CreERT2}$ animals

subcutaneous tamoxifen (Tam; SIGMA-Aldrich; T5648) administration (1 mg per pup) was performed 2 to 3 hrs after electroporation.

3.3.3. Immunohistochemistry

Mice were sacrificed by an intraperitoneal overdose of pentobarbital followed by perfusion with Ringer Lactate solution and 4% paraformaldehyde (PFA) dissolved in 0.1 M phosphate buffer (PB; pH 7.4). Brains were removed and postfixed for 12-48 hrs at 4° C in 4% PFA and sectioned in 50 µm thick coronal serial sections. When necessary, antigen retrieval was performed for 20 minutes in citrate buffer (pH 6) at 80° C, then cooled for 20 minutes at room temperature and washed in 0.1 M PB. Blocking was done in TNB buffer (0.1 M PB; 0.05% Casein; 0.25% Bovine Serum Albumin; 0.25% TopBlock) with 0.4% triton-X (TNB-Tx). Sections were incubated over night at 4° C with the following primary antibodies in TNB-Tx: Rabbit anti-Hopx (1:400; Santa Cruz; sc-30216); Mouse anti-Hopx (1:400; Santa Cruz; sc-398703); Goat anti-DCX (1:500; Santa Cruz; sc-8066); Mouse anti-Olig2 (1:1500; Millipore; MABN50); Mouse anti-GFAP (1:500; Millipore; MAB3402); Chicken anti-GFP (1:1000; AVES LABS; GFP-1020); Rabbit anti-RFP (1:1500; MBL; PM005); Rabbit anti-S100β (1:5000; SWANT); Chicken anti-βGal (1:4000; Abcam; ab9361); Goat anti-Mcm2 (1:300; Santa Cruz; sc-9839); Mouse anti-Sox2 (1:100; Santa Cruz; sc-365823). Following extensive washing in 0.1 M PB with 0.4% triton-X (PB-Tx), sections were incubated with appropriate secondary antibodies conjugated with Alexafluor 488, 555 or 647 (1:500; Life Technologies) for 2 hrs at room temperature. Sections were washed and counterstained with Dapi (1:5000; Life Technologies; D1306). To increase the signal from βGal, a biotinylated secondary antibody (1:500; Jackson) was used in combination with a TSA amplification kit according to manufacturer's protocol (Life Technologies; T-20932).

3.3.4. FACsorting and qPCR

Hes5::EGFP (with C57BL/6 background) of the age P2-P4 were used for sorting for NSCs as previously described and using the same parameters (Azim et al. 2015). 4 to 5 animals of one litter was used for 1 "n" number. Microdissection of SVZ domains (dorso-medial; dorso-lateral and lateral) was performed in RNase free, sterile conditions. Tissues were dissociated using a

trypsin-based Neural Dissociation Kit (Miltenyi Biotec, Bergisch Gladbach, Germany). For additional purification of the Hes5-EGFP population, an APC conjugated NSC antibody against the transmembrane-protein prominin-1 (1:100; ebiosciences) was applied for 15 mins at RT, before suspension was subjected to Fluorescence Activated Cell Sorting (FACS Aria III; BD Bioscience, Franklin Lakes, New Jersey, USA). Dead cells were excluded by forward and sideward scatter. Gating settings were gained using an EGFP- wildtype animal and a prominin-1 isotype control conjugated to APC (rat anti-IgG; 1:100, ebiosciences). Brightest 30% of $EGFP^+$ cells, which where $prominin\text{-}1^+$ were collected directly into RNA lysis buffer and snap-frozen for further gene expression analysis. RNA extraction was performed using the RNeasy microkit (Qiagen; 74004) following manufacturer's guidelines. RNA amplification of 3 ng input material was done using the Nugene Pico Ovation WT kit (NuGen Technologies, Inc., San Carlos, CA) like described previously. 50 ng RNA per sample was used for cDNA synthesis (Superscript; Life Technologies; Carlsbad, CA, USA). qPCR was performed according to the procedures described elsewhere (Azim et al., 2012b, Azim et al., 2014b), with the LightCycler 480 (Roche, Basel, Switzerland). All reactions were performed in duplicates or triplicates and GAPDH was used as reference gene. Primers used were custom made by Qiagen (EGFP, Eomes, Hopx, Pcna, Sp8) or designed with the Primer Express 1.5 software and produced by Eurofins (Schönenwerd, Switzerland):

GAPDH:	fw_CGTCCCGTAGACAAAATGGT,	rv_TTGATGGCAACAATCTCCAC;
Aldh1l1:	fw_CAGTAAACCTCCTGGCCAAA,	rv_CCCTGTTTTCCCTACTTCCC;
Aqp4:	fw_TGAGCTCCACATCAGGACAG,	rv_TCCAGCTCGATCTTTTGGAC;
Dct:	fw_GCATCTGTGGAAGGGTTGTT,	rv_ACTCCTTCCTGAATGGGACC;
DCX:	fw_CTGACTCAGGTAACGACCAAGAC,	rv_TTCCAGGGCTTGTGGGTGTAGA;
Dlx2:	fw_CTTCTTGAACTTGGATCGGC,	rv_AGACCCAGTATCTGGCCCTG;
Ebf1:	fw_GGTGGAAGTCACACTGTCGTAC,	rv_GTAACCTCTGGAAGCCGTAGTC;
Fgfr3:	fw_ACAGGTGGTCATGGCAGAAGCT,	rv_CTCCATCTCAGATACCAGGTCC;
Gli1:	fw_CTCAAACTGCCCAGCTTAACCC,	rv_TGCGGCTGACTGTGTAAGCAGA;
Gli3:	fw_CGAGAACAGATGTCAGCGAG,	rv_TGAGGCTGCATAGTGATTGC;

Hes5:	fw_GTAGTCCTGGTGCAGGCTCT,	rv_AACTCCAAGCTGGAGAAGGC;
Id3:	fw_GCGTGTCATAGACTACATCCTCG,	rv_GTCCTTGGAGATCACAAGTTCCG;
Lef1:	fw_CGTCACACATCCCGTCAGATGTC,	rv_TGGGTGGGGTGATCTGTCCAACG;
Olig1:	fw_AGCAAGCTCAAACGTTGGTT,	rv_GTTCTGTTTTTCAGGCTCGC;
Olig2:	fw_GACGATGGGCGACTAGACA,	rv_CAGCGAGCACCTCAAATCTA;
PDGFRα:	fw_AGAAAATCCGATACCCGGAG,	rv_AGAGGAGGAGCTTGAGGGAG;
Plp1:	fw_GGGCCCCTACCAGACATCTA,	rv_TCCTTCCAGCTGAGCAAAGT;
Tcf7:	fw_TGCCTTCAATCTGCTCATGCC,	rv_GTGTGGACTGCTGAAATGTTCG;
Vax1:	fw_CTCTACAGGCTGGAGATGGAGT,	rv_GCTTAGTCCGCCGATTCTGGAA.

3.3.5. Meta-analysis of Transcriptional Profiles

To generate the lists of transcription factors and transcriptional regulators that are enriched in dNSCs and lNSCs, we made use of our recently published transcriptional datasets (Azim et al., 2015; GSE60905). We analysed the dataset on the "Gene Expression Omnibus" (https://www.ncbi.nlm.nih.gov/geo/) for transcripts that are differentially expressed between dNSCs and lNSCs (≥1.8 fold enrichment and p-values <5%). Finally, we selected transcripts for transcription factor activity and regulation of transcription using "DAVID Analysis Wizard" (https://david.ncifcrf.gov/). Lists of transcripts were analysed for enrichments in the neuronal, astrocytic or oligodendrocytic lineage using the transcriptional dataset of the Barres group (Cahoy et al., 2008; GSE9566). Heatmaps were produced using a self-made R script "Heatmap Generator", which enables us to compare and generate heatmaps from different datasets available on the "Gene Expression Omnibus" (GEO).

3.3.6. Quantifications and Statistics

Images were acquired using a Leica DM5500 epifluorescent microscope, a Leica TCS SPE II and a TCS SP5 confocal microscope (Leica Microsystems GmbH, Wetzlar, Germany). Images were quantified using ImageJ-win64 or assembled as representative pictures with LAS X,

ImageJ and Photoshop (CS4). Statistical analysis was done with Microsoft Excel 2013 and GraphPad Prism 7. All data are showed as mean ± SEM and statistical significance was calculated using the unpaired t-test (<0.05=*, <0.01=**, <0.001=***, <0.0001=****).

3.4. Results

3.4.1. *Hopx* is Enriched in NSCs of the dSVZ, as well as in the Astrocytic Lineage

In a previous study, the transcriptome of spatially distinct domains of the postnatal SVZ were deciphered to reveal the existence of different transcriptional networks in region-specific NSCs (Azim et al. 2015). This transcriptional heterogeneity was further examined here by analysis of transcription factors and transcriptional regulators (defined hereafter as TFs) as well as their association with defined neural lineages. Focusing on TFs only, 112 were differentially expressed between the subpopulations of NSCs (dNSCs: 61; lNSCs: 51; **Figures 1A and S1A to S1C**). Those enriched dorsally were confirmed by examining in situ databases (http://www.brain-map.org/), and by immunohistochemistry (**Figures 1C and 1D**). Among transcripts enriched in dNSCs (**Figure 1B**), 5 out of the top 10 (*NeuroD6, Eomes, NeuroD1, Tbr1, Neurog2*) were major determinants of the glutamatergic neuronal lineage (Schuurmans et al., 2004; Hevner et al., 2006; Brill et al., 2009; Winpenny et al., 2011). For further examining TFs association with defined neural lineages, we made use of previously published datasets to perform a meta-analysis (Cahoy et al., 2008). Interestingly, this analysis revealed that TF enriched in dNSCs formed at least 3 clusters defined as astroglial (18/61), neuronal (15/61) and oligodendroglial (11/61; **Figure 1E**). In contrast, clustering of lNSCs enriched TFs defined a single large neuronal cluster (42/51), while the oligodendroglial cluster was small (3/51) and the astroglial absent (**Figure S1E**). These observations support the greater diversity of lineages arising from the dSVZ compared to the lSVZ that generates almost exclusively interneurons (reviewed in Fiorelli et al., 2015 and Azim et al., 2016).

We then focused our analysis on *Hopx*, an atypical homeodomain protein, which was interestingly enriched in both dNSCs (rank 7; 7 fold enriched in dNSCs) and the astrocytic lineage population (**Figures 1A, 1B and 1E**). Immunodetection of Hopx confirmed that it was

not expressed in migrating neuroblasts (DCX^+) of the RMS and in oligodendrocytes ($Olig2^+$) of the corpus callosum (CC; **Figures 1F and 1G**). In contrast, Hopx was expressed by astrocytes in the corpus callosum ($GFAP^+$; **Figure 1H**), in agreement with the transcriptional meta-analysis (**Figure 1E**). This pattern of expression suggests that Hopx might play a role in regulating neural stemness and/or fate choice.

Figure 1. A meta-analysis of TF enrichment in dNSCs in highlighting their association with distinct neural lineages.
(A): Heatmap showing enrichment of 61 TFs in dNSCs compared to their lateral counterparts (≥1,8 folds and p.Value<0,05).
(B): Top 10 TFs enriched in dNSCs.
(C, D): Dorsal enrichment of select transcripts was confirmed using Allen Brain Atlas for Eomes (C) and by immunohistochemistry (Hopx) (D).
(E): Heatmap of dNSCs enriched TFs reveals 3 clusters corresponding to specific neural lineages: oligodendrocytes (purple, 11/61); astrocytes (yellow, 18/61); neurons (turquoise, 15/61). Hopx is highlighted in bold and associates to the astrocytic lineage.
(F-H): Confirmation of lineage-specific enrichment of Hopx by immunohistochemistry. Hopx is largely absent in neuroblasts in the RMS (DCX, F) and oligodendrocytes in the CC (Olig2, G), but is observed in astrocytes of the CC (GFAP, H).
Scale bars: C, D = 500 μm; H = 25 μm. Abbreviations: CC, corpus callosum; dNSC, dorsal neural stem cell; lNSC, lateral neural stem cell; RMS, rostral migratory stream; OPC, oligodendrocyte precursor cell. ⟶

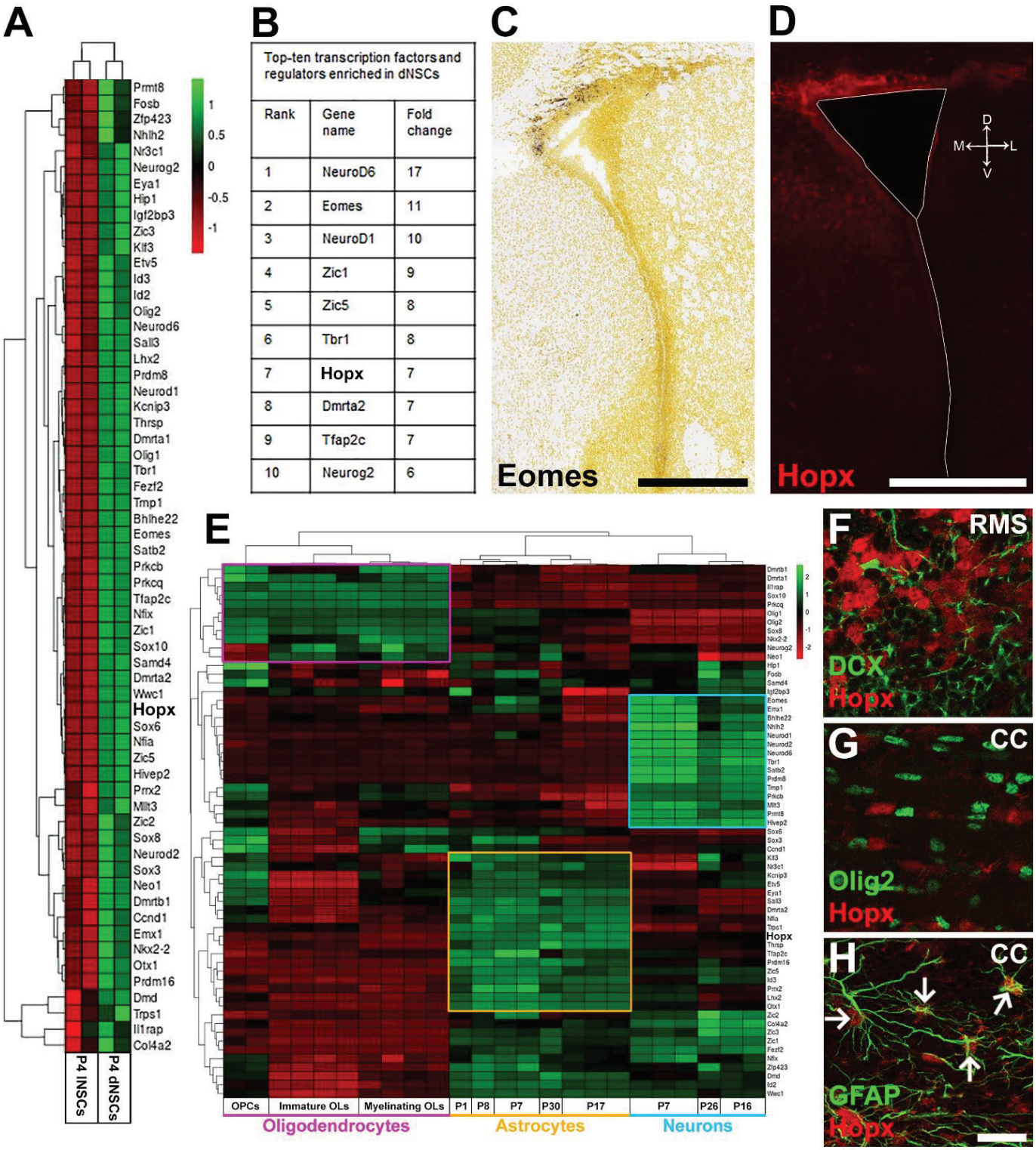
A
B
C
D
E
F
G
H
Top-ten transcription factors and regulators enriched in dNSCs
Rank
Gene name
Fold change
1 NeuroD6 17
2 Eomes 11
3 NeuroD1 10
4 Zic1 9
5 Zic5 8
6 Tbr1 8
7 Hopx 7
8 Dmrta2 7
9 Tfap2c 7
10 Neurog2 6
Eomes
Hopx
D
M
L
V
RMS
DCX
Hopx
CC
Olig2
Hopx
CC
GFAP
Hopx
P4 INSCs
P4 dNSCs
OPCs
Immature OLs
Myelinating OLs
P1
P8
P7
P30
P17
P7
P26
P16
Oligodendrocytes
Astrocytes
Neurons

3.4.2. Hopx Expression Reveals Intraregional Heterogeneity within the dSVZ

Using two distinct antibodies, we found Hopx expression to be restricted to the dSVZ, while it was consistently absent from its lateral counterpart (**Figures 2A and S2**; for quantifications the rabbit anti Hopx antibody was used), in agreement with our transcriptomic analysis (see above). A high Hopx expression was already detectable along the dorsal region of the VZ/SVZ at embryonic day 16 (E16). At early postnatal time points (P1) its expression remained high, but declined sharply thereafter in the young adult SVZ. Throughout its period of expression, a clear mediolateral gradient persisted, with the highest expression observed in the medial aspects of the dorsal wall and declining in the lateral aspects of the dorsal wall (i.e. high medial-to-lateral expression), which has not yet been described for any other gene.

We next investigated Hopx expression in postnatal dNSCs in the Hes5::EGFP mouse line, which efficiently labels NSCs, as characterized previously (Azim et al., 2015; Giachino et al., 2014). Quantification of Hopx expression in the dSVZ of this mouse line, revealed that most, but not all (70.1±5.0%) Hes5::EGFP$^+$ cells in the dSVZ expressed Hopx. Due to the unexpected mediolateral gradient in Hopx expression in the dSVZ, quantifications of EGFP$^+$/Hopx$^+$ cells were performed in the medial and lateral subdomains. There was a significantly higher overlap in the medial subdomain of the dSVZ (90.9±6.6%; dmSVZ) compared to the lateral subdomain (53.7±6.2%; dlSVZ; **Figure 2B**). These results were confirmed by performing GFP-electroporations (EPOs) of the dSVZ. Pups were sacrificed 8 hrs following EPO labeling the cells in direct contact with the lumen of the ventricle, i.e. those with radial glia (RG) morphology, as previously described (Azim et al. 2015; Tiveron et al., 2017). Similar results were obtained with 76.0±2.4% of the electroporated (GFP$^+$) cells expressing Hopx, which were significantly larger in the dorso-medial subdomain, compared to its dorso-lateral counterpart (93.0±2.4% vs. 69.3±3.4%; **Figure 2C**).

Taken together Hopx expression pattern in dNSCs suggests entirely novel functional differences in the dSVZ and implies for the first time intraregional heterogeneity of the dorsal wall.

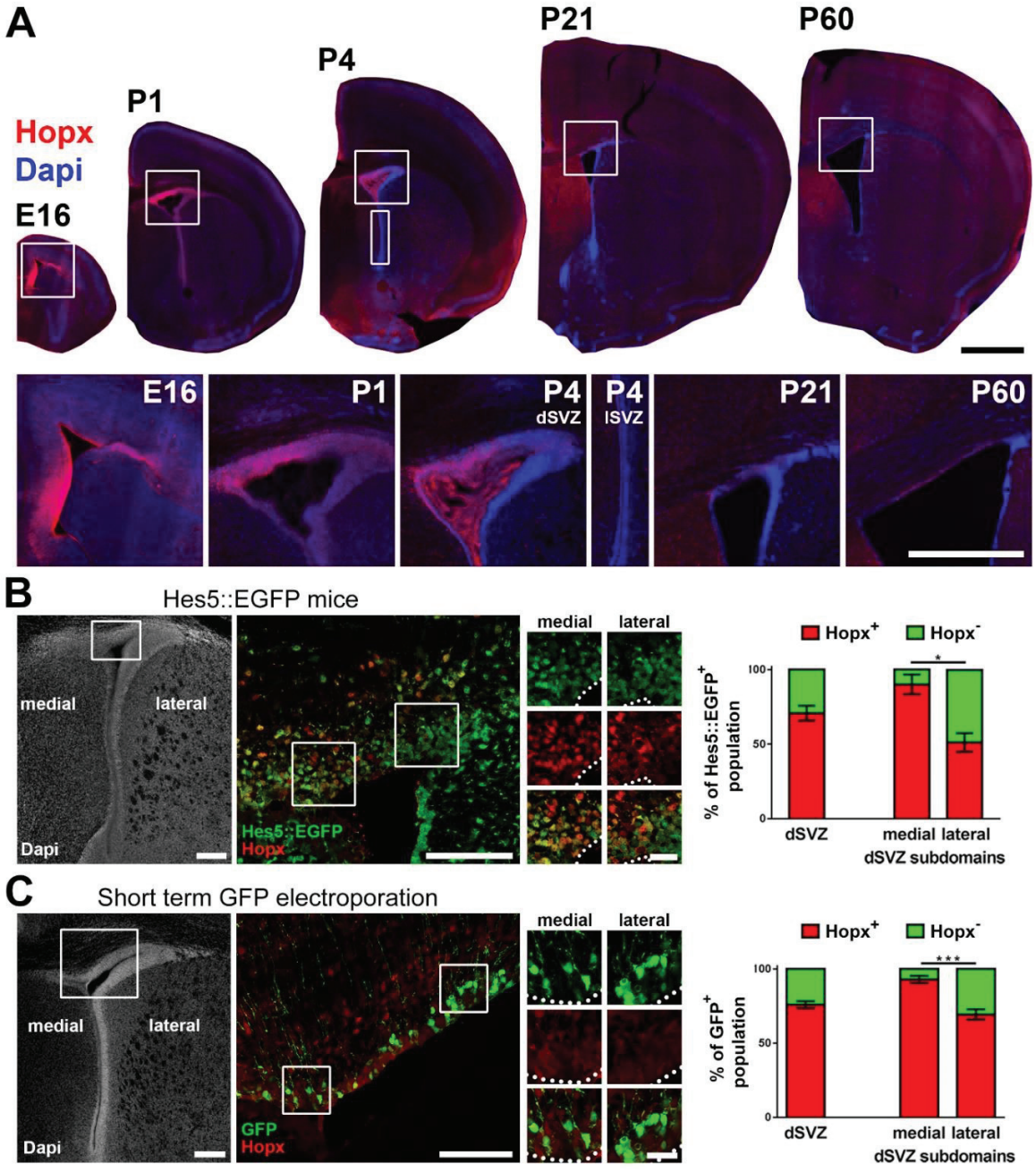

Figure 2. Hopx shows a complex spatial and temporal expression pattern during forebrain development.

(A): Representative micrographs of Hopx expression in coronal sections at E16, P1, P4, P21 and P60 (top panels). Higher magnifications (lower panel) show high expression in the embryo (E16) and at early postnatal stages (P1, P4) and a decline thereafter (P21, P60).

Embryonal and early postnatal ages (E16, P1, P4) show a clear expression gradient in the dorsal wall from medial high to lateral low.

(B, C): Analysis of Hopx expression in dNSCs was performed in Hes5::EGFP mice (B) and after short-term (8 hrs) targeted electroporation of a pCX-GFP plasmid (C). →

Quantifications were performed in rostral LV section (Dapi overviews; Bregma: 1,2-0) in the complete extent of the dorsal microdomain as well as in its medial and lateral subdomains (higher magnification). Crops show a high degree of overlap of Hopx with Hes5::EGFP and GFP positive cells, respectively. Degree of overlap was higher in the medial subdomain (Crops and Graphs).
Animals: (B) n=3; (C) n=6.
Scale bars: A (overview) = 1 mm; A (crops) = 500 µm; B+C (Dapi overview) = 200 µm; B+C (higher magnification) = 100 µm; B+C (crops) = 25 µm.
Abbreviations: dSVZ, dorsal subventricular zone; lSVZ, lateral subventricular zone.

3.4.3. Hopx Defines Dorsal SVZ Microdomains with Distinct Lineage Outputs

Expression of Hopx by astrocytes and a regional enriched subpopulation of dNSCs suggests further transcriptional heterogeneity within the dSVZ microdomain. To further investigate these observations, we microdissected the medial and lateral parts of the dSVZ (dmSVZ and dlSVZ, respectively) and isolated NSCs (dmNSCs; dlNSCs) based on their expression of Hes5::EGFP, as previously described (Azim et al. 2015). We performed qPCR to compare the expression of lineage-specific markers in regional NSC populations (**Figures 3B and 3C**).

We selected transcripts found to be enriched in NSCs, as well as in defined neural lineages (Azim et al., 2015; Cahoy et al., 2008) and compared their expression level by qPCR. Transcripts were all enriched in NSCs of all regions compared to the dSVZ, thereby validating our FACs strategy. In addition, there was no overall regional enrichment of stem cell markers (*Hes5, EGFP*; Basak and Taylor, 2007) and proliferation marker (*Pcna*; Yu et al., 1992) within the different NSC populations, although the neuroblast marker, *Dcx* was enriched in lNSCs, consistent with a greater number of neuroblasts generated by this SVZ microdomain (Yang et al., 2004; **Figure 3A, top panel**). Markers for the astrocytic, oligodendrocytic and neuronal lineages were confirmed using the transcriptional dataset from the Barres group (Cahoy et al., 2008; **Figure S3**). Markers which were highly specific to astrocytes (*Acq4, Aldh1l1, Fgf3, Id3*), including Hopx, were expressed in dmNSCs including *Hopx* (**Figure 3B, top panel**). Markers for the oligodendrocyte lineage (*PDGFRa, Plp1, Olig1, Olig2, Dct*) showed a more homogeneous distribution along the dSVZ, but seem also to be biased to the dmNSCs population (**Figure 3B, middle panel**). Finally, proneuronal genes (*Eomes, Sp8, Dlx2, Vax1, Ebf1*) were generally enriched in dlNSCs or in lNSCs (**Figure 3B, bottom panel**), implying

spatial segregation of lineages in the dSVZ. Taken together, astroglial markers, including Hopx, exhibit a converse expression gradient in dNSCs compared to neuronal markers (**Figure 3C**). Interestingly, target genes for patterning molecules, i.e. Wnt and Shh, showed that Wnt signaling is homogenously distributed throughout the dorsal wall (*Tcf, Lef1*) whereas, *Gli1* is highly expressed in lNSCs (**Figure 3A, bottom panel**). Another signaling pathway target gene, *Id3*, used as a readout for Bmp signaling, showed very high enrichment in dmNSCs (**Figure 3B, top panel**; Azim et al., 2014b; Ihrie et al., 2011; Hollnagel et al., 1999).

To test if NSCs harbored by those two subdomains are biased to generate specific neural progenies, we performed targeted EPO of the dmSVZ and dlSVZ (**Figure 3D**). At a short time point (i.e. 12 hrs) electroporation of both microdomains resulted in efficient GFP expression in numerous radial glial cells (data not shown). At later time points (14 days post electroporation, dpe) the high efficiency of the targeted EPO was still evident, as assessed by analysis of the GFP optical density in the dSVZ (**Figure S4**). This was done using our recently developed software "FlashMap" (**Chapter 1**). Both regions had given rise to a large cohort of progenies whose distribution and fate appeared to be strikingly different (**Figures 3C-F**). Thus, in accordance to the transcriptional profile of dlNSCs, we found a large population of GFP^+ neurons in the OB (93.3±11.1) following dorso-lateral EPO, while that derived from the dorso-medial EPO remained small (11.1±1.8; **Figures 3E to 3G**). Contrary, the population of astrocytes around the LV, assessed by morphology and GFAP expression (**Figures 3H and 3I**), was substantially larger after dorso-medial EPO than after dorso-lateral EPO (34.6.5±6.3 vs. 16.5±4.1; **Figure 3J**). Taken together, dmNSCs are clearly biased to the generation of the astrocytic lineage (74.9±3.0% astrocytes vs. 25.1±3.0% neurons), while dlNSCs mainly produce neurons (15.2±3.8% astrocytes vs. 84.8±3.8% neurons; **Figure 3K**).

Altogether, these findings suggest a high degree of heterogeneity within the dSVZ, with subdomains containing NSCs biased towards either an astrocytic or a neuronal fate.

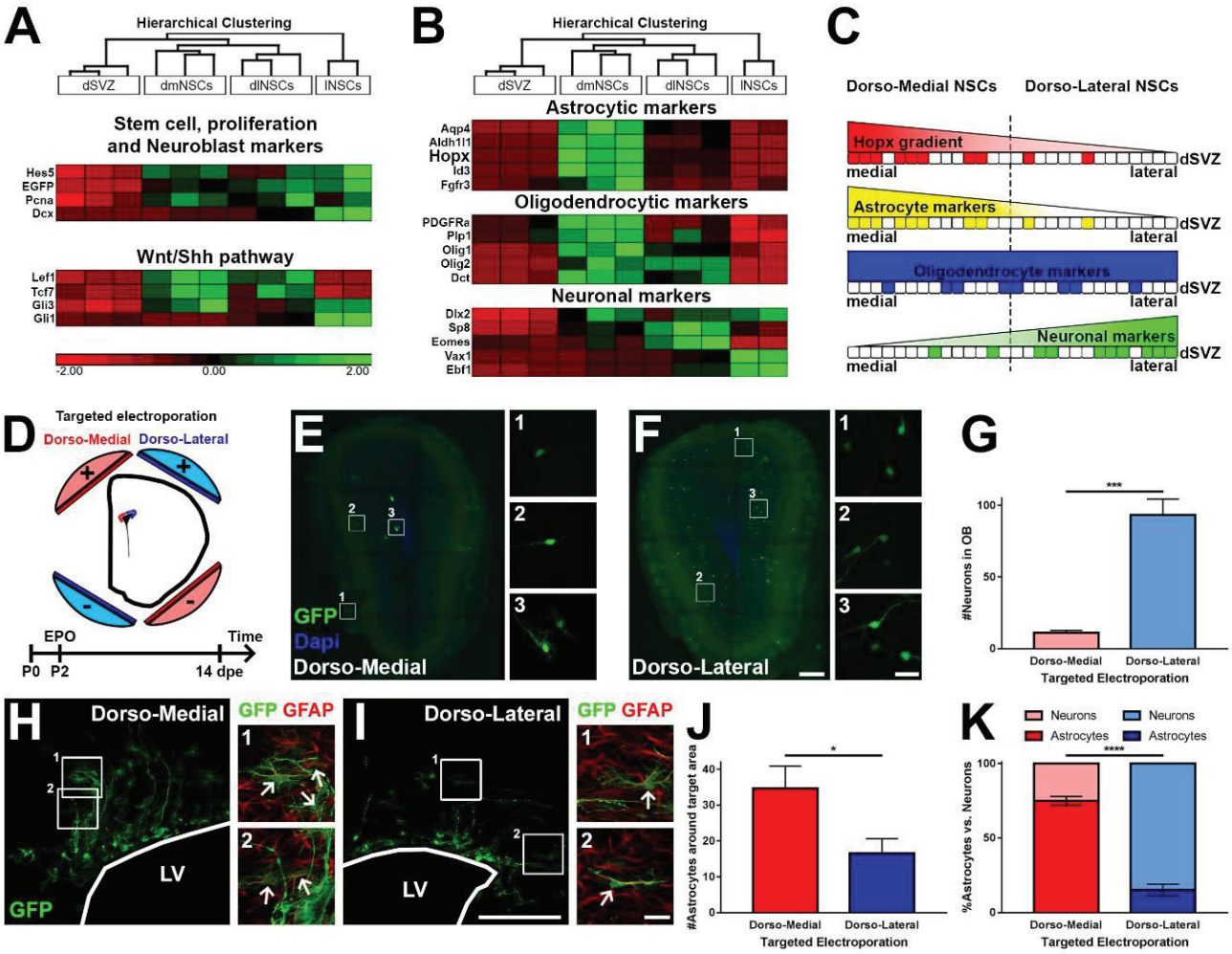

Figure 3. Lineage-specific markers highlight acquisition of divergent cell fates by NSCs located in different dSVZ subdomains.

(A+B): Heatmaps show enrichment of transcripts in NSCs of distinct SVZ regions (dmNSCs, dlNSCs, lNSCs) against the dorsal environment (dSVZ). Transcripts of stem cell, proliferation and neurogenesis markers (A; top panel) and Wnt/Shh pathways specific markers were analysed (A; bottom panel). Selected markers of the astrocytic lineage and Hopx (B; top panel), oligodendrocytic lineage (B; middle panel) and the neuronal lineage (B; bottom panel) were analysed. Astrocytic and neuronal markers show regional enrichment (in dmNSCs and dlNSCs, respectively), while oligodendrocytic makers were more homogeneously distributed along the dSVZ. Note that Hopx transcripts were enriched in dmNSCs.

(C): Scheme representing the counter gradients of the expression of Hopx (red) and astrocytic markers (yellow) versus the expression of neuronal markers (green) in dNSCs. Oligodendrocytic markers (blue) do not show such a clear spatial enrichment.

(D): Dorso-medial and dorso-lateral targeted electroporations highlight divergent lineage outputs of the two dorsal subdomains. Scheme shows the orientation of the electrodes for the targeted electroporation at P2 and sacrificing of animals at 14 dpe. ⟶

(E-F): Representative micrographs of OB sections after dm and dlEPO (E+F). Cell counts of OB neurons indicate that neurogenesis of the dSVZ is mainly provided by dlNSCs (G).
(H-J): Representative micrographs of LV containing sections after dm and dlEPO. Cells with astrocytic fates were identified according to their morphology and GFAP expression (H+I). Cell counts of astrocytes indicate that astrogenesis of the dSVZ is mainly provided by dmNSCs (J).
(K): Graph of the fractions of astrocytic and neuronal progenies from NSCs of these two subdomains. It highlights that dmNSCs are biased to the production of astrocytes, while dlNSCs mainly produce neurons.
Animals: (A) 4-5 per n; (B) dmEPO, n=4; (B) dlEPO, n=5.
Scale Bars: F+I (overviews) = 200 µm; F+I (crops) = 25 µm.
Abbreviations: dpe, days post electroporation; dSVZ, dorsal subventricular zone; dmNSCs, dorso-medial NSCs; dlNSCs, dorso-lateral NSCs; lNSCs, lateral NSCs; EPO, electroporation.

3.4.4. Hopx Expressing NSCs are Biased to Acquire an Astroglial Fate

To confirm a direct relationship between Hopx expression and the generation of distinct neural lineages, we fate-mapped Hopx expressing NSCs. We co-electroporated an inducible fluorescent plasmid (pFloxpA-DsRED express) with a GFP plasmid (pCX-GFP) in the dSVZ of P1 $Hopx^{CreERT2}$ mice and analyzed brain sections at 7 and 21 dpe (**Figures 4A and 4B**). Activation of the Cre-recombinase in $Hopx^{+}$ NSCs led to DsRED/GFP expression (hereafter called DsRED) in electroporated cells and their progenies, while the $Hopx^{-}$ lineage expressed GFP only (**Figure 4C**). Electroporated cells distribution and cell fate were assessed at both time points on serial sections encompassing the LV and the OB (**Figures 4D and 4E**). Our results reveal the presence of $DsRED^{+}$ and GFP^{+} cells at both 7 and 21 dpe (**Figure 4F**). Remarkably, while the majority of GFP^{+} cells were found in the OB (7 dpe: 66.2±2.1%; 21 dpe: 77.7±2.5%), where they acquired the typical morphology of granule neurons, the majority of $DsRED^{+}$ cells remained in close proximity to the dSVZ, i.e. in the corpus callosum (7 dpe: 64.6±5.6%; 21 dpe: 63.8±6.8%) at both time points (**Figure 4G**). To confirm the early acquisition of distinct neural fates by $Hopx^{+}$ and $Hopx^{-}$ NSCs, we investigated GFAP expression by $DsRED^{+}$ and GFP^{+} in the periventricular regions at 21 dpe. This analysis confirmed that the fraction of $GFAP^{+}$ astrocytes produced by $Hopx^{+}$ NSCs was approximately twice as much as the fraction generated by $Hopx^{-}$ NSCs (59.2±7.1% vs. 32.8±4.3%, **Figure 4H**).

Taken together, these findings validate for the first time that the dSVZ consists of two subdomains harboring specialized NSC populations biased to acquire distinct fates (medial: astrocytes; lateral: neurons). Furthermore, our results identify Hopx as a marker of a subpopulation of NSCs biased to generate astrocytes.

Figure 4. Fate mapping of Hopx$^+$ and Hopx$^-$ lineages by electroporation of an inducible fluorescence plasmid.
(A-C): EPO of a pCX-GFP and an inducible pFloxpA-DsRed plasmid (1:2; A) allows lineage tracing of both populations at short- (7 dpe) and long-term (21 dpe; B). This approach results in GFP only progenies from Hopx$^-$ NSCs, whilst Hopx$^+$ NSCs give rise to DsRED/GFP (or DsRED) progenies (C).
(D+E): Representative micrographs at 21 dpe of a LV (D) and OB (E) section. Astrocytic fate was assessed according to morphology and GFAP expression (D, crops).
(F): Graph of absolute numbers of recombined cells (red) and GFP$^+$ (green) in LV and OB sections at 7 dpe and 21 dpe.
(G): Graph showing the fractions of recombined and GFP$^+$ cells harbored by LV and OB sections at 7 dpe and 21 dpe.
(H): Graph showing the fractions of cells from the recombined and GFP population exhibiting astrocytic traits 7 dpe and 21 dpe.
Animals: 7 dpe, n=5; 21 dpe, n=4.
Scale bars: D (Dapi overview and fluorescence overview) = 100 µm; D (crops) = 25 µm; E (Dapi overview) = 500 µm; E (fluorescence overview) = 250 µm; E (crops) = 50 µm.
Abbreviations: dEPO, dorsal electroporation; dpe, days post electroporation; dSVZ, dorsal subventricular zone; LV, lateral ventricle; NSCs, neural stem cells; OB, olfactory bulb; Tam, tamoxifen. →

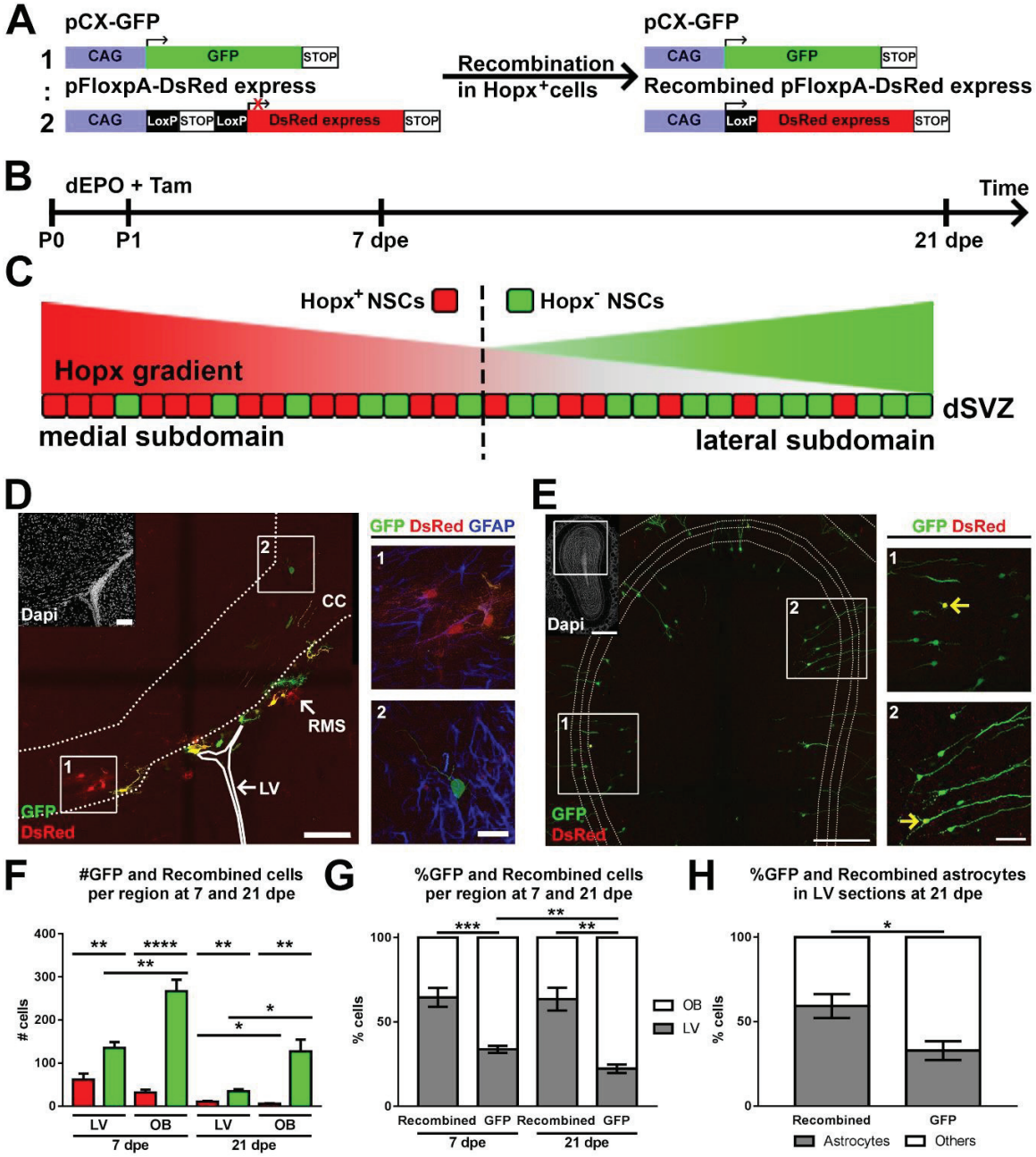

3.4.5. Expression of Hopx is Partly Dispensable During Astrogenesis

To further explore the role of Hopx in regulating lineage specification in the postnatal dSVZ, we performed loss and gain of function (LoF; GoF) experiments and analysed the effects of these manipulations on the expression of the astrocytic markers, GFAP and S100β in the corpus callosum at P19 and 19 dpe, respectively (**Figures 5A and 5B**). First, the effect of Hopx loss in astrocytes was analysed by fate mapping the phenotypes of LacZ expressing astroglia in

both *Hopx* KO ($Hopx^{LacZ/LacZ}$) and *Hopx* heterozygous ($Hopx^{WT/LacZ}$) mice. Quantifications of S100β and/or GFAP in β-galactosidase (βGal) expressing cells revealed no significant differences in their numbers. The majority of $βGal^+$ cells, in both backgrounds, maintained their astrocytic identity, shown by their expression of GFAP (Het: 86.0±2.3%; KO: 86.7±3.7%). However these populations were nearly free of S100β expression, which labels a fraction of GFAP astrocytes (**Figure 5C**). These results are largely in agreement with those obtained by the GoF approach. Hopx overexpression only resulted in minor, non-significant changes in the fraction of $S100β^-$ $GFAP^+$ cells following Hopx overexpression (increase from 40.9±7.1% to 56.5±3.7%), while the other two groups ($GFAP^-$ $S100β^+$; $GFAP^+$ $S100β^+$) were slightly decreased (**Figure 5D**). Interestingly, the number of cells expressing GFAP in the CC was however dramatically increased following Hopx GoF (**Figure 5E**). Together, these results suggest that Hopx is not a major determinant for astroglial specification of postnatal NSCs. The expansion of the cohort of GFAP expressing cells observed following Hopx GoF, rather suggests its role in amplifying the number of astrocytes being produced or their survival.

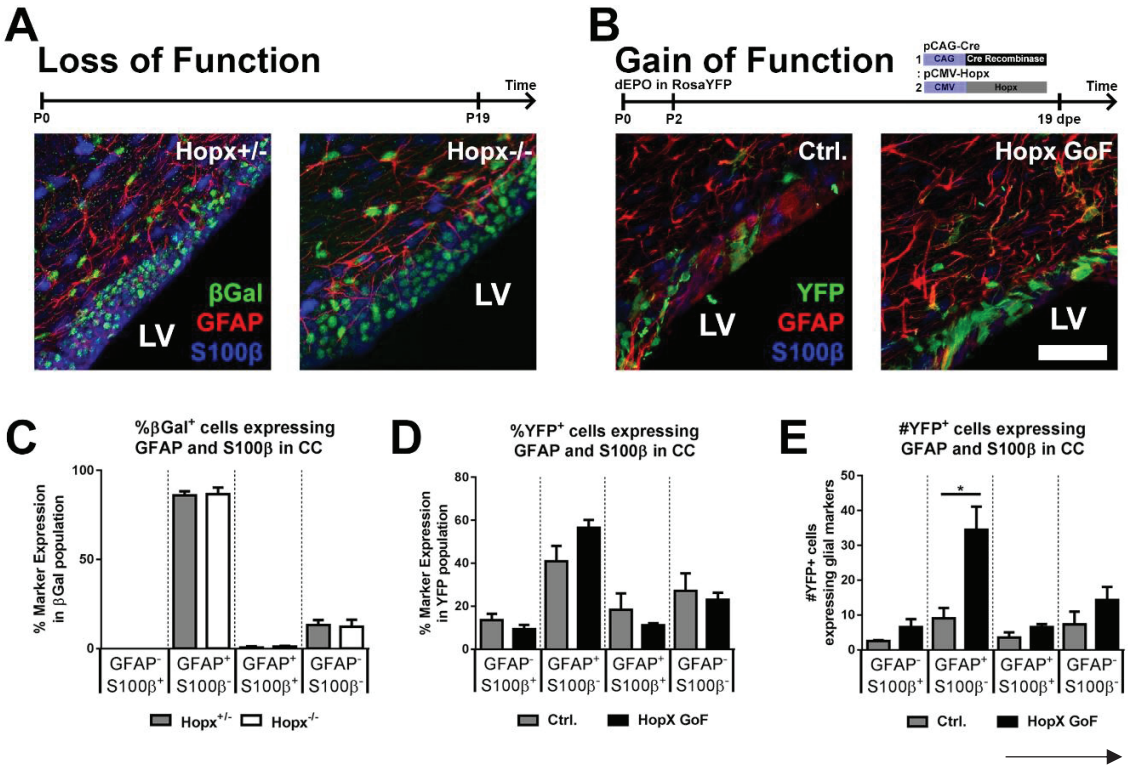

Figure 5. Hopx LoF and GoF approaches.
(A): *Hopx* KO and heterozygous animals were used to analyse the βGal$^+$ populations at P19.
(B): GoF experiments were performed by dorsal electroporation of pCAG-Cre and pCMV-Hopx plasmids (1:2) into RosaEYFP animals. Animals were sacrificed 19 dpe. Analysis of YFP$^+$ cells was performed in the CC.
(C-E): Quantifications of co-expression of S100β and GFAP in the βGal and YFP populations were performed in the CC. No differences in the fractions expressing S100β and/or GFAP were observed after *Hopx* KO or overexpression (C+D).
However, the total size of the YFP expressing population was increased after Hopx overexpression, notably the GFAP$^+$ fraction.
Animals: (C) Hopx$^{+/-}$, n=4; (C) Hopx$^{-/-}$, n=4; (D) Ctrl., n=4; (D) GoF, n=4.
Scale Bar: B = 50 μm. Abbreviations: dEPO, dorsal electroporation; dpe, days post electroporation; LV, lateral ventricle; Ctrl., control; GoF, gain of function; LoF, loss of function.

3.4.6. Hopx Overexpression Regulates the Appearance of Outer Radial Glial Cells

Driven by these observations as well as by recent reports of Hopx expression in outer radial glial cells in humans (Pollen et al., 2015 ; Thomsen et al., 2016), we next aimed at more directly assessing the effect of Hopx overexpression on NSCs behavior by sacrificing the animals at an earlier time point, i.e. 4 dpe (**Figure 6A**). Interestingly, we found a 200% enrichment of YFP$^+$ cells presenting a typical radial morphology, whilst non-RG like cells were less affected (**Figures 6B and 6C**). The fraction of RG cells and none-RG cells were uniformly increased along the medial to lateral aspects of the dSVZ (**Figure S5**). In line with these results quantifications confirmed an increased fraction of RG cells, expressing Mcm2 4 dpe in the dSVZ (Hopx GoF: 73.6±4.5%; Ctrl.: 60.6±3.7%; **Figures. 6D and 6E**). Remarkably, some of the RG cells observed following Hopx overexpression showed characteristics of oRG, a discrete population of ectopically located RG cells observed during corticogenesis in mice (Wang et al., 2011), which becomes predominant in humans. These oRG morphology exhibited a long basal process, no apical process, and were located away from the LV surface (most of them were found in the CC) where they maintained expression of NSC markers (i.e. Mcm2, Sox2; **Figures 6F and 6G**). To investigate the later consequences of the induction of this large population RG/oRG cells, the number of YFP$^+$ cells in the dSVZ, RMS and OB (**Figures 6H to 6L**), were quantified at 19 dpe. At this late time point, an increased number of glial cells in the CC (**Figure 5E**) could be detected, as well as a significant increase in the

number of neurons in the OB (**Figure 6L**). However, no ectopic neurons were observed in the cortex after Hopx overexpression, indicating that the increased neurogenesis remains destined to the OB.

Taken together, these observations indicate that Hopx overexpression increases RG cells number and induces the appearance of oRG shortly after electroporation, resulting in an increased germinal activity and a larger number of astrocytes and neurons being produced.

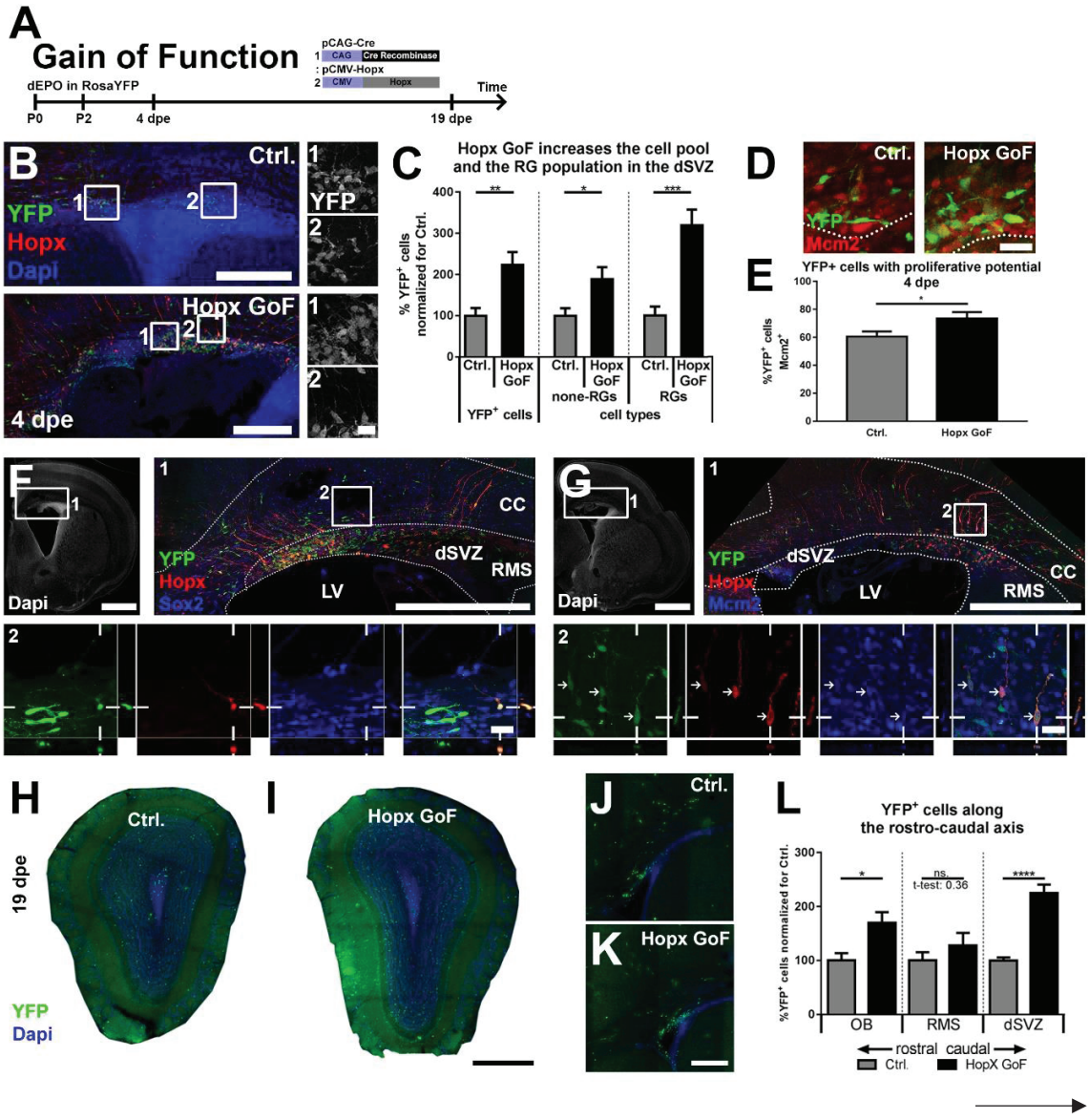

Figure 6. Hopx overexpression enlarges the pool of RG cells and results in an increased germinal activity.
(A): Quantifications were performed at 4 and at 19 dpe.
(B-E): The YFP^+ populations were analyzed for RG morphology (B+C) and proliferative potential (D+E) at 4 dpe. The population of RG cells, but also none-RG cells were increased following Hopx overexpression (C). A higher fraction of the YFP population was positive for the proliferation marker Mcm2 (E).
(F+G): YFP^+ cells with characteristics of oRG were observed 4 dpe, showing Sox2 (F) and Mcm2 (G) co-expression.
(H-L): The enlarged population of RG cells after Hopx overexpression results in an increased overall population of YFP cells at 19 dpe.
Animals: 4 dpe Ctrl., n=7; 4 dpe GoF, n=5; 19 dpe Ctrl., n=5; 19 dpe GoF, n=6.
Scale bars: B (overviews) = 250 µm; B (crop) = 25 µm; E = 25 µm; G+H (Dapi overviews) = 1 mm; G+H (fluorescence overview) = 500 µm; G+H (crops) = 25 µm; J+L = 500 µm.
Abbreviations: dEPO, dorsal electroporation; dpe, days post electroporation; Ctrl., control; GoF, gain of function; CC, corpus callosum; dSVZ, dorsal subventricular zone; RMS, rostral migratory stream; LV, lateral ventricle.

3.5. Discussion

In this study, we show that TFs of specific neural lineages are enriched in specific regions of the postnatal SVZ in agreement with their capacity to produce defined neural cell types. By selecting one of these transcripts, we show that NSCs are spatially segregated and primed to differentiate towards specific neural fates. Our results further identify Hopx as a marker of NSCs heterogeneity and suggest its association with the emergence of germinal traits observed during primate corticogenesis.

The diversity of neural subtypes generated by NSCs of the SVZ after birth is much larger than first believed. The concept of SVZ regionalisation in which the genesis of distinct neural lineages are spatially and temporally regulated is being increasingly investigated (reviewed in Fiorelli et al., 2015; Azim et al., 2016). NSCs located in SVZ microdomains originate from distinct regions of the developing forebrain (Fuentealba et al., 2015) and generate a large diversity of neural cells, including neuronal subtypes depending on the expression of specific transcriptional programmes (Merkle et al., 2007; Merkle et al., 2014; Fernández et al., 2011; Young et al., 2007). Consequently, expression of defined TFs is likely to directly correlate with the acquisition of specific neural fates, a concept that we have explored in the present study. We took advantage of the whole genome transcriptome of region-specific postnatal NSCs that we have recently resolved. Our analysis revealed that the major class of mRNA

transcripts differing in expression in region-specific NSCs, were transcriptional regulators, rather than the expression of receptors for signaling pathways, signaling ligands or metabolic processes (Azim et al., 2015). Additionally, meta-analysis of TFs expressed in dorsal and lateral NSCs with datasets of distinct neural lineages (Cahoy et al., 2008) highlighted transcriptional networks that correspond to the lineages derived from microdomain-specific NSCs. Together, our results suggest that NSCs are primed to acquire specific fates by the early expression of lineage-specific TFs. Such an early priming is supported by a recent single cell RNA-Seq characterization of SVZ NSCs (Llorens-Bobadilla et al., 2015), as well as by observations made in other tissues (Kim et al., 2016).

Exploring the spatial heterogeneity and restricted nature of NSCs in generating specific neural lineages will be greatly facilitated by the identification of regionalized NSCs markers. In this study, we identified Hopx as such a marker. Using two separate approaches, we show that Hopx expression is confined to a subpopulation of dNSCs, while it is consistently absent from lNSCs. These observations do not support recent reports highlighting expression of Hopx in quiescent NSCs, as these cells can also be found in the lateral SVZ (Codega et al., 2014). Our results rather suggest an association of Hopx with the astrocytic lineage, although they do not support a direct role of Hopx in specifying astrocytes. Indeed, Hopx loss of function and gain of function experiments revealed that it is redundant during initial astrogenesis from dNSCs, and suggest that it acts as a modulator of differentiation and acquisition of specific astrogenic traits such as GFAP expression, such as previously reported in other cell lineages (Obarzanek-Fojt et al., 2011). Importantly, although Hopx expression is observed in a subpopulation of NSCs that rapidly loses its ability to produce neurons but instead produces astrocytes, it cannot be considered as a pan-astrocytic marker. Indeed, whereas astrogenesis can be observed throughout the brain, Hopx expression is restricted to a subdomain of the postnatal dSVZ, namely its dorso-medial most region and is therefore likely to be associated with the generation of a subpopulation of astrocytes. Astrocytes heterogeneity has been recently highlighted in a number of studies. Fate mapping studies revealed that astrocytes are allocated to spatial domains in accordance with their embryonic sites of origin in the ventricular zone (Tsai et al., 2012). Further, transcriptomic analysis of astrocytes isolated from various brain regions reveal heterogeneous expression of several astrocytic markers, including Hopx (Morel et al., 2017). Interestingly, Hopx was reported to show a gradient, with higher expression levels in the dorsal

forebrain (cortex/hippocampus) compared to ventral subcortical (thalamus/hypothalamus) regions. Regional differences in astrocytes have been recently shown to influence neuronal synaptogenesis and maturation through secretion of several extracellular matrix proteins (Eroglu and Barres, 2010). In addition, density of astrocytes vary greatly between brain regions (Azevedo et al., 2009). The role of Hopx in influencing regional astrocytes properties and/or density remains to be explored.

Remarkably, postnatal Hopx overexpression increased the number of RG cells and induced the appearance of ectopic located cells resembling oRG. While oRG cells are rare in embryonic mice (Wang et al., 2011), their number increases dramatically in primates to form a secondary germinal region (i.e. the outer SVZ, or oSVZ) that contributes to the expansion of upper cortical layers during embryogenesis (Lewitus et al., 2013, Smart, 2002). Recently, a number of studies have reported Hopx expression in human oRG (Pollen et al., 2015; Thomsen et al., 2016). Furthermore, ectopic overexpression of the hominoid-specific gene *Tbc1d3* into radial glia in rodents, induces Hopx positive oRGs that contributes to cortical folding (Ju et al., 2016). In line with these observations, our overexpression results propose a novel instructive role of Hopx in oRG cells formation. They further reveal that ectopically generated oRG cells generated after birth may result in an increased olfactory neuronal yields. Taken together, our results suggest differential outputs of Hopx overexpression in dorso-medial and dorso-lateral NSCs, which are respectively $Hopx^{+}$ and $Hopx^{-}$. Thus, Hopx overexpression results in consolidating astroglial fates, in gliogenic NSCs, whilst inducing an RG phenotype in those primed to produce neurons. Consequently, Hopx regulates uniquely the numbers of both astrocytes and neurons as revealed by our quantifications.

The mechanisms by which Hopx mediates its functions remains largely unknown. Hopx is an atypical TF, which does not bind DNA per se. Therefore, it is likely modulating other TFs and/or effectors of signaling pathways at the post-transcriptional level. An interaction of Hopx with SRF has for example been demonstrated during cardiac development (Shin et al., 2002), but is unlikely to occur in the SVZ where SRF expression is remains low (data not shown). A more likely function of Hopx is the modulation of dorsally active signaling pathways. Our results show an activity of Bmp and Wnt pathways in dNSCs (see also Azim et al., 2014a; Azim et al., 2017), which have been demonstrated to link astrogenesis with neurogenesis during corticogenesis (Gross et al., 1996; Nakashima et al., 2001; Tiberi et al., 2012).

Reciprocal signaling between Bmp and Wnt has been reported in multiple progenitor populations (He et al., 2004; Kandyba et al., 2013; Plikus et al., 2008; Song et al., 2014; Genander et al., 2014). It is tempting to speculate that Hopx expression in the dorsal SVZ plays a role in the integration of these two signaling pathways as recently demonstrated in cardiomyoblasts (Jain et al., 2015). Future studies aimed at manipulating the activity of these two signaling pathways in *Hopx* KO animals may allow addressing these questions and investigate the role of extrinsic signals integration in lineage fate specification of neighbouring populations of NSCs. Other signaling pathways are likely to influence the pattern of Hopx expression and may have been involved in the evolution in the pattern of Hopx expression observed in primates. It is interesting to note that Hopx expression in the mouse SVZ follows the pattern of maturation of ependymal cells which might gradually restrict RG cells contact with the cerebrospinal fluid (Spassky et al., 2005). This combined with the expression of Hopx in oRG which lack apical processes in primates, suggest that an unknown cerebrospinal fluid derived signal may regulate Hopx expression. Such a signal might counteract or modulate Shh signaling which was recently identified in regulating oRG cell formation (Wang et al., 2016). Interestingly, Shh manipulation in mice results in oRG and gyri formation in the medial most aspect of the cortex, where high Hopx expression is evident. Expression of Hopx in primate oRG might have evolved from this original pattern of expression for the dual coupling of oRG cells and cortex expansion.

In summary, our work identifies for the first time that the dSVZ is much more heterogeneous than previously thought in terms of spatial segregation and early-priming of NSCs in generating specific neural lineages. The abundant expression of the TF Hopx contributes to the intraregional heterogeneity of the dSVZ in rodents, while its overexpression suggests its association with changes observed in germinal regions throughout evolution.

3.6. Acknowledgments

The authors would like to thank Jonathan A. Epstein for kindly sharing the $Hopx^{CreERT2}$ mouse line and Daniel Hohl for sharing the $Hopx^{LacZ/WT}$ knockin mouse line. Further, we like to thank Xavier Morin and Colette Dehay for providing plasmids for these experiments. We are grateful to Bruno Fischer and Anahi Hurtado-Chong for their technical assistance and Vanessa Donega

for critical reading of the manuscript. This study was supported by a Grant from the "Programme Avenir Lyon Saint-Etienne" and S.Z. was further supported by a Doc.Mobility fellowship from the Swiss National Science Foundation (SNF; grant number P1SKP3_168418). Other support was received from a SNF project grant NRP63 to O.R. (grant number 406340_128291) and SNF Advanced Post-doc mobility fellowship to K.A. (grant number P300P3_154614).

3.7. Supplementary Figures

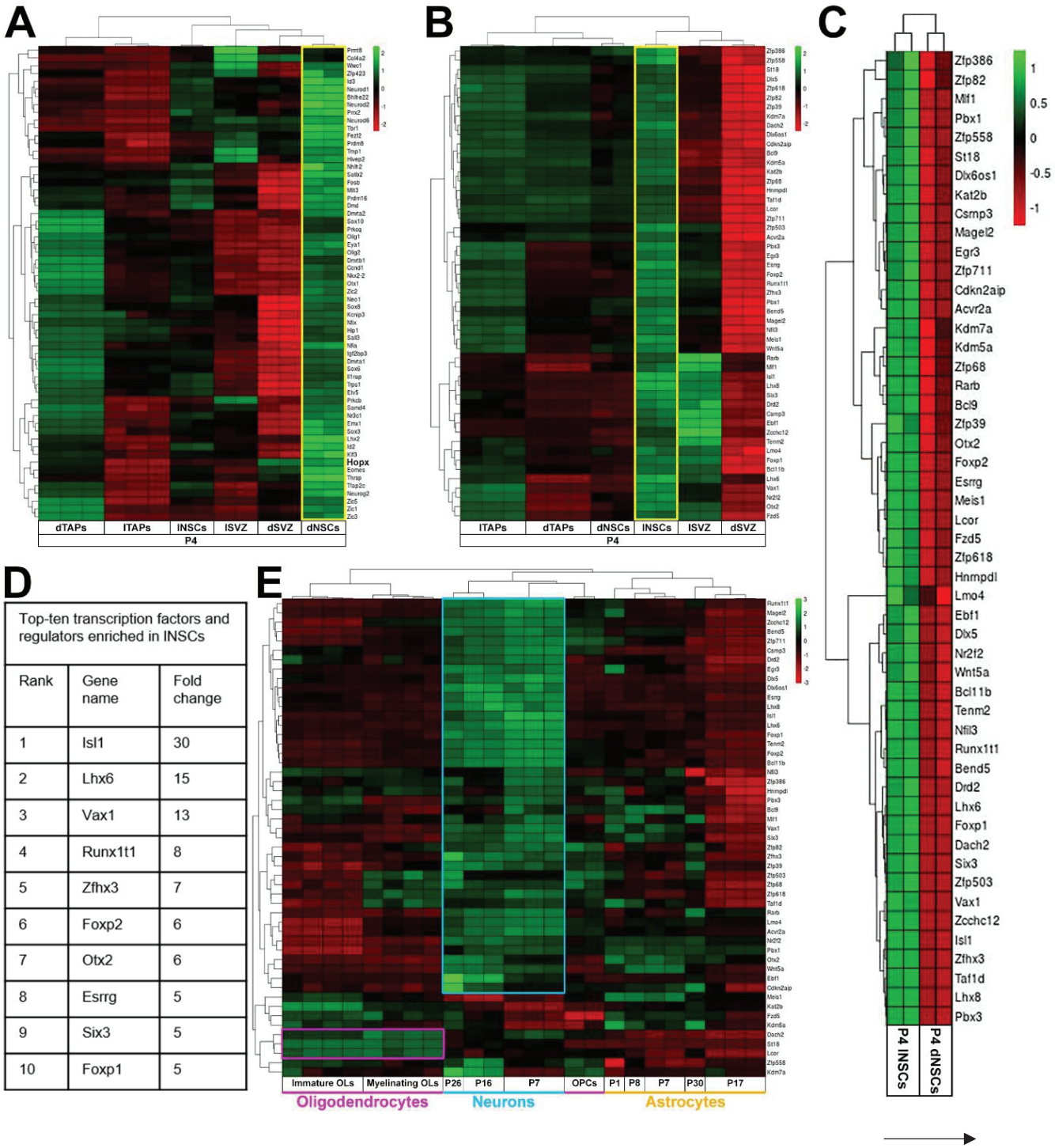

Figure S1. Analysis of TFs enriched in regionally separated NSC population.
(A+B): Heatmaps confirming the enrichment of selected TF transcripts in dNSC (vs. lNSCs (A)) and lNSCs (vs. dNSCs (B)), including the transcriptional profile in TAPs and the environment (SVZ) of those two regions.
(C): Heatmap of in P4 lNSCs enriched TFs compared to their dorsal counterparts (≥1,8 folds and p.Value<0,05).
(D): List of the top ten TFs enriched in lNSCs.
(E): Lineage-specific meta-analysis of lNSC TFs using the dataset from the Barres group: oligodendrocytes (purple, 3/51); astrocytes (yellow, 0/51); neurons (turquoise, 42/51).
Abbreviations: transient amplifying progenitors, TAPs; neural stem cells, NSCs; subventricular zone, SVZ; oligodendrocytye precursor cells, OPCs.

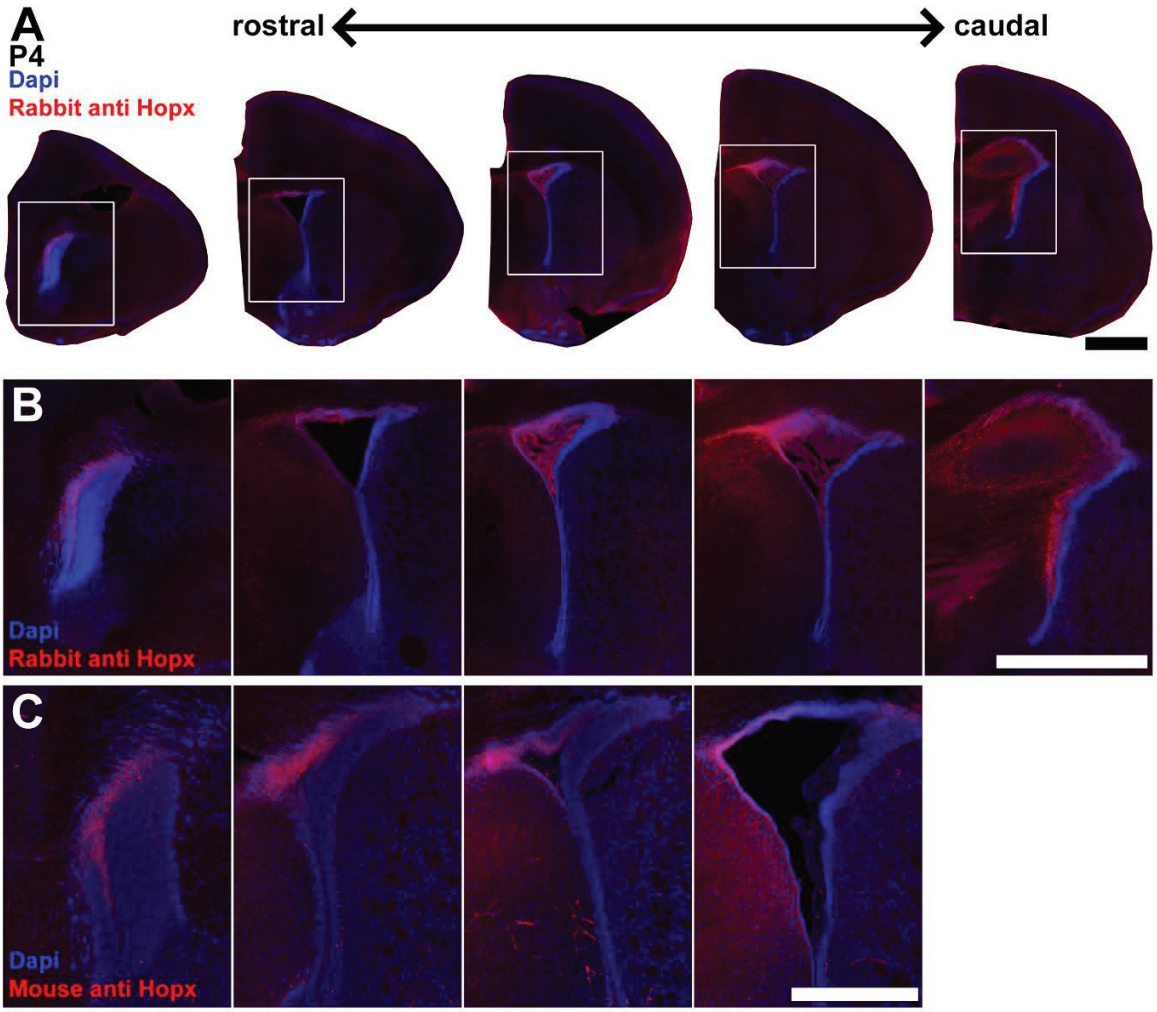

Figure S2. Spatial heterogeneity of Hopx expression at P4.
(A-C): Representative pictures demonstrate Hopx expression in a P4 animal along the rostro-caudal axis. The top and middle panel show overviews (A) and higher magnification pictures (B) of tissue stained with the rabbit anti Hopx antibody. The bottom panel shows higher magnification pictures of tissue stained with the mouse anti Hopx antibody (C). Note that both antibodies exhibit the same spatial pattern of Hopx expression.
Scale bars: A+B = 1 mm; C = 500 µm.

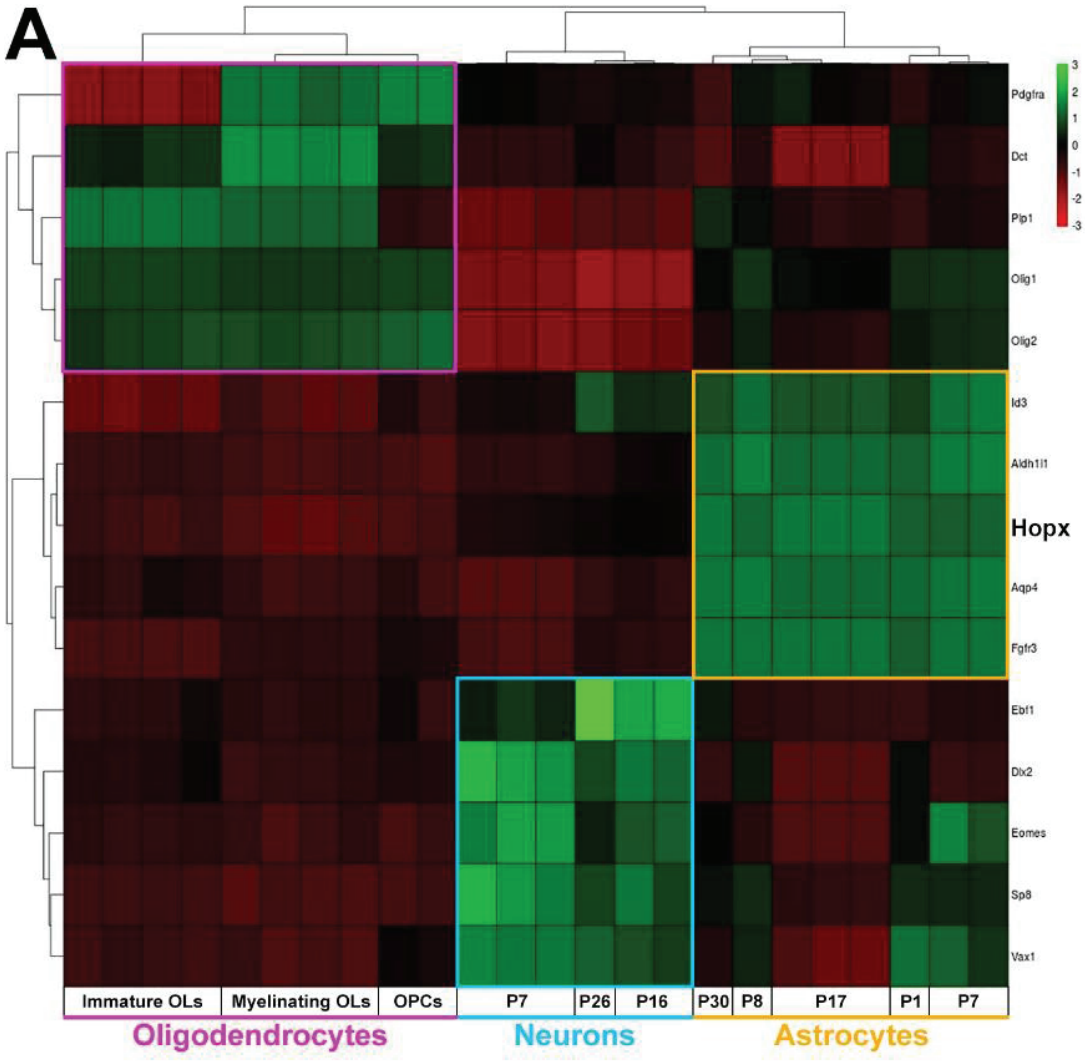

Figure S3. Confirmation of lineage specificity of selected transcripts using the dataset from the Barres group.
5 transcripts of the oligodendrocytic lineage (*PDGFRa, Dct, Plp1, Olig1, Olig2*), 5 of the neuronal lineage (*Ebf1, Dlx2, Eomes, Sp8, Vax1*) and 5 of the astrocytic lineage (*Id3, Aldh1l1, Hopx, Aqp4, Fgfr3*) were selected.

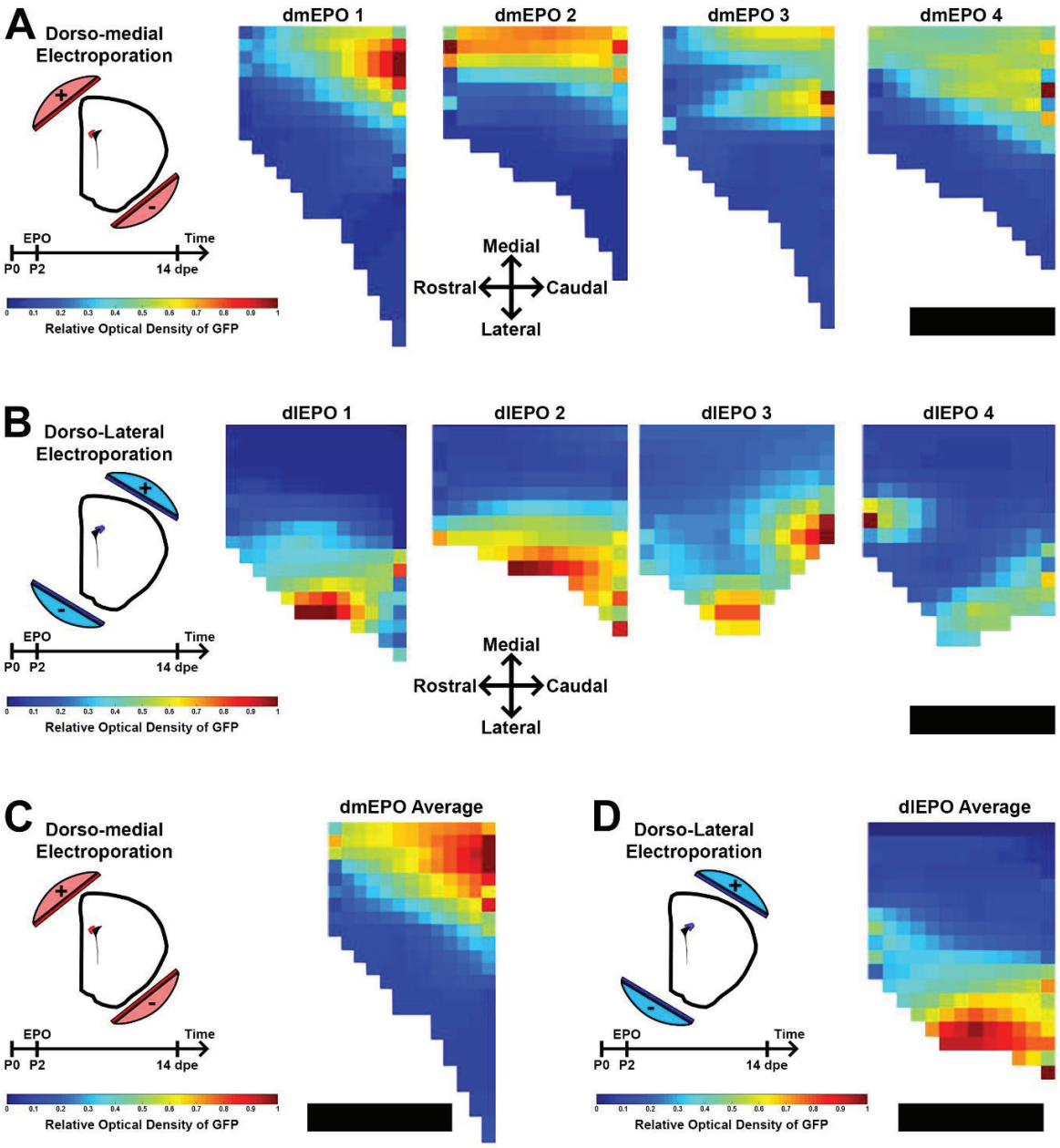

Figure S4. Optical density measurements of GFP reveal the high efficiency of targeted dorso-medial and dorso-lateral EPO.

(A+B): Heatmaps representing the relative optical density of GFP expression in the dorsal SVZ of different individuals following dorso-medial (A) or dorso-lateral EPO (14 dpe; B). Heatmaps are color coded (0 = dark blue; highest measured value = dark red) and generated with our recently developed software "FlashMap" (**Chapter 1**). Heatmap orientation is: left = rostral; right = caudal; top = medial; bottom = lateral.

(C+D): Heatmaps representing the averaged values of 4 animals those received dorso-medial (C) or dorso-lateral EPO (D). →

Animals: dmEPO, n=4; dlEPO, n=4.
Scale bars: A-D = 500 μm
Abbreviations: dpe, days post electroporation; EPO, electroporation; dmEPO, dorso-medial electroporation; dlEPO, dorso-lateral electroporation; SVZ, subventricular zone.

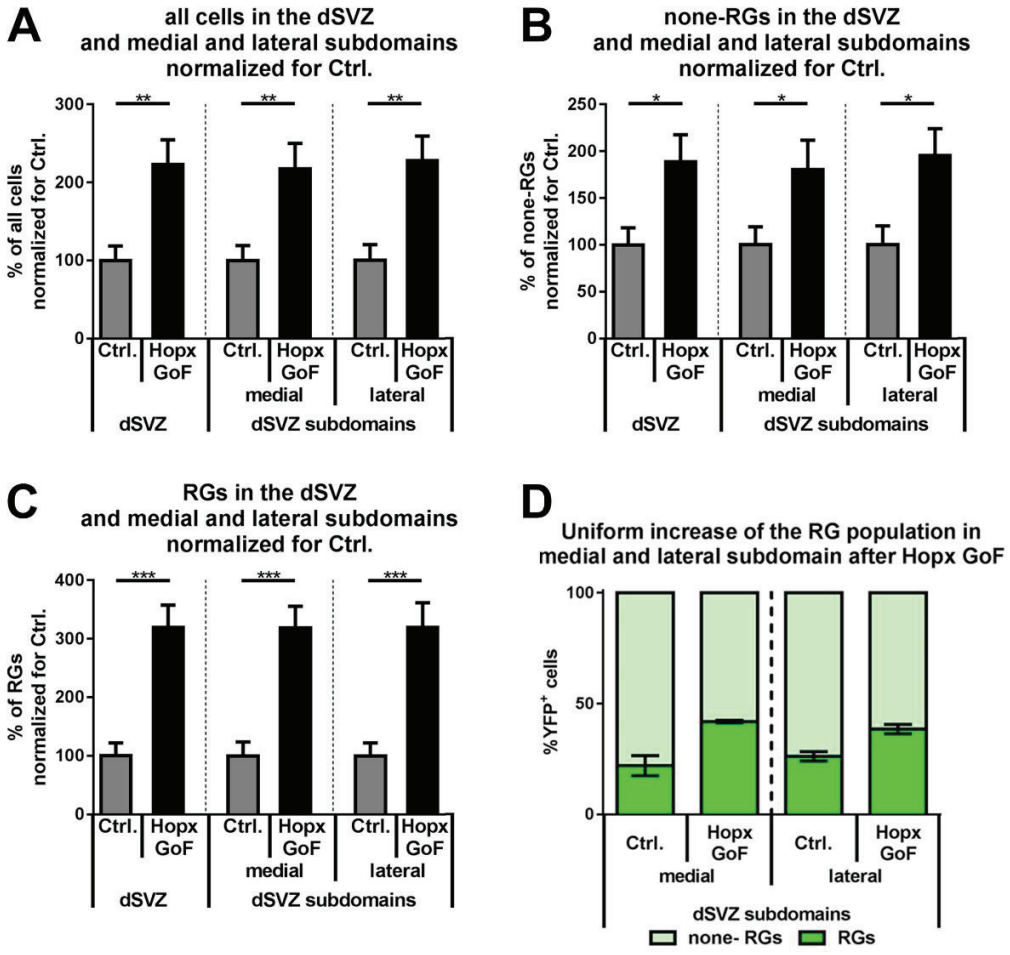

Figure S5. No difference in enlargement of the population after Hopx overexpression along the dSVZ.

(A-C): Full population (A), none-RG cells (B) and RG (C) are increased 4 days following Hopx overexpression. No difference in the enlargement between the medial and the lateral subdomain of the dSVZ was observed. Graphs are presented in percentage of the change normalized for control.

(D): The fractions of the RG population were equally increased in the medial and the lateral subdomain of the dSVZ following Hopx GoF.

Animals: Ctrl., n=7; GoF, n=5.

Abbreviations: Ctrl., control; dSVZ, dorsal subventricular zone; GoF, gain of function; RG, radial glia.

4. General Discussion

4.1. Summary and Open Questions

Germinal regions are not homogeneous, but highly heterogeneous. This heterogeneity relies on transcriptional differences, which underline the production of divergent cell lineages. New methods allow generating enormous transcriptional datasets to identify genes differentially expressed between distinct domains of germinal regions. Recently we demonstrated an unexpected level of transcriptional heterogeneity between the dorsal and lateral subventricular zone (SVZ), as well as in the neural stem cells (NSCs) and transient amplifying progenitors (TAPs) harbored by those microdomains. These findings underline the need to develop appropriate tools to integrate spatial information to the study of gene expression within the SVZ. To this end, we have developed a new tool, i.e. "FlashMap", to analyze and map protein expression along the full rostro-caudal and dorso-ventral extent of the SVZ (**Chapter 1**).

Germinal region heterogeneity does not stop at the mesoscopic scale (i.e. at the regional scale), but probably goes beyond. The second chapter of my thesis indeed suggests that previously described SVZ microdomains (Azim et al., 2015; for review Fiorelli et al., 2015) can be further subdivided. My results further support existence of a heterogeneity at the microscopic scale, i.e. at the cellular scale. Thus, neighboring NSCs appear to express different transcription factors that influence them respective behaviors and guide them through the acquisition of different fates. In the chapter 2 we described and discussed a new level of regional and lineage-specific heterogeneity in the dorsal SVZ based on Hopx expression (**Chapter 2**).

In the introduction of this thesis, I have discussed how advances in techniques have influenced our understanding of NSCs biology, from the macroscopic (i.e. the demonstration of persisting germinal regions in the postnatal brain) to the mesoscopic scale (the subdivision of these germinal regions in microdomains). It is likely that emerging techniques will now allow us to investigate this heterogeneity at the microscopic scale. The development of new approaches is a pre-requisite to perform these studies. Indeed, current approaches such as BrdU injection, regular electroporation (EPO), as well as most transgenesis approaches only allow studying NSCs at the population level. This does not allow concluding if neuron subtypes, astrocytes and oligodendrocytes arise from single NSCs, or if multiple subpopulations of unipotent NSCs co-exist. Here I will discuss current evidences, including my own results, supporting

heterogeneity at the cellular level. I will also discuss how single cell approaches in transcriptomic and histology are currently changing our understanding of NSCs identity.

4.2. The Potency of Postnatal NSCs: From a Population of Multipotent NSCs to Populations of Restricted NSCs

In vivo and *in vitro* evidences indicate that NSCs gradually lose their potency and get more and more restricted throughout central nervous system (CNS) development.

4.2.1. *Drosophila* Neuroblasts as a Model of Progressive Restriction

Drosophila neural precursors (i.e. neuroblasts) have been extensively studied, as a model to investigate the progressive fate restriction and plastic potential of NSCs. These precursors have been shown to sequentially express the transcription factors (TFs) Hunchback, Krüppel, Pdm and Castor. These transcription factors have been suggested (at least Hunchback and Krüppel) to be necessary and sufficient for the sequential generation of distinct neuronal subtypes. Thus, neuronal subtypes produced at different time points, inherit and maintain the expression of these TFs, while they are rapidly downregulated in neuroblasts (**Figure 1A**). This temporal expression defines the fate and spatial destination of the newborn neurons. For example, the expression of Hunchback and Krüppel in early born neurons defines their deep layer position as well as the development of long axons (Isshiki et al., 2001; Pearson and Doe, 2003). Such temporal cues are called temporal identity factors (Kohwi and Doe, 2013). A lack of Hunchback or Krüppel expression in neuroblasts leads to a lack of the corresponding progeny. On the other hand, forced expression of one of these early factors leads to a forced generation of the corresponding progeny. However, this effect is only observed until the fifth division (Isshiki et al., 2001; **Figure 1B**). Therefore, it has been suggested that there is a temporal competence window during which such manipulations can be successfully performed (Cleary and Doe, 2006; Kohwi and Doe, 2013).

Taken together, *Drosophila* neuroblasts represent a relevant example for the sequential generation of distinct cell types, and support a progressive loss of their competence over time.

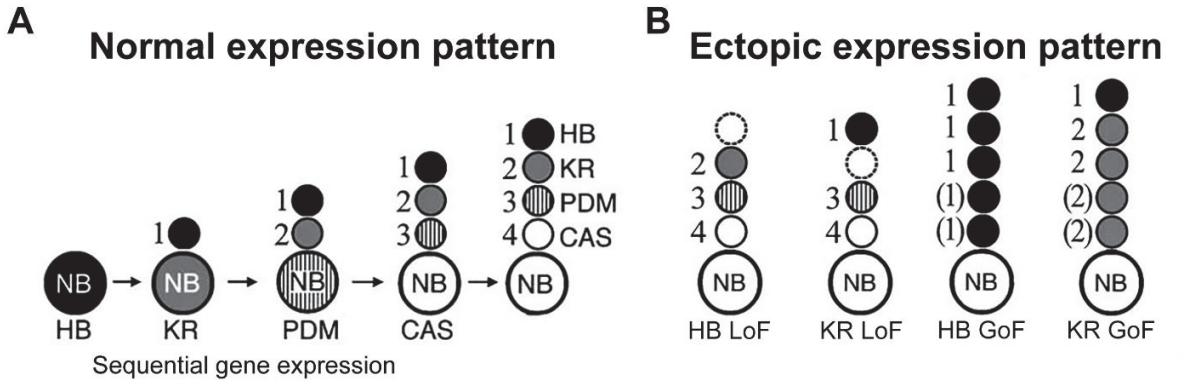

Figure 1. *Drosophila* neuroblasts as a model of progressive fate restriction.
(A): Illustration of the sequential expression of Hunchback (HB), Krüppel (KR), Pdm and Castor (CAS) by *Drosophila* neuroblasts (NB). While this gene expression is transient in neuroblasts, progenies retain gene expression and acquire a gene specific fate.
(B): Illustration of the effects resulting from a disturbance of this sequence. Ablation of HB or KR leads to a lack of the respective progenies. Forced expression of HB or KB leads to a forced generation of the corresponding progenies (modified from (Isshiki et al., 2001)).
Abbreviations: NB, Neuroblast; HB, Hunchback; KR, Krüppel; Cas, Castor; LoF, loss of function; GoF, gain of function.

4.2.2. *In Vitro* and *In Vivo* Evidences Suggest that Cortical Progenitors Progressively Lose Their Potency to Produce Early Born Neurons

In vitro experiments suggest a similar situation in mammals. Time-lapse video microscopy in clonal cultures of cortical progenitors demonstrated their generation of distinct progenies following a strict sequence, i.e. first neurons then glial cells (Qian et al., 2000). Regarding the neurogenesis phase, another level of sequential lineage generation has been demonstrated. It has been shown that the order of neuron subtypes generation, destined to different cortical layers, is intrinsically programmed and preserved *in vitro*. Further, the competence of cortical progenitors appears to become increasingly restricted. Noticeably, mid-gestational progenitors can still be manipulated to generate early neuronal fates, while late-gestational progenitors have lost this competence (Shen et al., 2006). Interestingly, adult NSCs exhibit a lineage restriction and appear to be bipotent *in vitro*. Clones have been found to consist of neurons and astrocytes or oligodendrocytes and astrocytes. However, neurons and oligodendrocytes were never found within the same clone (Ortega et al., 2013). Taken together, this *in vitro*

experiments suggest not only a sequential fashion of embryonal lineage and subtype generation, but also a certain degree of potency restriction postnatally.

This progressive loss of competence by progenitor cells has also been shown *in vivo* by transplantation experiments. Early heterochronic (temporal) transplantation approaches have found that the potential of different progenitor populations to generate distinct neuronal subtypes becomes gradually restricted over time (for review Gaiano and Fishell, 1998). For instance, cycling progenitors from late stages of the ferret corticogenesis, keep their intrinsic restriction, even if transplanted into an early stage environment. Indeed they keep generating upper layer neurons and fail to produce deep cortical layers, which are normally generated at this age (Frantz and McConnell, 1996). In contrast, early progenitors are able to adapt to the host environment to generate upper layer neurons, when transplanted into a late stage environment (Desai and McConnell, 2000). These original experiments support a gradual fate restriction of cortical progenitors, a model that is still accepted today.

More recent observations question this fate restriction and suggest that postnatal and adult stem cells can give rise to a larger diversity of cell types than previously thought. Thus, *ex vivo* experiments showed that postnatal and adult SVZ explants have the capacity to generate pyramidal neurons. In this experiments, adult SVZ explants were exposed to an embryonic environment by juxtaposing them to organotypic slices of the pallium. Neurons were produced by the SVZ explants, which invaded the pallium. Their expression of Tbr1 suggested their acquisition of a glutamatergic phenotype, although their maturation could not be investigated at long term (Sequerra et al., 2010).

These observations challenge the current model of a gradual fate restriction proposed by McConnell. They suggest that postnatal and adult NSCs, under specific experimental conditions, can generate cell types produced at earlier developmental time points. These discrepancies may be explained by the identity of the transplanted cells. While in the first two studies only cycling progenitors were transplanted, the third study used SVZ explants, which also contain quiescent NSCs. These quiescent NSCs have been recently suggested to have an embryonic origin. Thus, a subpopulation of radial glial cells would become quiescent between the embryonic day 13.5 (E13.5) and E15.5 (Furutachi et al., 2015; Fuentealba et al., 2015) and remain in the SVZ, to be “reactivated” at postnatal time points. It is tempting to speculate that

these cells may keep their competence to generate cortical neurons (for review Donega and Raineteau, 2017).

Altogether, these observations suggest a complex cellular heterogeneity of the postnatal SVZ, with the presence of subpopulations of NSCs showing distinct competences juxtaposed. Addressing this complexity cannot be done at the population level, but requires the development of clonal approaches to follow the fate of individual NSCs.

4.3. Clonal Approaches in Histology

Original *in vivo* clonal approaches rely on the permanent but sparse labeling of NSCs within the germinal region of interest. This allows following the fates of single NSCs over extended periods. These approaches are, however, time-consuming, in particular when progenies distribute throughout large areas. Sparse labeling is suitable for clonal analyses in the adult dentate gyrus (DG), as clones stay relatively close to their region of origin (<150 μm within 2 months; Bonaguidi et al., 2011). Sparse labeling can also be used for clonal analyses of embryonal NSCs. While these progenies migrate longer distances, they distribute along cortical columns regardless of the cell type (Gao et al., 2014). This allows to differentiate clones if the labeling is achieved sparsely. However, the situation in the postnatal SVZ is strikingly different. In addition to their migration of long distances, different lineages are destined for different destinations. Therefore, just one single NSCs should be labeled per animal. This is, however, very time-consuming and almost impossible to achieve, guarantee and control. Later approaches have tried to circumvent this main limitation. They make use of multiple markers for a retrospective identification of single clones. These techniques include bar coding of progenitors and multicolor approaches.

4.3.1. Sparse Labeling as a First Approach for Clonal Analyses

First attempts were made by infusing low titers of a retrovirus in the ventricular system of rat embryos. Postnatal analyses of multiple animals suggested neuronal- or glial-specific clones in the cortex and striatum. In addition, neuronal clones were often found to be restricted to

specific (deep or superficial) cortical layers. These results support the coexistence of fate restricted progenitors in the developing CNS (Krushel et al., 1993).

Later studies made use of the Cre-Lox system to perform clonal analyses after inducing minimal recombination. The mouse line expressing Cre under the control of the Thy-1.2 promoter can be used for achieving such "sparse recombination". Their crossing with Z/EG mice leads to sparse labeling of radial glia (RG) cells in embryos, which give rise to cortical columns. Estimations of the diversity of lineages within single columns in adult mice, revealed that 95% contained both astrocytes and neurons. Interestingly, the astrocytes were found to be generated later than neurons. While columns are completely free of astrocytes at E18, cells with immature astrocytic morphologies appear at the postnatal day 1 at the apical end of the columns. The number of astrocytes observed in the columns increases substantially with age (Magavi et al., 2012). These results contrast with those obtained with the retroviral approach (see above), as they indicate that most RG cells are bipotent, i.e. are first generating neurons and then astrocytes at late embryonic stages. However, it is possible that these two approaches result in the labeling of distinct progenitor populations.

Further clonal experiments were performed in adult mice. Bonaguidi et al. developed a single cell lineage tracing approach in the DG. This approach was based on the administration of low tamoxifen doses into nestin-CreERT2-Z/EG mice. Minimal recombination rates in the DG allow to distinguish clones with a high degree of confidence. Self-renewal of RG-like cells, the NSCs of the DG, and also multipotency of a significant fraction of clones was demonstrated. However, the fraction of multi-lineage clones (producing both neurons and astrocytes) was rather low compared to the single-lineage clones (1 month post injection: 12.9% multi-lineage clones vs. 80.6% single-lineage clones vs. 6.5% undifferentiated clones; 2 months post injection: 19.2% vs. 73.1% vs. 7.7%; Bonaguidi et al., 2011). One can conclude that there are indeed multipotent NSCs cells present in the adult DG, but they represent a minor fraction. Indeed, most NSCs appear to be committed to produce a single cell type, and are therefore unipotent. It is unlikely that these "unipotent" clones generate other cell types overtime. Thus, the germinal region of the adult hippocampus harbor a heterogeneous population of NSCs, with only a minority of them being multipotent.

The situation might be similar in the SVZ, which shows an even greater transcriptional heterogeneity than the subgranular zone of the dentate gyrus (Fiorelli et al., 2015). Performing such experiments in the SVZ is however more challenging. Indeed, cells produced by SVZ NSCs have the capability to migrate long distances to diverse forebrain regions (Fernández et al., 2011; Bayraktar et al., 2015). Performing a clonal analysis at long survival time points, therefore require the systematic sampling of a large region extending from the olfactory bulb (OB) to the lateral ventricle.

To address this issue and to maximize the number of "clones" one can study in a single animal, multicolor approaches have been developed. The MADM (mosaic analysis with double markers) is such an approach. It is based on interchromosomal recombination driven by a Cre-recombinase (Zong et al., 2005). It relies on the use of only two markers, which makes it suitable to investigate embryonic rather than postnatal SVZ NSCs potency. Sparse labeling of RGs by administration of low concentrations of tamoxifen allows to study individual clones during corticogenesis. Single clones were shown to give rise to both deep and superficial neurons if recombination was initiated between E10 and E13. Recombination at a later time point (i.e. E15) were mainly composed of superficial neurons only. This is in agreement with the inside-out sequence of neuron production during corticogenesis. Astrocytes and oligodendrocytes were also detected in clones. However, just 1 clone out of 6 harbored glia cells. This indicates that only a minor fraction of cortical RGs are truly multipotent and make the neurogenic to gliogenic switch (Gao et al., 2014). The discrepancy between the findings of Magavi (95% multi-lineage clones; Magavi et al., 2012) and Gao (17% multi-lineage clones; Gao et al., 2014) might be explained by differential induction of recombination. While Gao induced recombination not before E10, Magavi used the Thy-1.2 promoter to trigger Cre expression, which might be active already earlier.

4.3.2. Bar Coding of Progenitors Exhibits a Subpopulation of Embryonal NSCs Entering Quiescence for Postnatal Preservation

Another elegant, but also very challenging clonal approach, makes use of a QmGFP-OL retroviral library to integrate unique bar codes into different embryonic ventricular NSCs.

GFP^+ progenies from embryonal infected NSCs can be detected postnatally in the OB, cortex, striatum, septum and hippocampus. The clonal relationship between cells is unraveled by examining the different bar codes across the entire population of GFP^+ cells. This "tour de force" experiment allowed to demonstrate that postnatal OB interneurons and cortical, hippocampal, striatal or septal neurons are mostly unrelated. Further, it has been shown that most adult NSCs originate at E13.5-E15.5 by entering quiescence at this time. These NSCs keep their regional identity from E15.5 on, to generate distinct progenies in the adult OB (Fuentealba et al., 2015). These findings were corroborated by another group, which independently demonstrated that adult NSCs originate from embryonic stem cells that enter quiescence around E13.5-E15.5 (Furutachi et al., 2015).

4.4. Development of Multicolor Approaches for High Throughput Clonal Analysis

A solution for accurate and concomitant analysis of multiple clones in histology appears to be the development of multicolor approaches. A number of those approaches have been developed in the recent years, which remain to be fully exploited in the context of postnatal germinal activity.

4.4.1. Brainbow Inaugurated the Era of Multicolor Clonal Approaches

The Brainbow technique, is a powerful Cre mediated excision and/or inversion approach that stochastically labels multiple neighboring cells with cell specific color-codes. It has the power to label cells with approximately 89 distinct colors, which are different enough for discrimination (Livet et al., 2007). The beauty of this method is that the color coding is driven by Cre-recombinases. This allows the use of different Cre or $CreER^{T2}$ reporter mice, which careful selection leads to a more accurate analysis. Further, the administration of minimal doses of tamoxifen may restrict the number of recombination to ensure the singularity of specific color codes. Cre-recombinases may also be electroporated into specific microdomains for spatial restriction and control of the number of recombination. Interestingly, the Brainbow technique is one of the rare techniques that was first developed in the mice CNS, then adapted

to other tissues and species (for review Weissman and Pan, 2015). For example another mouse line expressing the Brainbow-cassette under an ubiquitous promoter allowed investigations in the intestine (R26R-Confetti; Snippert et al., 2010). Further, the approach has been adapted to species like *Drosophila melanogaster* (Hampel et al., 2011) and zebrafish (Pan et al., 2011). Even a clonal deletion system in plants has been developed based on Brainbow (Wachsman et al., 2011). As a practical example of the applicability of the Brainbow-cassette, it has been used to demonstrate a limited self-renewal of adult SVZ NSCs (Calzolari et al., 2015).

Further, the Brainbow-cassette has been integrated into plasmids for EPO approaches. The approach is called MAGIC (multiaddressable genome-integrative color) and consists of Brainbow-cassette transposon vectors, with specific expression in the cytoplasm (Cytbow), the cell membrane (Palmbow), the nuclei (Nucbow) or the mitochondria (Mitbow). The adaptation of Brainbow to the targeted EPO method does not only add a spatial component to the method, but also ensures its suitability for other species than mice, as illustrated in the chicken (Loulier et al., 2014).

4.4.2. StarTrack Gives Insights into Restricted Potency of NSC Populations

Another elegant multicolor approach, StarTrack, was developed by the López-Mascaraque laboratory. StarTrack consists of 6 fluorescence proteins (mT-Sapphire, mCerulean, EGFP, YFP, mKO, mCherry), each targeted to the cell nucleus (by human H2B histone fusion) or cytoplasm. The *PiggyBac* transposon system is used to stochastically integrate them into the genome, leading to unique color-codes of those 12 features in distinct NSCs. The inheritance of these color-codes by progenies ensures efficient clonal analysis. Fluorescent protein expression was initially driven by human GFAP promoters to investigate astrocyte heterogeneity. Briefly, *in utero* EPO experiments revealed that fibrous and protoplasmic clones are largely non-overlapping and emerge from separate lineages. In the case of pial clones, which reside in a region containing both protoplasmic and fibrous-like (pial) astrocytes, it has been shown that nearly 90% of the clones consist of one single astrocyte subtype. Clones showed mostly radial distribution and reside in a highly spatially restricted area in the corpus callosum, the cortex or cortical surface. Finally, single clones were constantly observed to be

associated with one specific blood vessel (García-Marqués and López-Mascaraque, 2013). These observations confirm the maintenance of an inherited spatial relationship of RG cells and their astrocytic progeny.

Interestingly, this GFAP promoter driven plasmid mix also allowed the investigation of NG2 glia, which are referred as oligodendrocyte progenitors (Zhu et al., 2008). This is due to the weak activity of the human GFAP promoter in the NG2 lineage, as described elsewhere (Matthias et al., 2003). Remarkably, these clones remained small during embryogenesis and early postnatal ages, but form the largest clones of the adult brain with an average of 170 cells extending up to 1.1 mm along the rostro-caudal axis (García-Marqués et al., 2014).

The natural limitation of StarTrack for investigation of the NSCs potency is its selective expression in astrocytes (and NG2 glia), which is inherent to the use of the human GFAP promoter (García-Marqués and López-Mascaraque, 2013; García-Marqués et al., 2014). To circumvent this limitation, the López-Mascaraque lab developed a similar set of transposons under a ubiquitous promoter (UbC-StarTrack). In addition to the 12 fluorescence protein carriers and integration helper plasmid (CMV-hyPBase), a tamoxifen inducible Cre-Lox system was developed to further refine the method (**Figure 2A**). This allows a degradation of non-integrated transposons, and therefore preventing subsequent changes in color-codes. UbC-StarTrack has already been tested *in vitro* (HEK cells), *ex vivo* (embryonic brain slices) and *in vivo in utero*. It has been shown to efficiently label cells of the neuronal, astroglial and oligodendroglial lineages (Figueres-Oñate et al., 2016). During the last year of my PhD, I attempted to establish this method in the lab to study the competence of individual postnatal NSCs to produce cells of distinct lineages (**Figure 2B**).

Figure 2. The UbC-StarTrack technique is a powerful tool for clonal analysis of dorsal SVZ neural stem cells.
(A): The UbC-StarTrack technique combines different transposon constructs that allow the random expression of combinations of fluorescent proteins. 12 constructs coding for cytoplasmic vs. nuclear (H2B) fluorescent proteins (mT-Sapphire: Ex. 399 – Em. 511; mCerulean: Ex. 433 – Em. 475; EGFP: Ex. 488 – Em. 507; YFP: Ex. 514 – Em. 527; mKO: Ex. 548 – Em. 559; mCherry: Ex. 587 – Em. 610) are used. The presence of the hyPBase transposase allows their random integration into the electroporated cells genome. ⟶

Non-integrated constructs are subsequently eliminated by activation of a co-electroporated Cre-recombinase, allowing unique combination of fluorescent proteins to be expressed by single neural stem cells and their progeny.
(B): Preliminary results show successful implementation of this method, as demonstrated in the representative pictures of the SVZ following dorsal EPO.
Note that expression of the fluorescence proteins is observed at different frequencies resulting in different color coding of single clones. Some constructs are integrated at a lower frequency (e.g. mCerulean; mKO) therefore facilitating the clonal quantitative analysis.
Scale bar: B (overview) = 1 mm; B (crops) = 200 µm. Abbreviations: EPO, electroporation; SVZ, subventricular zone.

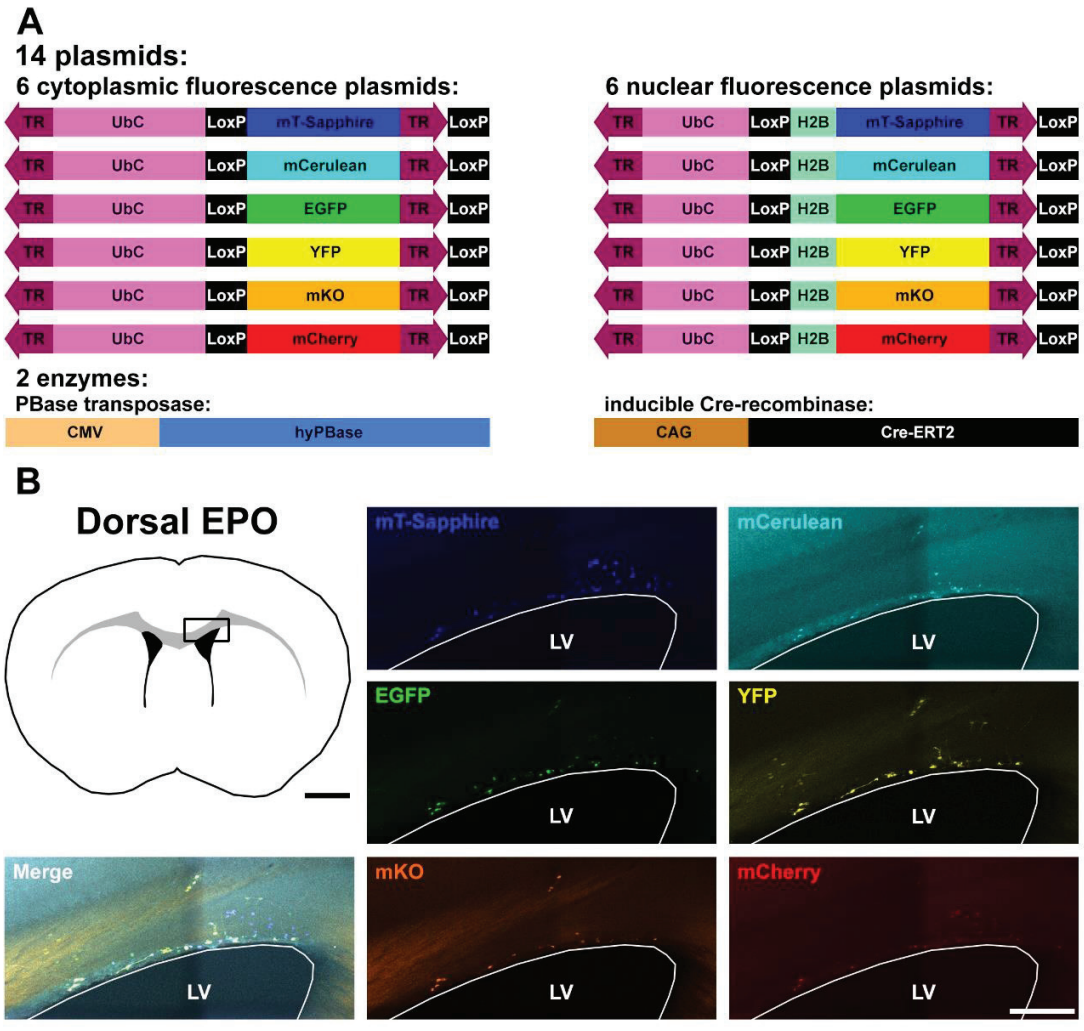

4.4.3. CLoNE – an Inducible Multicolor Approach

The concomitant detection of 6 fluorochromes (and multiple combination of them) is often challenging, as it requires the use of a high-end confocal microscope equipped with a white laser. Another multicolor EPO approach, CLoNe (Clonal Labeling of Neural progenies; García-Moreno et al., 2014), has been developed with a more limited number of fluorescence proteins (4 instead of 6, i.e. mT-Sapphire, EGFP, EYFP, mCherry; UbC-StarTrack contains in addition mCerulean and mKO). Each fluorophore plasmid however comes in 3 different variants for nuclear (human H2B histone sequence), cell membrane (palmitoylation sequence) or cytoplasmic (no specific localization sequence) expression. Thus although color codes are less numerous, the differential color distribution in the 3 cell compartments allows discrimination of a large number of clones. Another major difference to other methods, is the use of a Cre-recombinase to restrict expression to a specific cell type and/or stage of differentiation. The selective expression of the Cre-recombinase to NSCs population, and or to specific lineages, can then be achieved by the use of specific promoters (e.g. pEmx2-Cre; $Tbr2^{Cre}$).

Together, these multicolor approaches underline the need to develop methodologies to study NSCs heterogeneity and their lineage commitment in health and disease. It is likely that an ongoing development of such approaches will occur in the coming years. For example, it might be interesting to add a temporal aspect to color code induction by using tamoxifen inducible $CreER^{T2}$-recombinases. This could be done by the use of transgenic mouse lines or by the use of integrable plasmids controlled by ubiquitous or restricted promoters. $CreER^{T2}$-recombinases could also be the method of choice to achieve sparse recombination in order to guarantee the singularity of the color codes.

4.5. Clonal Approaches in Transcriptomic

Transcriptional profiling is classically performed on a population of cells (bulk analysis). Recently, methods have been developed to achieve transcriptional profiling of single cells. These approaches are very complementary. While bulk analyses give insights into transcriptional changes occurring during differentiation and lineage commitment, single cell analysis allows investigating the heterogeneity existing within a cell population.

4.5.1. Bulk Analysis Reveals Transcriptional Specificities of Postnatal Germinal Regions

For bulk analysis, cell populations of interest are enriched by FACS, based on their expression of specific markers. Their mRNA is extracted then analyzed by microarrays, qPCR or RNA sequencing approaches.

These methods gave us deeper insights into transcriptional differences that exist in distinct neural lineages (i.e. in maturing astrocytes, neurons and oligodendrocytes), between SVZ and DG NSCs and SVZ NSCs of different levels of activation. For example Aldh1l1 has been identified to be highly specific for the astrocytic lineage and subsequently became a widely used marker. Further, it has been found that the two macroglia lineages, i.e. astrocytes and oligodendrocytes, are transcriptionally as far apart from each other, as they are from neurons (Cahoy et al., 2008). Comparisons of transcriptional profiles of DG and SVZ NSCs identified IGF2 to be highly enriched in the DG. In this region, IGF2 was shown to control the NSCs proliferation through AKT-signaling (Bracko et al., 2012). In the SVZ the early expression of neuronal markers in NSCs has been demonstrated. This is in agreement with our findings suggesting an early priming of NSCs (**Chapter 2; Figures 1 and S1**). Further, the importance of cilia- and Ca-dependent pathways were emphasized (Beckervordersandforth et al., 2010). Thus, transcriptional profiling reveal specificities of both DG and SVZ NSCs. Another study investigated an additional level of heterogeneity within NSCs. Based on the expression of the EGF receptor in activated NSCs they were discriminated from their quiescent counterparts. This allowed to discover multiple markers for these two stages and uncovered signaling pathways that may be targeted by small bioactive molecules to regulate NSCs activity (Codega et al., 2014). Our own work added a spatial dimension to the transcriptional profiling of the postnatal SVZ. The dorsal and lateral SVZ microdomains were microdissected and their transcriptional profiles compared. This comparative analysis, which was also applied to the NSCs and TAPs they contain, demonstrated an unexpected high level of transcriptional heterogeneity (Azim et al., 2015). This study also revealed transcriptional regulators as major hallmarks that sustain postnatal SVZ regionalization.

Accumulating datasets from various germinal regions and cell types can be combined to perform transcriptional meta-analysis. For example our datasets from regionalized NSCs

populations (Azim et al., 2015) were combined with a lineage-specific dataset (Cahoy et al., 2008). Such meta-analysis reveal remarkable differences in the lineage priming of regionalized NSC populations (Azim et al., 2016). While the dorsal population expresses increased levels of diverse neural lineages (astrocytes, neurons, oligodendrocytes; **Chapter 2; Figure 1**), the lateral population seems to be particularly primed towards the neuronal lineage (**Chapter 2; Figure S1**), as suggested elsewhere (Beckervordersandforth et al., 2010). We demonstrated how such meta-analyses can expose previously ignored factors, as the dorsally enriched astrocyte marker Hopx, for further investigation (**Chapter 2**). It is likely that many other regionally expressed genes will be identified by such meta-analyses. An accurate tool for rapid expression analyses of such markers along the full extent of the SVZ was long missing. We closed this gap by developing "FlashMap" (**Chapter 1**).

4.5.2. Single Cells Analysis Refines Current Transcriptional Knowledge

New approaches allow breaking down cell populations to investigate their transcriptional heterogeneity at the single cell level. Single cells are captured in micro-chambers and their mRNA isolated and sequenced. This allows comparing the transcriptome of multiple cells to highlight similarities (i.e. clusters of cells) and differences (i.e. separate clusters).

Single cell RNA-sequencing was recently performed on adult NSCs from the SVZ. This allowed identifying several clusters of cells, which present different states of activation. Therefore, it demonstrated that NSC activation follows a sequence of transitions: dormant cells (quiescent NSCs type 1) first enter a primed quiescent state (quiescent NSCs type 2) before becoming activated (activated NSCs type 1). This sequence is paralleled by a downregulation of the glycolytic metabolism and of Notch and Bmp signaling, while protein synthesis and lineage-specific TFs are upregulated (Llorens-Bobadilla et al., 2015). A similar study was performed in the DG. A pseudo-timed reconstruction of the NSCs activation process revealed multiple new markers (Shin et al., 2015).

Together, these published results strongly support our own results (**Chapter 2**). Indeed, distinct NSCs populations appear to be primed towards a certain lineage by expressing lineage-specific markers, which are absent in others. For instance, Llorens-Bobadilla et al. tested the expression

profile of lineage specific TFs. They showed that dorsal/glutamatergic markers (Emx1, Eomes, Neurod4, Neurog2), GABAergic markers (Dlx1, Dlx2, Gsx1, Gsx2), and oligodendroglial markers (Ascl1, Etv1, Olig2), assembled in separate clusters of cells. Therefore, their observations describe a new level of heterogeneity within the NSC population and suggest a fate-restriction of different populations to different lineages (Llorens-Bobadilla et al., 2015). Taken together, this supports the idea of lineage-restricted, regionally enriched populations of NSCs. The fate mapping of one of these populations, described in the **Chapter 1** of this thesis, further supports this idea.

4.6. Perspectives – Push Technical Advances Further

This thesis manuscript focused on technical advances, which appear as the main driving force of new discoveries in research. Reciprocally, acquisition of new knowledge leads to the constant development of state of art techniques. The same logic may apply to "FlashMap" in order to increase its applicability and user friendliness. This will allow identifying other highly regionalized TFs. Ultimately, this will increase our knowledge of the mechanisms influencing activation of quiescent NSCs, pushing self-renewal and guiding lineage restriction with the ultimate goal to manipulate germinal activity in the injured or diseased brain.

4.6.1. "FlashMap" Evolves into "FlashMap 2.0"

Several modifications could be done to further improve "FlashMap". First, while it already allows a rapid spatial analysis of TFs expression pattern, it does not yet allow a systematic temporal analysis. In this context, a modified "FlashMap" version would allow to produce heatmaps at different embryonic and postnatal time points. Morphing of these maps, would then allow integrating temporal changes that may occur in the pattern of expression of selected TFs. This would reveal their peak of expression, as well as possible changes in their expression pattern over time. Second, major improvements may be implemented to speed up the analysis process. Automation of region of interest positioning (dorsal, lateral and medial SVZ microdomains) by selection of their borders only (dorso-medial, dorso-lateral and ventral corners) would be of major interest. Further, it might be useful to automatically subdivide them (e.g. dorsal and ventral parts of the lateral SVZ). Third, another useful add-on would allow the

analysis to be repeated in multiple animals. In this context, "FlashMap 2.0" would include not only the capacity to generate heatmaps for single animals, but also to generate a heatmap representing the averaged data from a group of animals. Finally, future versions may allow the analyses presented in **Chapter 1,** to be performed in other regions than the SVZ. Indeed, other germinal regions such as the DG or the pallium of the developing forebrain, also present an easily recognizable cytoarchitecture, which could be probed in a similar way.

4.6.2. Hopx as a First Marker of a Subpopulation of Committed NSCs

We demonstrated that Hopx defines a temporal restricted and new level of spatial heterogeneity within the dorsal SVZ. Hopx appears to be expressed in NSCs biased to acquire an astrocytic fate. Although these results are suggestive of subpopulations of "committed" NSCs coexisting in the postnatal SVZ, they do not allow to fully study the competence of these cells. A clonal analysis of dorsal NSCs and of their progenies will be necessary to conclude on the existence of multiple subpopulations of unipotent NSCs. During the course of my thesis I made some first attempts to use the UbC-StarTrack approach. The goal of this experiments was to explore the potency of the dorsal NSC population. Following dorsal EPO (**Figure 2B**) the brain was analyzed for cortical astrocytes and their color code was identified (**Figures 3A and 3B**). It was planned to subsequently analyze the neurons in the entire OB for the same color and compartment combinations (**Figure 3C**). However, these experiments could not have been achieved due to time issues.

I believe that a careful consideration of current protocols will be necessary to perform those experiments. It is probably that a mix between UbC-StarTrack (Figueres-Oñate et al., 2016), CLoNe (García-Moreno et al., 2014) and dorsal EPO into $Hopx^{CreERT2}$ mice (Takeda et al., 2011) will be necessary to perform these complicated experiments. I would favor the 6 fluorophores in 2 cellular compartments (UbC-StarTrack) over the 4 fluorophores in 3 cellular compartments approach (CLoNe). Indeed, the quantification with just two cellular compartments is already particularly challenging. Discriminating a third cellular compartment would require the acquisition of high resolution confocal images, at high magnification. Although this could be achieved in a small volume of tissue, it represents an unreasonable

amount of work if the entire forebrain is analyzed. I would also favor the use of the Cre-Lox system proposed by CLoNe (lox-stop-lox-fluorophore), as it would allow to restrict the analysis to a subpopulation of NSCs of interest, i.e. dorsal NSCs, or Hopx-expressing NSCs.

Figure 3. Illustration of clonal analysis using UbC-StarTrack.
(A+B): Representative micrographs show cortical astrocytes exhibiting unique color codes. Multicellular (A) and single cell astrocytic (B) clones were identified in the cortex and their color codes in the nucleus and the cytoplasm were analyzed.
(C): Representative micrographs show differentially labeled neurons in the OB. It was initially planned to analyze the entire OB for color codes that were discovered in cortical astrocytic clones. Such an extensive and time-consuming analysis could allow to make clearer assumptions about the potency of postnatal NSCs.
Scale bar: A+B = 50 µm; C (overview) = 1 mm; C (crops) = 100 µm. Abbreviations: OB, olfactory bulb; NSC, neural stem cell. ⟶

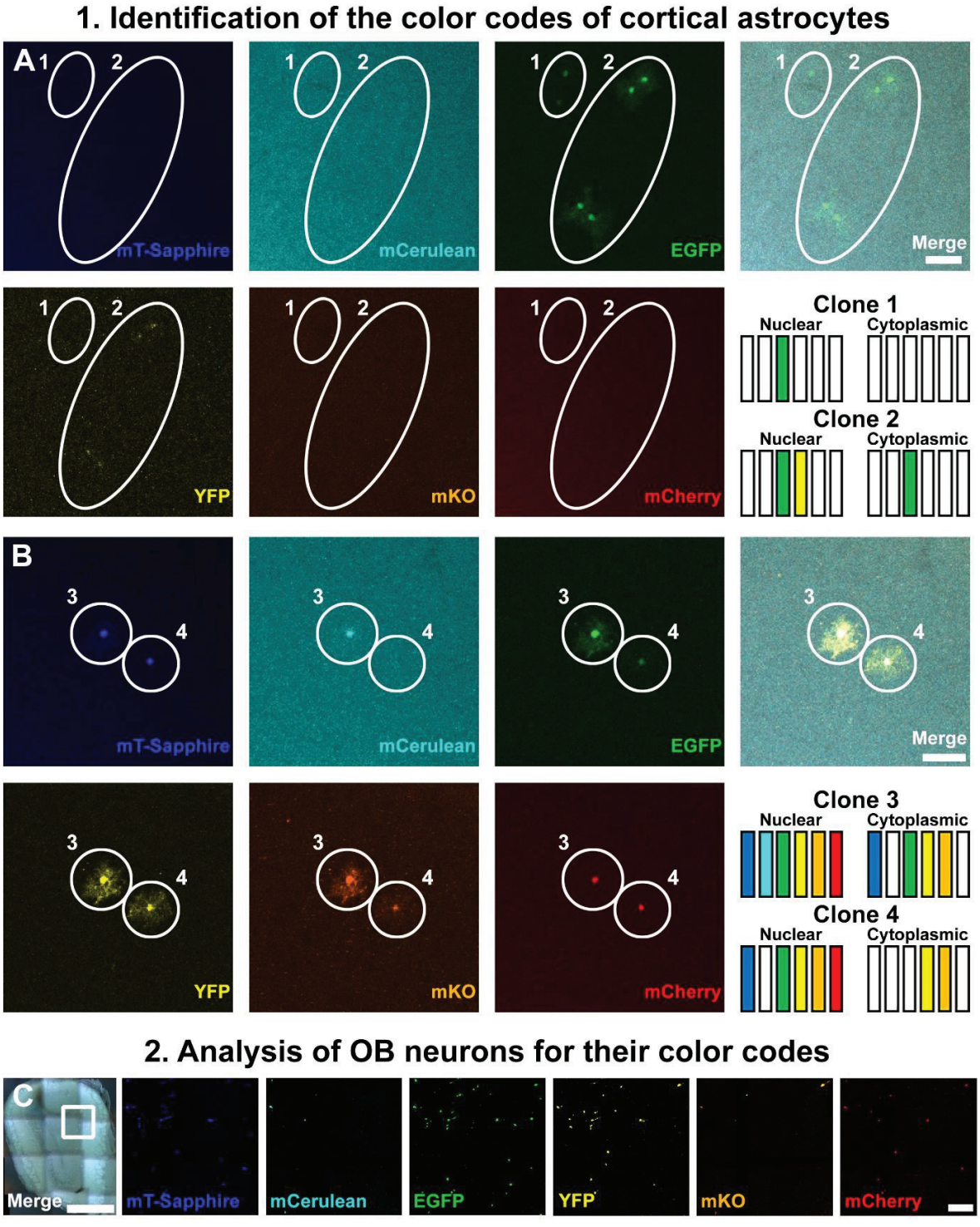
1. Identification of the color codes of cortical astrocytes
A
1
2
mT-Sapphire
mCerulean
EGFP
Merge
YFP
mKO
mCherry
Clone 1
Nuclear
Cytoplasmic
Clone 2
Nuclear
Cytoplasmic
B
3
4
mT-Sapphire
mCerulean
EGFP
Merge
YFP
mKO
mCherry
Clone 3
Nuclear
Cytoplasmic
Clone 4
Nuclear
Cytoplasmic
2. Analysis of OB neurons for their color codes
C
Merge
mT-Sapphire
mCerulean
EGFP
YFP
mKO
mCherry

4.6.3. Exploring NSCs Heterogeneity Beyond Hopx

Our transcriptional meta-analysis provides a list of enriched TFs in the dorsal NSCs and lateral NSCs, as well as their relation to selected neural lineages. This list may be screened for further TFs of interest. In addition, it is important to mention that such analysis should not be restricted to TFs. Indeed, other genes such as those coding for cell adhesion molecules might be powerful restrictors of NSCs potency. In embryonal brains, for example, striatal and cortical progenitors differ in their expression of cell adhesion molecules (Götz et al., 1996). Such cell adhesion molecules have been suggested to restrict the potential of NSCs for heterotopic integration (Olsson, 1998) and therefore they might be candidates to investigate fate restriction in general.

In conclusion, my study on Hopx adds a piece of knowledge to the puzzle of a full understanding of NSCs potency and restriction. This and other studies, which added additional pieces on their side, were driven by the continuous development and refinement of state of the art techniques. However, further investigations, the development of new key techniques and revolutionary ideas are absolutely necessary to decipher and understand NSCs biology in more details. This includes the decoding and understanding of the various signaling pathways, the expression of different TF combinations, the control of specific epigenetic mechanisms and much more.

A broad understanding of NSCs biology may pave the way of the development of future therapeutic approaches in the diseased or damaged brain.

5. Bibliography

Acampora, D., Mazan, S., Lallemand, Y., Avantaggiato, V., Maury, M., Simeone, A., and Brûlet, P. (1995). Forebrain and midbrain regions are deleted in Otx2-/- mutants due to a defective anterior neuroectoderm specification during gastrulation. Development *121*, 3279–3290.

Aihara, H., and Miyazaki, J. (1998). Gene transfer into muscle by electroporation in vivo. Nat. Biotechnol. *16*, 867–870.

Akhtar, A.A., Molina, J., Dutra-Clarke, M., Kim, G.B., Levy, R., Schreiber-Stainthorp, W., Danielpour, M., and Breunig, J.J. (2015). A transposon-mediated system for flexible control of transgene expression in stem and progenitor-derived lineages. Stem Cell Reports *4*, 323–331.

Allen, E. (1912). The cessation of the mitosis in the central nervous system of the albino rat. J. Comp. Neurol *22*, 547–569.

Altman, J. (1963). Autoradiographic investigation of cell proliferation in the brains of rats and cats. Anat. Rec. *145*, 573–591.

Altman, J. (1969). Autoradiographic and Histological Studies o Postnatal Neurogenesis. J. Comp. Neurol. *137*, 433–457.

Altman, J., and Das, G.D. (1965). Autoradiographic and histological evidence of postnatal hippocampal neurogenesis in rats. J. Comp. Neurol. *124*, 319–335.

Altman, J., and Das, G.D. (1967). Postnatal neurogenesis in the guinea-pig. Nature *214*, 1098–1101.

Anderson, S.A., Eisenstat, D.D., Shi, L., and Rubenstein, J.L.R. (1997a). Interneuron Migration from Basal Forebrain to Neocortex: Dependence on Dlx Genes. Science (80-.). *278*, 474–476.

Anderson, S. a, Qiu, M., Bulfone, a, Eisenstat, D.D., Meneses, J., Pedersen, R., and Rubenstein, J.L. (1997b). Mutations of the homeobox genes Dlx-1 and Dlx-2 disrupt the striatal subventricular zone and differentiation of late born striatal neurons. Neuron *19*, 27–37.

Ang, S.L., Jin, O., Rhinn, M., Daigle, N., Stevenson, L., and Rossant, J. (1996). A targeted mouse Otx2 mutation leads to severe defects in gastrulation and formation of axial mesoderm and to deletion of rostral brain. Development *122*, 243–252.

Angevine, J.B., and Sidman, R.L. (1961). Autoradiographic study of cell migration during histogenesis of cerebral cortex in the mouse. Nature *192*, 766–768.

Arnold, S.J., Huang, G., Cheung, A.F.P., Era, T., Nishikawa, S., Bikoff, E.K., Molnár, Z., Robertson, E.J., and Groszer, M. (2008). The T-box transcription factor Eomes/Tbr2 regulates neurogenesis in the cortical subventricular zone. Genes Dev. *22*, 2479–2484.

Aruga, J., Yokota, N., Hashimoto, M., Furuichi, T., Fukuda, M., and Mikoshiba, K. (1994). A novel zinc finger protein, zic, is involved in neurogenesis, especially in the cell lineage of cerebellar granule cells. J Neurochem *63*, 1880–1890.

Asanoma, K., Matsuda, T., Kondo, H., Kato, K., Kishino, T., Niikawa, N., Wake, N., and Kato, H. (2003). NECC1, a candidate choriocarcinoma suppressor gene that encodes a homeodomain consensus motif. Genomics *81*, 15–25.

Azevedo, F.A.C., Carvalho, L.R.B., Grinberg, L.T., Farfel, J.M., Ferretti, R.E.L., Leite, R.E.P., Filho, W.J., Lent, R., and Herculano-Houzel, S. (2009). Equal numbers of neuronal and nonneuronal cells

make the human brain an isometrically scaled-up primate brain. J. Comp. Neurol. *513*, 532–541.

Azim, K., Fiorelli, R., Zweifel, S., Hurtado-Chong, A., Yoshikawa, K., Slomianka, L., and Raineteau, O. (2012a). 3-Dimensional Examination of the Adult Mouse Subventricular Zone Reveals Lineage-Specific Microdomains. PLoS One *7*, e49087.

Azim, K., Fiorelli, R., Zweifel, S., Hurtado-Chong, A., Yoshikawa, K., Slomianka, L., and Raineteau, O. (2012b). 3-Dimensional Examination of the Adult Mouse Subventricular Zone Reveals Lineage-Specific Microdomains. PLoS One *7*, e49087.

Azim, K., Fiorelli, R., Zweifel, S., Hurtado-Chong, A., Yoshikawa, K., Slomianka, L., and Raineteau, O. (2012c). 3-Dimensional Examination of the Adult Mouse Subventricular Zone Reveals Lineage-Specific Microdomains. PLoS One *7*, e49087.

Azim, K., Raineteau, O., and Butt, A.M. (2012d). Intraventricular injection of FGF-2 promotes generation of oligodendrocyte-lineage cells in the postnatal and adult forebrain. Glia *60*, 1977–1990.

Azim, K., Zweifel, S., Klaus, F., Yoshikawa, K., Amrein, I., and Raineteau, O. (2013). Early decline in progenitor diversity in the marmoset lateral ventricle. Cereb. Cortex *23*, 922–931.

Azim, K., Fischer, B., Hurtado-Chong, A., Draganova, K., Cantù, C., Zemke, M., Sommer, L., Butt, A., and Raineteau, O. (2014a). Persistent Wnt / b -Catenin Signaling Determines Dorsalization of the Postnatal Subventricular Zone and Neural Stem Cell Specification into Oligodendrocytes and Glutamatergic Neurons. Stem Cells *23*, 1301–1312.

Azim, K., Rivera, A., Raineteau, O., and Butt, A.M. (2014b). GSK3β regulates oligodendrogenesis in the dorsal microdomain of the subventricular zone via Wnt-β-catenin signaling. Glia *62*, 778–779.

Azim, K., Hurtado-Chong, A., Fischer, B., Kumar, N., Zweifel, S., Taylor, V., and Raineteau, O. (2015). Transcriptional Hallmarks of Heterogeneous Neural Stem Cell Niches of the Subventricular Zone. Stem Cells *33*, 2232–2242.

Azim, K., Berninger, B., and Raineteau, O. (2016). Mosaic subventricular origins of forebrain oligodendrogenesis. Front. Neurosci. *10*, 1–7.

Azim, K., Angonin, D., Marcy, G., Pieropan, F., Rivera, A., Donega, V., Cantù, C., Williams, G., Berninger, B., Butt, A.M., et al. (2017). Pharmacogenomic identification of small molecules for lineage specific manipulation of subventricular zone germinal activity. PLoS Biol. *15*, 1–27.

Basak, O., and Taylor, V. (2007). Identification of self-replicating multipotent progenitors in the embryonic nervous system by high Notch activity and Hes5 expression. Eur. J. Neurosci. *25*, 1006–1022.

Batista-Brito, R., Close, J., Machold, R., and Fishell, G. (2008). The distinct temporal origins of olfactory bulb interneuron subtypes. J. Neurosci. *28*, 3966–3975.

Bayraktar, O.A., Fuentealba, L.C., Alvarez-Buylla, A., and Rowitch, D.H. (2015). Astrocyte development and heterogeneity. Cold Spring Harb. Perspect. Biol. *7*, a020362.

Beckervordersandforth, R., Tripathi, P., Ninkovic, J., Bayam, E., Lepier, A., Stempfhuber, B., Kirchhoff, F., Hirrlinger, J., Haslinger, A., Lie, D.C., et al. (2010). In vivo fate mapping and expression analysis reveals molecular hallmarks of prospectively isolated adult neural stem cells. Cell Stem Cell *7*, 744–758.

Berger, J., Eckert, S., Scardigli, R., Guillemot, F., Gruss, P., and Stoykova, A. (2004). E1-Ngn2/Cre is a new line for regional activation of Cre recombinase in the developing CNS. Genesis *40*, 195–199.

Bergmann, O., Liebl, J., Bernard, S., Alkass, K., Yeung, M.S.Y., Steier, P., Kutschera, W., Johnson, L., Landén, M., Druid, H., et al. (2012). The Age of Olfactory Bulb Neurons in Humans. Neuron *74*, 634–639.

Bhardwaj, R.D., Curtis, M.A., Spalding, K.L., Buchholz, B.A., Fink, D., Bjork-Eriksson, T., Nordborg, C., Gage, F.H., Druid, H., Eriksson, P.S., et al. (2006). Neocortical neurogenesis in humans is restricted to development. Proc. Natl. Acad. Sci. *103*, 12564–12568.

Bignami, A., and Dahl, D. (1974). Astrocyte-specific protein and neuroglial differentiation. An immunofluorescence study with antibodies to the glial fibrillary acidic protein. J. Comp. Neurol. *153*, 27–37.

Bonaguidi, M.A., Wheeler, M.A., Shapiro, J.S., Stadel, R.P., Sun, G.J., Ming, G.L., and Song, H. (2011). In vivo clonal analysis reveals self-renewing and multipotent adult neural stem cell characteristics. Cell *145*, 1142–1155.

Boutin, C., Diestel, S., Desoeuvre, A., Tiveron, M.-C., and Cremer, H. (2008). Efficient In Vivo Electroporation of the Postnatal Rodent Forebrain. PLoS One *3*, e1883.

Boutin, C., Hardt, O., de Chevigny, A., Coré, N., Goebbels, S., Seidenfaden, R., Bosio, A., and Cremer, H. (2010). NeuroD1 induces terminal neuronal differentiation in olfactory neurogenesis. Proc. Natl. Acad. Sci. U. S. A. *107*, 1201–1206.

Bracko, O., Singer, T., Aigner, S., Knobloch, M., Winner, B., Ray, J., Clemenson, G.D., Suh, H., Couillard-Despres, S., Aigner, L., et al. (2012). Gene Expression Profiling of Neural Stem Cells and Their Neuronal Progeny Reveals IGF2 as a Regulator of Adult Hippocampal Neurogenesis. J. Neurosci. *32*, 3376–3387.

Brill, M.S., Snapyan, M., Wohlfrom, H., Ninkovic, J., Jawerka, M., Mastick, G.S., Ashery-Padan, R., Saghatelyan, A., Berninger, B., and Götz, M. (2008). A dlx2- and pax6-dependent transcriptional code for periglomerular neuron specification in the adult olfactory bulb. J. Neurosci. *28*, 6439–6452.

Brill, M.S., Ninkovic, J., Winpenny, E., Hodge, R.D., Ozen, I., Yang, R., Lepier, A., Gascón, S., Erdelyi, F., Szabo, G., et al. (2009). Adult generation of glutamatergic olfactory bulb interneurons. Nat. Neurosci. *12*, 1524–1533.

Bulfone, A., Puelles, L., Porteus, M.H., Frohman, M.A., Martin, G.R., and Rubenstein, J.L.R. (1993). Spatially restricted expression of Dlx-1, Dlx-2 (Tes-1), Gbx-2, and Wnt-3 in the embryonic day 12.5 mouse forebrain defines potential transverse and longitudinal segmental boundaries. J. Neurosci. *13*, 3155–3172.

Bulfone, A., Smiga, S.M., Shimamura, K., Peterson, A., Puelles, L., and Rubenstein, J.L.R. (1995). T-Brain-1: A homolog of Brachyury whose expression defines molecularly distinct domains within the cerebral cortex. Neuron *15*, 63–78.

Bulfone, A., Wang, F., Hevner, R., Anderson, S., Cutforth, T., Chen, S., Meneses, J., Pedersen, R., Axel, R., and Rubenstein, J.L.R. (1998). An olfactory sensory map develops in the absence of normal projection neurons or GABAergic interneurons. Neuron *21*, 1273–1282.

Bulfone, A., Martinez, S., Marigo, V., Campanella, M., Basile, A., Quaderi, N., Gattuso, C., Rubenstein, J.L.R., and Ballabio, A. (1999). Expression pattern of the Tbr2 (Eomesodermin) gene during mouse and chick brain development. Mech. Dev. *84*, 133–138.

Cahoy, J.D., Emery, B., Kaushal, A., Foo, L.C., Zamanian, J.L., Christopherson, K.S., Xing, Y., Lubischer, J.L., Krieg, P.A., Krupenko, S.A., et al. (2008). A Transcriptome Database for Astrocytes , Neurons , and Oligodendrocytes : A New Resource for Understanding Brain Development and

Function. J. Neurosci. *28*, 264–278.

Calvin, N.M., and Hanawalt, P.C. (1988). High-Efficiency Transformacion of Bacterial cells by Electroporation. J. Bacteriol. *170*, 2796–2801.

Calzolari, F., Michel, J., Baumgart, E.V., Theis, F., Götz, M., and Ninkovic, J. (2015). Fast clonal expansion and limited neural stem cell self-renewal in the adult subependymal zone. Nat. Neurosci. *18*, 490–492.

Carleton, A., Petreanu, L.T., Lansford, R., Alvarez-Buylla, A., and Lledo, P.-M. (2003). Becoming a new neuron in the adult olfactory bulb. Nat. Neurosci. 507–518.

Casarosa, S., Fode, C., and Guillemot, F. (1999). Mash1 regulates neurogenesis in the ventral telencephalon. Development *126*, 525–534.

Cavanagh, B.L., Walker, T., Norazit, A., and Meedeniya, A.C.B. (2011). Thymidine analogues for tracking DNA synthesis. Molecules *16*, 7980–7993.

Chen, F., Kook, H., Milewski, R., Gitler, A.D., Lu, M.M., Li, J., Nazarian, R., Schnepp, R., Jen, K., Biben, C., et al. (2002). Hop is an unusual homeobox gene that modulates cardiac development. Cell *110*, 713–723.

Cleary, M.D., and Doe, C.Q. (2006). Regulation of neuroblast competence: multiple temporal identity factors specify distinct neuronal fates within a single early competence window. Genes Dev. *20*, 429–434.

Codega, P., Silva-Vargas, V., Paul, A., Maldonado-Soto, A.R., DeLeo, A.M., Pastrana, E., and Doetsch, F. (2014). Prospective Identification and Purification of Quiescent Adult Neural Stem Cells from Their In Vivo Niche. Neuron *82*, 545–559.

Cohen, I., Sivron, T., Lavie, V., Blaugrund, E., and Schwartz, M. (1994). Vimentin immunoreactive glial cells in the fish optic nerve: Implications for regeneration. Glia *10*, 16–29.

Craddock, V.M. (1981). Shortening of life span caused by administration of 5-bromodeoxyuridine to neonatal rats. Chem. Biol. Interact. *35*, 139–144.

Deneen, B., Ho, R., Lukaszewicz, A., Hochstim, C.J., Gronostajski, R.M., and Anderson, D.J. (2006). The Transcription Factor NFIA Controls the Onset of Gliogenesis in the Developing Spinal Cord. Neuron *52*, 953–968.

Desai, A.R., and McConnell, S.K. (2000). Progressive restriction in fate potential by neural progenitors during cerebral cortical development. Development *127*, 2863–2872.

Doetsch, F., and Alvarez-Buylla, a (1996). Network of tangential pathways for neuronal migration in adult mammalian brain. Proc. Natl. Acad. Sci. U. S. A. *93*, 14895–14900.

Doetsch, F., García-Verdugo, J.M., and Alvarez-Buylla, a (1997). Cellular composition and three-dimensional organization of the subventricular germinal zone in the adult mammalian brain. J. Neurosci. *17*, 5046–5061.

Doetsch, F., Caillé, I., Lim, D. a, García-Verdugo, J.M., and Alvarez-Buylla, a (1999). Subventricular zone astrocytes are neural stem cells in the adult mammalian brain. Cell *97*, 703–716.

Donega, V., and Raineteau, O. (2017). Postnatal Neural Stem Cells: Probing Their Competence for Cortical Repair. Neurosci. *23*, 1–11.

Donega, V., Marcy, G., Lo Giudice, Q., Zweifel, S., Angonin, D., Fiorelli, R., Abrous, D.N., Rival-

Gervier, S., Koehl, M., Jabaudon, D., et al. (2018). Transcriptional Dysregulation in Postnatal Glutamatergic Progenitors Contributes to Closure of the Cortical Neurogenic Period. Cell Rep. *22*, 2567–2574.

Downing, M., and Schweigert, B.S. (1956). Rôle of vitamin B12 in nucleic acid metabolism. IV. Metabolism of C14-labeled thymidine by Lactobacillus leichmannii. J. Biol. Chem. *220*, 521–526.

Eriksson, P.S., Perfilieva, E., Eriksson, T.B., Alborn, A.-M., Nordborg, C., Peterson, D.A., and Gage, F.H. (1998). Neurogenesis in the adult human hippocampus. Nat. Med. *4*, 1313–1317.

Ernst, A., Alkass, K., Bernard, S., Salehpour, M., Perl, S., Tisdale, J., Possnert, G., Druid, H., and Frisén, J. (2014). Neurogenesis in the striatum of the adult human brain. Cell *156*, 1072–1083.

Eroglu, C., and Barres, B.A. (2010). Regulation of synaptic connectivity by glia. Nature *468*, 223–231.

Faedo, A., Ficara, F., Ghiani, M., Aiuti, A., Rubenstein, J.L.R., and Bulfone, A. (2002). Developmental expression of the T-box transcription factor T-bet/Tbx21 during mouse embryogenesis. Mech. Dev. *116*, 157–160.

Falcão, A.M., Palha, J.A., Ferreira, A.C., Marques, F., Sousa, N., and Sousa, J.C. (2012). Topographical analysis of the subependymal zone neurogenic niche. PLoS One *7*, 1–12.

Feil, R., Brocard, J., Mascrez, B., LeMeur, M., Metzger, D., and Chambon, P. (1996). Ligand-activated site-specific recombination in mice. Proc. Natl. Acad. Sci. *93*, 10887–10890.

Fernández, M.E., Croce, S., Boutin, C., Cremer, H., and Raineteau, O. (2011a). Targeted electroporation of defined lateral ventricular walls: a novel and rapid method to study fate specification during postnatal forebrain neurogenesis. Neural Dev. *6*, 13.

Fernández, M.E., Croce, S., Boutin, C., Cremer, H., and Raineteau, O. (2011b). Targeted electroporation of defined lateral ventricular walls: a novel and rapid method to study fate specification during postnatal forebrain neurogenesis. Neural Dev. *6*, 13.

Figueres-Oñate, M., García-Marqués, J., and López-Mascaraque, L. (2016). UbC-StarTrack, a clonal method to target the entire progeny of individual progenitors. Sci. Rep. *6*, 33896.

Fiorelli, R., Azim, K., Fischer, B., and Raineteau, O. (2015). Adding a spatial dimension to postnatal ventricular-subventricular zone neurogenesis. Development *142*, 2109–2120.

Fischer, K. (1967). Subependymale Zellproliferationen und Tumordisposition brachycephaler Hunderassen. Acta Neuropathol. *8*, 242–254.

Fischer, B., Azim, K., Hurtado-Chong, A., Ramelli, S., Fernández, M., and Raineteau, O. (2014). E-proteins orchestrate the progression of neural stem cell differentiation in the postnatal forebrain. Neural Dev. *9*, 1–14.

Fode, C., Ma, Q., Casarosa, S., Ang, S.L., Anderson, D.J., and Guillemot, F. (2000). A role for neural determination genes in specifying the dorsoventral identity of telencephalic neurons. Genes Dev. *14*, 67–80.

Fogarty, M., Grist, M., Gelman, D., Marin, O., Pachnis, V., and Kessaris, N. (2007). Spatial Genetic Patterning of the Embryonic Neuroepithelium Generates GABAergic Interneuron Diversity in the Adult Cortex. J. Neurosci. *27*, 10935–10946.

Frantz, G.D., and McConnell, S.K. (1996). Restriction of late cerebral cortical progenitors to an upper-layer fate. Neuron *17*, 55–61.

Friedkin, M., Tilson, D., and Roberts, D. (1956). Studies of deoxyribonucleic acid biosynthesis in embryonic tissues with thymidine-C14. J. Biol. Chem. *220*, 627–637.

Fromm, M., Taylor, L.P., and Walbot, V. (1985). Expression of genes transferred into monocot and dicot plant cells by electroporation. Proc. Natl. Acad. Sci. *82*, 5824–5828.

Fuentealba, L.C., Rompani, S.B., Parraguez, J.I., Obernier, K., Romero, R., Cepko, C.L., and Alvarez-buylla, A. (2015). Embryonic Origin of Postnatal Neural Stem Cells Article Embryonic Origin of Postnatal Neural Stem Cells. Cell *161*, 1644–1655.

Furutachi, S., Miya, H., Watanabe, T., Kawai, H., Yamasaki, N., Harada, Y., Imayoshi, I., Nelson, M., Nakayama, K.I., Hirabayashi, Y., et al. (2015). Slowly dividing neural progenitors are an embryonic origin of adult neural stem cells. Nat. Neurosci. *18*.

Gaiano, N., and Fishell, G. (1998). Transplantation as a tool to study progenitors within the vertebrate nervous system. J. Neurobiol. *36*, 152–161.

Gao, P., Postiglione, M.P., Krieger, T.G., Hernandez, L., Wang, C., Han, Z., Streicher, C., Papusheva, E., Insolera, R., Chugh, K., et al. (2014). Deterministic progenitor behavior and unitary production of neurons in the neocortex. Cell *159*, 775–788.

García-Marqués, J., and López-Mascaraque, L. (2013). Clonal identity determines astrocyte cortical heterogeneity. Cereb. Cortex *23*, 1463–1472.

García-Marqués, J., Nùñez-Llaves, R., and López-Mascaraque, L. (2014). NG2-Glia from Pallial Progenitors Produce the Largest Clonal Clusters of the Brain: Time Frame of Clonal Generation in Cortex and Olfactory Bulb. J. Neurosci. *34*, 2305–2313.

García-Moreno, F., Vasistha, N.A., Begbie, J., and Molnár, Z. (2014). CLoNe is a new method to target single progenitors and study their progeny in mouse and chick. Development *141*, 1589–1598.

Ge, W.P., Miyawaki, A., Gage, F.H., Jan, Y.N., and Jan, L.Y. (2012). Local generation of glia is a major astrocyte source in postnatal cortex. Nature *484*, 376–381.

Genander, M., Cook, P.J., Ramsköld, D., Keyes, B.E., Mertz, A.F., Sandberg, R., and Fuchs, E. (2014). BMP Signaling and Its pSMAD1/5 Target Genes Differentially Regulate Hair Follicle Stem Cell Lineages. Cell Stem Cell *15*, 619–633.

Gerdes, J., Lemke, H., Baisch, H., Wacker, H., Schwab, U., and Stein, H. (1984). Cell cycle analysis of a cell proliferation-associated human nuclear antigen defined by the monoclonal antibody Ki-67. J. Immunol. *133*, 1710–1715.

Giachino, C., Basak, O., Lugert, S., Knuckles, P., Obernier, K., Fiorelli, R., Frank, S., Raineteau, O., Alvarez-Buylla, A., and Taylor, V. (2014). Molecular diversity subdivides the adult forebrain neural stem cell population. Stem Cells *32*, 70–84.

Gómez-Lopera, J.F., Martínez-Aroza, J., Robles-Pérez, A.M., and Román-Roldán, R. (2000). Analysis of edge detection by using the Jensen-Shannon divergence. J. Math. Imaging Vis. *13*, 35–56.

Götz, M., Wizenmann, A., Reinhardt, S., Lumsden, A., and Price, J. (1996). Selective adhesion of cells from different telencephalic regions. Neuron *16*, 551–564.

Gould, E., Tanapat, P., McEwen, B.S., Flügge, G., and Fuchs, E. (1998). Proliferation of granule cell precursors in the dentate gyrus of. Proc. Natl. Acad. Sci. *95*, 3168–3171.

Gould, E., Reeves, A.J., Fallah, M., Tanapat, P., Gross, C.G., and Fuchs, E. (1999). Hippocampal neurogenesis in adult Old World primates. Proc. Natl. Acad. Sci. *96*, 5263–5267.

Gould, E., Vail, N., Wagers, M., and Gross, C.G. (2001). Adult-generated hippocampal and neocortical neurons in macaques have a transient existence. Proc. Natl. Acad. Sci. U. S. A. *98*, 10910–10917.

Gratzner, H.G. (1982). Monoclonal Antibody to 5-Bromo- and 5-Iododeoxyuridine : A New Reagent for Detection of DNA Replication Placental Mononuclear Phagocytes as a Source of Interleukin-1. Science (80-.). *218*, 474–475.

Gratzner, H.G., Leif, R.C., Ingram, D.J., and Castro, A. (1975). The use of antibody specific for bromodeoxyuridine for the immunofluorescent determination of DNA replication in single cells and chromosomes. Exp. Cell Res. *95*, 88–94.

Grinberg, I., and Millen, K. (2005). The ZIC gene family in development and disease. Clin. Genet. *67*, 290–296.

Gross, R.E., Mehler, M.F., Mabie, P.C., Zang, Z., Santschi, L., and Kessler, J.A. (1996). Bone morphogenetic proteins promote astroglial lineage commitment by mammalian subventricular zone progenitor cells. Neuron *17*, 595–606.

Hampel, S., Chung, P., Mckellar, C.E., Hall, D., Looger, L.L., and Simpson, J.H. (2011). *Drosophila* Brainbow : a recombinase-based fluorescence labeling technique to subdivide neural expression patterns. Nat. Methods *8*, 253–259.

He, X.C., Zhang, J., Tong, W.-G., Tawfik, O., Ross, J., Scoville, D.H., Tian, Q., Zeng, X., He, X., Wiedemann, L.M., et al. (2004). BMP signaling inhibits intestinal stem cell self-renewal through suppression of Wnt–β-catenin signaling. Nat. Genet. *36*, 1117–1121.

Hevner, R.F., Hodge, R.D., Daza, R. a M., and Englund, C. (2006). Transcription factors in glutamatergic neurogenesis: conserved programs in neocortex, cerebellum, and adult hippocampus. Neurosci. Res. *55*, 223–233.

Hollnagel, A., Oehlmann, V., Heymer, J., Rühter, U., and Nordheim, A. (1999). Id Genes Are Direct Targets of Bone Morphogenetic Protein Induction in Embryonic Stem Cells. J. Biol. Chem. *274*, 19838–19845.

Hsieh-Li, H.M., Witte, D.P., Szucsik, J.C., Weinstein, M., Li, H., and Potter, S.S. (1995). Gsh-2, a murine homeobox gene expressed in the developing brain. Mech. Dev. *50*, 177–186.

Hughes, W.L., Bond, V.P., Brecher, G., Cronkite, E.P., Painter, R.B., Quastler, H., and Sherman, F.G. (1958). Cellular Proliferation in the Mouse as Revealed by Autoradiography with Tritiated Thymidine. Proc. Natl. Acad. Sci. *44*, 476–483.

Ihrie, R.A., Shah, J.K., Harwell, C.C., Levine, J.H., Guinto, C.D., Lezameta, M., Kriegstein, A.R., and Alvarez-Buylla, A. (2011). Persistent Sonic hedgehog Signaling in Adult Brain Determines Neural Stem Cell Positional Identity. Neuron *71*, 250–262.

Isshiki, T., Pearson, B., Holbrook, S., and Doe, C.Q. (2001). *Drosophila* neuroblasts sequentially express transcription factors which specify the temporal identity of their neuronal progeny. Cell *106*, 511–521.

Itasaki, N., Bel-Vialar, S., and Krumlauf, R. (1999). "Shocking" developments in chick embryology: electroporation and in ovo gene expression. Nat. Cell Biol. *1*, E203-7.

Jacobson, M. (1991). Developmental Neurobiology.

Jain, R., Li, D., Gupta, M., Manderfield, L.J., Ifkovits, J.L., Wang, Q., Liu, F., Liu, Y., Poleshko, a.,

Padmanabhan, a., et al. (2015). Integration of Bmp and Wnt signaling by Hopx specifies commitment of cardiomyoblasts. Science (80-.). *348*, aaa6071-aaa6071.

Ju, X.C., Hou, Q.Q., Sheng, A.L., Wu, K.Y., Zhou, Y., Jin, Y., Wen, T., Yang, Z., Wang, X., and Luo, Z.G. (2016). The hominoid-specific gene TBC1D3 promotes generation of basal neural progenitors and induces cortical folding in mice. Elife *5*, 1–25.

Kahoud, R.J., Elsen, G.E., Hevner, R.F., and Hodge, R.D. (2014). Conditional ablation of Tbr2 results in abnormal development of the olfactory bulbs and subventricular zone-rostral migratory stream. Dev. Dyn. *243*, 440–450.

Kandyba, E., Leung, Y., Chen, Y.-B., Widelitz, R., Chuong, C.-M., and Kobielak, K. (2013). Competitive balance of intrabulge BMP/Wnt signaling reveals a robust gene network ruling stem cell homeostasis and cyclic activation. Proc. Natl. Acad. Sci. *110*, 1351–1356.

Kaplan, M.S. (1983). Proliferation of subependymal cells in the adult primate CNS: differential uptake of DNA labelled precursors. J. Hirnforsch. *24*, 23–33.

Kaplan, M.S., and Hinds, J.W. (1977). Neurogenesis in the adult rat: electron microscopic analysis of light radioautographs. Science *197*, 1092–1094.

Kaufman, E.R. (1988). The role of deoxyribonucleotide metabolism in 5-bromo-2 â€™ -deoxyuridine mutagenesis in mammalian cells. Mutat. Res. *200*, 149–155.

Kessaris, N., Fogarty, M., Iannarelli, P., Grist, M., Wegner, M., and Richardson, W.D. (2006). Competing waves of oligodendrocytes in the forebrain and postnatal elimination of an embryonic lineage. Nat. Neurosci. *9*, 173–179.

Kim, T.H., Saadatpour, A., Guo, G., Saxena, M., Cavazza, A., Desai, N., Jadhav, U., Jiang, L., Rivera, M.N., Orkin, S.H., et al. (2016). Single-cell transcript profiles reveal multilineage priming in early progenitors derived from Lgr5+ intestinal stem cells. Cell Rep. *16*, 2053–2060.

Kirschenbaum, B., and Goldman, S. a (1995). Brain-derived neurotrophic factor promotes the survival of neurons arising from the adult rat forebrain subependymal zone. Proc. Natl. Acad. Sci. U. S. A. *92*, 210–214.

Kohwi, M., and Doe, C.Q. (2013). Temporal fate specification and neural progenitor competence during development. Nat. Rev. Neurosci. *14*, 823–838.

Kohwi, M., Petryniak, M. a, Long, J.E., Ekker, M., Obata, K., Yanagawa, Y., Rubenstein, J.L.R., and Alvarez-Buylla, A. (2007). A subpopulation of olfactory bulb GABAergic interneurons is derived from Emx1- and Dlx5/6-expressing progenitors. J. Neurosci. *27*, 6878–6891.

Kojima, Y., Tam, O.H., and Tam, P.P.L. (2014). Timing of developmental events in the early mouse embryo. Semin. Cell Dev. Biol. *34*, 65–75.

Kriegstein, A., and Alvarez-Buylla, a (2009). The glial nature of embryonic and adult neural stem cells. Annu. Rev. Neurosci. *32*, 149–184.

Krushel, L.A., Johnston, J.G., Fishell, G., Tibshirani, R., and van der Kooy, D. (1993). Spatially localized neuronal cell lineages in the developing mammalian forebrain. Neuroscience *53*, 1035–1047.

Kuwajima, T., Nishimura, I., and Yoshikawa, K. (2006). Necdin Promotes GABAergic Neuron Differentiation in Cooperation with Dlx Homeodomain Proteins. J. Neurosci. *26*, 5383–5392.

Lacar, B., Young, S.Z., Platel, J.-C., and Bordey, A. (2010). Imaging and recording subventricular

zone progenitor cells in live tissue of postnatal mice. Front. Neurosci. *4*, 1–16.

Lawrence, P.A. (1992). The Making of a Fly.

Lee, J.E. (1997). Basic helix-loop-helix genes in neural development. Curr. Opin. Neurobiol. *7*, 13–20.

Levison, S.W., and Goldman, J.E. (1993). Both oligodendrocytes and astrocytes develop from progenitors in the subventricular zone of postnatal rat forebrain. Neuron *10*, 201–212.

Levison, S.W., Chuang, C., Abramson, B.J., and Goldman, J.E. (1993). The migrational patterns and developmental fates of glial precursors in the rat subventricular zone are temporally regulated. Development *119*, 611–622.

Lewis, P.D. (1968). Mitotic activity in the primate subependymal layer and the genesis of gliomas. Nature *217*, 974–975.

Lewitus, E., Kelava, I., and Huttner, W.B. (2013). Conical expansion of the outer subventricular zone and the role of neocortical folding in evolution and development. Front. Hum. Neurosci. *7*, 1–12.

Li, D., Takeda, N., Jain, R., Manderfield, L.J., Liu, F., Li, L., Anderson, S. a., and Epstein, J. a. (2015). Hopx distinguishes hippocampal from lateral ventricle neural stem cells. Stem Cell Res. *15*, 522–529.

Lin, J. (1991). Divergence Measures Based on the Shannon Entropy. IEEE Trans. Inf. Theory *37*, 145–151.

Livet, J., Weissman, T.A., Kang, H., Draft, R.W., Lu, J., Bennis, R.A., Sanes, J.R., and Lichtman, J.W. (2007). Transgenic strategies for combinatorial expression of fluorescent proteins in the nervous system. Nature *450*, 56–62.

Llorens-Bobadilla, E., Zhao, S., Baser, A., Saiz-Castro, G., Zwadlo, K., and Martin-Villalba, A. (2015). Single-Cell Transcriptomics Reveals a Population of Dormant Neural Stem Cells that Become Activated upon Brain Injury. Cell Stem Cell *17*, 329–340.

Lois, C., and Alvarez-Buylla, a (1993). Proliferating subventricular zone cells in the adult mammalian forebrain can differentiate into neurons and glia. Proc. Natl. Acad. Sci. U. S. A. *90*, 2074–2077.

Lois, C., and Alvarez-Buylla, a (1994). Long-distance neuronal migration in the adult mammalian brain. Science *264*, 1145–1148.

Lois, C., García-Verdugo, J.M., and Alvarez-Buylla, A. (1996). Chain migration of neuronal precursors. Science *271*, 978–981.

López-Juárez, A., Howard, J., Ullom, K., Howard, L., Grande, A., Pardo, A., Waclaw, R., Sun, Y.Y., Yang, D., Kuan, C.Y., et al. (2013). Gsx2 controls region-specific activation of neural stem cells and injury-induced neurogenesis in the adult subventricular zone. Genes Dev. *27*, 1272–1287.

Loulier, K., Barry, R., Mahou, P., Franc, Y. Le, Supatto, W., Matho, K.S., Loulier, K., Dupin, E., Benosman, R., Che, A., et al. (2014). Multiplex Cell and Lineage Tracking with Combinatorial Labels. Neuron *81*, 505–520.

Madisen, L., Zwingman, T.A., Sunkin, S.M., Oh, S.W., Zariwala, H.A., Gu, H., Ng, L.L., Palmiter, R.D., Hawrylycz, M.J., Jones, A.R., et al. (2010). A robust and high-throughput Cre reporting and characterization system for the whole mouse brain. Nat. Neurosci. *13*, 133–140.

Magavi, S., Friedmann, D., Banks, G., Stolfi, A., and Lois, C. (2012). Coincident Generation of Pyramidal Neurons and Protoplasmic Astrocytes in Neocortical Columns. J. Neurosci. *32*, 4762–4772.

Mairhofer, S., Zappala, S., Tracy, S.R., Sturrock, C., Bennett, M., Mooney, S.J., and Pridmore, T. (2012). RooTrak: Automated Recovery of Three-Dimensional Plant Root Architecture in Soil from X-Ray Microcomputed Tomography Images Using Visual Tracking. Plant Physiol. *158*, 561–569.

Mamber, C., Verhaagen, J., and Hol, E.M. (2010). In vivo targeting of subventricular zone astrocytes. Prog. Neurobiol. *92*, 19–32.

Matthias, K., Kirchhoff, F., Seifert, G., Hüttmann, K., Matyash, M., Kettenmann, H., and Steinhäuser, C. (2003). Segregated Expression of AMPA-Type Glutamate Receptors and Glutamate Transporters Defines Distinct Astrocyte Populations in the Mouse Hippocampus. J. Neurosci. *23*, 1750–1758.

McDermott, K.W.G., and Lantos, P.L. (1990). Cell proliferation in the subependymal layer of the postnatal marmoset, Callithrix jacchus. Dev. Brain Res. *57*, 269–277.

McGinnis, W., and Krumlauf, R. (1992). Homeobox genes and axial patterning. Cell *68*, 283–302.

Merkle, F.T., Mirzadeh, Z., and Alvarez-Buylla, A. (2007). Mosaic organization of neural stem cells in the adult brain. Science *317*, 381–384.

Merkle, F.T., Fuentealba, L.C., Sanders, T. a, Magno, L., Kessaris, N., and Alvarez-Buylla, A. (2014). Adult neural stem cells in distinct microdomains generate previously unknown interneuron types. Nat. Neurosci. *17*, 207–214.

Messier, B., Leblond, D.P., and Smart, I. (1958). Presence of DNA synthesis and mitosis in the brain of young adult mice. Exp. Cell Res. *14*, 224–226.

Mihalas, A.B., Elsen, G.E., Bedogni, F., Daza, R.A.M., Ramos-Laguna, K.A., Arnold, S.J., and Hevner, R.F. (2016). Intermediate Progenitor Cohorts Differentially Generate Cortical Layers and Require Tbr2 for Timely Acquisition of Neuronal Subtype Identity. Cell Rep. *16*, 92–105.

Morel, L., Chiang, M.S.R., Higashimori, H., Shoneye, T., Iyer, L.K., Yelick, J., Tai, A., and Yang, Y. (2017). Molecular and Functional Properties of Regional Astrocytes in the Adult Brain. J. Neurosci. 3956–16.

Mühlfriedel, S., Kirsch, F., Gruss, P., Stoykova, A., and Chowdhury, K. (2005). A roof plate-dependent enhancer controls the expression of Homeodomain only protein in the developing cerebral cortex. Dev. Biol. *283*, 522–534.

Muramatsu, T., Mizutani, Y., Ohmori, Y., and Okumura, J.I. (1997). Comparison of three nonviral transfection methods for foreign gene expression in early chicken embryos in ovo. Biochem. Biophys. Res. Commun. *230*, 376–380.

Nagai, T., Aruga, J., Minowa, O., Sugimoto, T., Ohno, Y., Noda, T., and Mikoshiba, K. (2000). Zic2 regulates the kinetics of neurulation. Proc. Natl. Acad. Sci. U. S. A. *97*, 1618–1623.

Nakashima, K., Takizawa, T., Ochiai, W., Yanagisawa, M., Hisatsune, T., Nakafuku, M., Miyazono, K., Kishimoto, T., Kageyama, R., and Taga, T. (2001). BMP2-mediated alteration in the developmental pathway of fetal mouse brain cells from neurogenesis to astrocytogenesis. Proc. Natl. Acad. Sci. U. S. A. *98*, 5868–5873.

Neumann, E., Schaefer-Ridder, M., Wang, Y., and Hofschneider, P.H. (1982). Gene transfer into mouse lyoma cells by electroporation in high electric fields. EMBO J. *1*, 841–845.

Noetzel, H., and Rox, J. (1964). Autoradiographische Untersuchungen über Zellteilung und Zellentwicklung im Gehirn der erwachsenen Maus und des erwachsenen Rhesus-Affen nach Injektion von radioaktivem Thymidin. Acta Neuropathol. *3*, 326–342.

Obarzanek-Fojt, M., Favre, B., Kypriotou, M., Ryser, S., Huber, M., and Hohl, D. (2011). Homeodomain-only protein HOP is a novel modulator of late differentiation in keratinocytes. Eur. J. Cell Biol. *90*, 279–290.

Olsson, M. (1998). Incorporation of mouse neural progenitors transplanted into the rat embryonic forebrain is developmentally regulated and dependent on regional and adhesive properties. Eur. J. Neurosci. *10*, 71–85.

Ortega, F., Gascón, S., Masserdotti, G., Deshpande, A., Simon, C., Fischer, J., Dimou, L., Chichung Lie, D., Schroeder, T., and Berninger, B. (2013). Oligodendrogliogenic and neurogenic adult subependymal zone neural stem cells constitute distinct lineages and exhibit differential responsiveness to Wnt signalling. Nat. Cell Biol. *15*, 602–613.

Pan, Y.A., Livet, J., Sanes, J.R., Lichtman, J.W., and Schier, A.F. (2011). Multicolor Brainbow Imaging in Zebrafish. Cold Spring Harb. Protoc. *2011*, 1–8.

Panzanelli, P., Fritschy, J.M., Yanagawa, Y., Obata, K., and Sassoè-Pognetto, M. (2007). GABAergic phenotype of periglomerular cells in the rodent olfactory bulb. J. Comp. Neurol. *502*, 990–1002.

Paredes, M.F., James, D., Gil-Perotin, S., Kim, H., Cotter, J.A., Ng, C., Sandoval, K., Rowitch, D.H., Xu, D., McQuillen, P.S., et al. (2016). Extensive Migration of Young Neurons into the Infant Human Frontal Lobe. Science (80-.). *354*, aaf7073-1to7.

Parras, C.M., Schuurmans, C., Scardigli, R., Kim, J., Anderson, D.J., and Guillemot, F. (2002). Divergent functions of the proneural genes Mash1 and Ngn2 in the specification of neuronal subtype identity. Genes Dev. *16*, 324–338.

Pearson, B.J., and Doe, C.Q. (2003). Regulation of neuroblast competence in *Drosophila*. Nature *425*, 624–628.

Pelc, S.R. (1956). The stripping-film technique of autoradiography. Int. J. Appl. Radiat. Isot. *1*, 172–177.

Peters, A., Palay, S.L., and Webster, H. deF (1991). The Fine Structure of the Nervous System.

Philippidou, P., and Dasen, J.S. (2013). Hox Genes: Choreographers in Neural Development, Architects of Circuit Organization. Neuron *80*, 12–34.

Pimeisl, I.M., Tanriver, Y., Daza, R.A., Vauti, F., Hevner, R.F., Arnold, H.H., and Arnold, S.J. (2013). Generation and characterization of a tamoxifen-inducible EomesCreER mouse line. Genesis *51*, 725–733.

Plikus, M. V, Mayer, J., Cruz, D. De, Baker, R.E., Maini, P.K., Maxson, R., and Chuong, C. (2008). Cyclic dermal BMP signaling regulates stem cell activation during hair regeneration. Nature *451*, 340–344.

Pollen, A. a., Nowakowski, T.J., Chen, J., Retallack, H., Sandoval-Espinosa, C., Nicholas, C.R., Shuga, J., Liu, S.J., Oldham, M.C., Diaz, A., et al. (2015). Molecular Identity of Human Outer Radial Glia during Cortical Development. Cell *163*, 55–67.

Ponti, G., Reitano, E., Aimar, P., Cattaneo, E., Conti, L., and Bonfanti, L. (2010). Neural-specific inactivation of ShcA functions results in anatomical disorganization of subventricular zone neural

stem cell niche in the adult brain. Neuroscience *168*, 314–322.

Ponti, G., Obernier, K., Guinto, C., Jose, L., Bonfanti, L., and Alvarez-Buylla, A. (2013). Cell cycle and lineage progression of neural progenitors in the ventricular-subventricular zones of adult mice. Proc. Natl. Acad. Sci. *110*, E1045–E1054.

Price, M., Lazzaro, D., Pohl, T., Mattei, M.G., Rüther, U., Olivo, J.C., Duboule, D., and Di Lauro, R. (1992). Regional expression of the homeobox gene Nkx-2.2 in the developing mammalian forebrain. Neuron *8*, 241–255.

Qian, X., Shen, Q., Goderie, S.K., He, W., Capela, A., Davis, A.A., and Temple, S. (2000). Timing of CNS cell generation: a programmed sequence of neuron and glial cell production from isolated murine cortical stem cells. Neuron *28*, 69–80.

Qiu, M., Bulfone, A., Martinez, S., Meneses, J.J., Shimamura, K., Pedersen, R.A., and Rubenstein, J.L.R. (1995). Null mutation of Dlx-2 results in abnormal morphogenesis of proximal first and second branchial arch derivatives and abnormal differentiation in the forebrain. Genes Dev. *9*, 2523–2538.

Qiu, M., Anderson, S., Chen, S., Meneses, J.J., Hevner, R., Kuwana, E., Pedersen, R.A., and Rubenstein, J.L.R. (1996). Mutation of the Emx-1 homeobox gene disrupts the corpus callosum. Dev. Biol. *178*, 174–178.

Qiu, M., Shimamura, K., Sussel, L., Chen, S., and Rubenstein, J.L.R. (1998). Control of anteroposterior and dorsoventral domains of Nkx-6.1 gene expression relative to other Nkx genes during vertebrate CNS development. Mech. Dev. *72*, 77–88.

Quastler, H., and Sherman, F.G. (1959). Cell population kinetics in the intestinal epithelium of the mouse. Exp. Cell Res. *17*, 420–438.

Rakic, P. (1985). Limits of Neurogenesis in Primates. Science (80-.). *227*, 1054–1056.

Reemst, K., Noctor, S.C., Lucassen, P.J., and Hol, E.M. (2016). The Indispensable Roles of Microglia and Astrocytes during Brain Development. Front. Hum. Neurosci. *10*, 566.

Reichard, P., and Estborn, B. (1951). Utilization of desoxyribosides in the synthesis of polynucleotids. J. Biol. Chem. *188*, 839–846.

Reynolds, B.A., and Weiss, S. (1992). Nervous System Generation of Neurons and Astrocytes from Isolated Cells of the Adult Mammalian Central Nervous System. Science (80-.). *255*, 1707–1710.

Rigau, J., Feixas, M., and Sbert, M. (2005). An Information-Theoretic Framework for Image Complexity. Comput. Aesthet. Graph. Vis. Imaging 177–184.

Rousselot, P., Lois, C., and Alvarezz-Buylla, A. (1995). Embryonic PSA-NCAM reveals changes of migrating neuroblasts between the lateral ventricle and the olfactory bulb of adult mice. J. Comp. Neurol. *351*, 51–61.

Rubenstein, J.L., Martinez, S., Shimamura, K., and Puelles, L. (1994). The embryonic vertebrate forebrain: the prosomeric model. Science *266*, 578–580.

Saba, R., Nakatsuji, N., and Saito, T. (2003). Mammalian BarH1 confers commissural neuron identity on dorsal cells in the spinal cord. J. Neurosci. *23*, 1987–1991.

Saito, T., and Nakatsuji, N. (2001). Efficient gene transfer into the embryonic mouse brain using in vivo electroporation. Dev. Biol. *240*, 237–246.

Saiz, N., and Plusa, B. (2013). Early cell fate decisions in the mouse embryo. Reproduction *145*,

R65–R80.

Salic, A., and Mitchison, T.J. (2008). A chemical method for fast and sensitive detection of DNA synthesis in vivo. Proc. Natl. Acad. Sci. U. S. A. *105*, 2415–2420.

Sanai, N., Tramontin, A.D., Quiñones-Hinojosa, A., Barbaro, N.M., Gupta, N., Kunwar, S., Lawton, M.T., McDermott, M.W., Parsa, A.T., Manuel-Garcia Verdugo, J., et al. (2004). Unique astrocyte ribbon in adult human brain contains neural stem cells but lacks chain migration. Nature *427*, 740–744.

Sanai, N., Nguyen, T., Ihrie, R.A., Mirzadeh, Z., Tsai, H.H., Wong, M., Gupta, N., Berger, M.S., Huang, E., Garcia-Verdugo, J.M., et al. (2011). Corridors of migrating neurons in the human brain and their decline during infancy. Nature *478*, 382–386.

Sauer, B. (1998). Inducible gene targeting in mice using the Cre/lox system. Methods *14*, 381–392.

Sauer, M.E., and Walker, B.E. (1959). Radioautographic Study of Interkinetic Nuclear Migration in the Neural Tube. Exp. Biol. Med. *101*, 557–560.

Schiffer, D., Giordana, M.T., Migheli, A., Giaccone, G., Pezzotta, S., and Mauro, A. (1986). Glial fibrillary acidic protein and vimentin in the experimental glial reaction of the rat brain. Brain Res. *374*, 110–118.

Schuurmans, C., Armant, O., Nieto, M., Stenman, J.M., Britz, O., Klenin, N., Brown, C., Langevin, L.-M., Seibt, J., Tang, H., et al. (2004). Sequential phases of cortical specification involve Neurogenin-dependent and -independent pathways. EMBO J. *23*, 2892–2902.

Sequerra, E.B., Miyakoshi, L.M., Fróes, M.M., Menezes, J.R.L., and Hedin-Pereira, C. (2010). Generation of glutamatergic neurons from postnatal and adult subventricular zone with pyramidal-like morphology. Cereb. Cortex *20*, 2583–2591.

Shen, Q., Wang, Y., Dimos, J.T., Fasano, C.A., Phoenix, T.N., Lemischka, I.R., Ivanova, N.B., Stifani, S., Morrisey, E.E., and Temple, S. (2006). The timing of cortical neurogenesis is encoded within lineages of individual progenitor cells. Nat. Neurosci. *9*, 743–751.

Shimamura, K., Hartigan, D.J., Martinez, S., Puelles, L., and Rubenstein, J.L.R. (1995). Longitudinal organization of the anterior neural plate and neural tube. Development *121*, 3923–3933.

Shin, C.H., Liu, Z., Passier, R., Zhang, C., Wang, D., Harris, T.M., Yamagishi, H., Richardson, J.A., Childs, G., Olson, E.N., et al. (2002). Modulation of Cardiac Growth and Development by HOP , an Unusual Homeodomain Protein. Cell *110*, 725–735.

Shin, J., Berg, D.A., Zhu, Y., Shin, J.Y., Song, J., Bonaguidi, M.A., Enikolopov, G., Nauen, D.W., Christian, K.M., Ming, G., et al. (2015). Single-Cell RNA-Seq with Waterfall Reveals Molecular Cascades underlying Adult Neurogenesis. Cell Stem Cell *17*, 360–372.

Sidman, R.L., Miale, I.L., and Feder, N. (1959). Cell proliferation and migration in the primitive ependymal zone; An autoradiographic study of histogenesis in the nervous system. Exp. Neurol. *1*, 322–333.

Simeone, A., Gulisano, M., Acampora, D., Stornaiuolo, A., Rambaldi, M., and Boncinelli, E. (1992a). Two vertebrate homeobox genes related to the *Drosophila* empty spiracles gene are expressed in the embryonic cerebral cortex. EMBO J. *11*, 2541–2550.

Simeone, A., Acampora, D., Gulisano, M., Stornaiuolo, A., and Boncinelli, E. (1992b). Nested expression domains of four homeobox genes in developing rostral brain. Nature *358*, 687–690.

Simeone, A., Acampora, D., Pannese, M., D'Esposito, M., Stornaiuolo, A., Gulisano, M., Mallamaci, A., Kastury, K., Druck, T., and Huebner, K. (1994). Cloning and characterization of two members of the vertebrate Dlx gene family. Proc. Natl. Acad. Sci. U. S. A. *91*, 2250–2254.

Smart, I. (1961). The subependymal layer of the mouse brain and its cell production as shown by radioautography after thymidine-H3 injection. J. Comp. Neurol. *116*, 325–347.

Smart, I.H.M. (2002). Unique Morphological Features of the Proliferative Zones and Postmitotic Compartments of the Neural Epithelium Giving Rise to Striate and Extrastriate Cortex in the Monkey. Cereb. Cortex *12*, 37–53.

Smart, I., and Leblond, C.P. (1961). Evidence for division and transformations of neuroglia cells in the mouse brain, as derived from radioautography after injection of thymidine-H3. J. Comp. Neurol. *116*, 349–367.

Snippert, H.J., van der Flier, L.G., Sato, T., van Es, J.H., van den Born, M., Kroon-Veenboer, C., Barker, N., Klein, A.M., van Rheenen, J., Simons, B.D., et al. (2010). Intestinal crypt homeostasis results from neutral competition between symmetrically dividing Lgr5 stem cells. Cell *143*, 134–144.

Song, J., McColl, J., Camp, E., Kennerley, N., Mok, G.F., McCormick, D., Grocott, T., Wheeler, G.N., and Munsterberg, A.E. (2014). Smad1 transcription factor integrates BMP2 and Wnt3a signals in migrating cardiac progenitor cells. Proc. Natl. Acad. Sci. *111*, 7337–7342.

Spalding, K.L., Bergmann, O., Alkass, K., Bernard, S., Salehpour, M., Huttner, H.B., Boström, E., Westerlund, I., Vial, C., Buchholz, B.A., et al. (2013). Dynamics of Hippocampal Neurogenesis in Adult Humans. Cell *153*, 1219–1227.

Spassky, N., Merkle, F.T., Flames, N., Tramontin, A.D., García-Verdugo, J.M., and Alvarez-Buylla, A. (2005). Adult ependymal cells are postmitotic and are derived from radial glial cells during embryogenesis. J. Neurosci. *25*, 10–18.

Srinivas, S., Watanabe, T., Lin, C.S., William, C.M., Tanabe, Y., Jessell, T.M., and Costantini, F. (2001). Cre reporter strains produced by targeted insertion of EYFP and ECFP into the ROSA26 locus. BMC Dev Biol *1*, 4.

St Johnston, D. (2002). The art and design of genetic screens: *Drosophila melanogaster*. Nat. Rev. Genet. *3*, 176–188.

Stoykova, a, and Gruss, P. (1994). Roles of Pax-genes in developing and adult brain as suggested by expression patterns. J. Neurosci. *14*, 1395–1412.

Tabata, H. (2015). Diverse subtypes of astrocytes and their development during corticogenesis. Front. Neurosci. *9*, 10.3389/fnins.2015.00114.

Takahashi, T., Nowakowski, R.S., and Caviness, V.S. (1995). The cell cycle of the pseudostratified ventricular epithelium of the embryonic murine cerebral wall. J. Neurosci. *15*, 6046–6057.

Takeda, N., Jain, R., LeBoeuf, M.R., Wang, Q., Lu, M.M., and Epstein, J. a (2011). Interconversion between intestinal stem cell populations in distinct niches. Science *334*, 1420–1424.

Tapscott, S.J., Lassar, A.B., Davis, R.L., and Weintraub, H. (1989). 5-Bromo-2 â€™ -Deoxyuridine Blocks Myogenesis by Extinguishing Expression of MyoDl. Science (80-.). *245*, 532–536.

Taylor, J.H., Woods, P.S., and Hughes, W.L. (1957). The Organization and Dupliation of Chromosomes as Revealed by Autoradiographic Studies using Tritium-Labelled Thymidine. Proc. Natl. Acad. Sci. *43*, 122–128.

Thomsen, E.R., Mich, J.K., Yao, Z., Hodge, R.D., Doyle, A.M., Jang, S., Shehata, S.I., Nelson, A.M., Shapovalova, N. V, Levi, B.P., et al. (2016). Fixed single-cell transcriptomic characterization of human radial glial diversity. Nat. Methods *13*, 87–93.

Tiberi, L., Vanderhaeghen, P., and van den Ameele, J. (2012). Cortical neurogenesis and morphogens: Diversity of cues, sources and functions. Curr. Opin. Cell Biol. *24*, 269–276.

Tiveron, M.-C., Beclin, C., Murgan, S., Wild, S., Angelova, A., Marc, J., Coré, N., de Chevigny, A., Herrera, E., Bosio, A., et al. (2017). Zic-proteins are repressors of dopaminergic forebrain fate in mice and C. elegans. J. Neurosci. *37*, 10611–10623.

Tong, C.K., and Alvarez-Buylla, A. (2014). SnapShot: Adult Neurogenesis in the V-SVZ. Neuron *81*, 220–220.e1.

De Toni, A., Zbinden, M., Epstein, J. a, Ruiz i Altaba, A., Prochiantz, A., and Caille, I. (2008). Regulation of survival in adult hippocampal and glioblastoma stem cell lineages by the homeodomain-only protein HOP. Neural Dev. *3*, 13.

Tsai, H.-H., Li, H., Fuentealba, L.C., Molofsky, A. V, Taveira-Marques, R., Zhuang, H., Tenney, A., Murnen, A.T., Fancy, S.P.J., Merkle, F., et al. (2012). Regional astrocyte allocation regulates CNS synaptogenesis and repair. Science *337*, 358–362.

Valerius, M.T., Li, H., Stock, J.L., Weinstein, M., Kaur, S., Singh, G., and Potter, S.S. (1995). Gsh-1: a novel murine homeobox gene expressed in the central nervous system. Dev. Dyn. *203*, 337–351.

Wachsman, G., Heidstra, R., and Scheres, B. (2011). Distinct Cell-Autonomous Functions of RETINOBLASTOMA-RELATED in Arabidopsis Stem Cells Revealed by the Brother of Brainbow Clonal Analysis System. Plant Cell *23*, 2581–2591.

Wang, L., Hou, S., and Han, Y.-G. (2016). Hedgehog signaling promotes basal progenitor expansion and the growth and folding of the neocortex. Nat. Neurosci. *19*, 888–896.

Wang, X., Tsai, J., LaMonica, B., and Kriegstein, A. (2011). A new subtype of progenitor cell in the mouse embryonic neocortex. Nat Neurosci *14*, 555–561.

Weghorst, C.M., Henneman, J.R., and Ward, J.M. (1991). Dose response of hepatic and renal DNA synthetic rates to continuous exposure of bromodeoxyuridine (BrdU) via slow-release pellets or osmotic minipumps in male B6C3F1 mice. J. Histochem. Cytochem. *39*, 177–184.

Weissman, T.A., and Pan, Y.A. (2015). Brainbow: New resources and emerging biological applications for multicolor genetic labeling and analysis. Genetics *199*, 293–306.

Winpenny, E., Lebel-Potter, M., Fernandez, M.E., Brill, M.S., Götz, M., Guillemot, F., and Raineteau, O. (2011a). Sequential generation of olfactory bulb glutamatergic neurons by Neurog2-expressing precursor cells. Neural Dev. *6*, 12.

Winpenny, E., Lebel-Potter, M., Fernandez, M.E., Brill, M.S., Götz, M., Guillemot, F., and Raineteau, O. (2011b). Sequential generation of olfactory bulb glutamatergic neurons by Neurog2-expressing precursor cells. Neural Dev. *6*, 12.

Wu, S.C.-Y., Meir, Y.-J.J., Coates, C.J., Handler, A.M., Pelczar, P., Moisyadi, S., and Kaminski, J.M. (2006). piggyBac is a flexible and highly active transposon as compared to Sleeping Beauty, Tol2, and Mos1 in mammalian cells. Proc. Natl. Acad. Sci. *103*, 15008–15013.

Xuan, S., Baptista, C.A., Balas, G., Tao, W., Soares, V.C., and Lai, E. (1995). Winged helix transcription factor BF-1 is essential for the development of the cerebral hemispheres. Neuron *14*,

1141–1152.

Yang, H.K.C., Sundholm-Peters, N.L., Goings, G.E., Walker, A.S., Hyland, K., and Szele, F.G. (2004). Distribution of Doublecortin Expressing Cells Near the Lateral Ventricles in the Adult Mouse Brain. J. Neurosci. Res. *76*, 282–295.

Yokochi, T., and Gilbert, D.M. (2007). Replication Labeling with Halogenated Thymidine Analogs. In Current Protocols in Cell Biology, p. Unit 22.10.

Yoshida, M., Suda, Y., Matsuo, I., Miyamoto, N., Takeda, N., Kuratani, S., and Aizawa, S. (1997). Emx1 and Emx2 functions in development of dorsal telencephalon. Development *124*, 101–111.

Young, K.M., Fogarty, M., Kessaris, N., and Richardson, W.D. (2007). Subventricular zone stem cells are heterogeneous with respect to their embryonic origins and neurogenic fates in the adult olfactory bulb. J. Neurosci. *27*, 8286–8296.

Yu, C.C.W., Woods, A.L., and Levison, D.A. (1992). The assessment of cellular proliferation by immunohistochemistry: A review of currently available methods and their applications. Histochem. J. *24*, 121–131.

Zhong, Y.F., and Holland, P.W.H. (2011). HomeoDB2: Functional expansion of a comparative homeobox gene database for evolutionary developmental biology. Evol. Dev. *13*, 567–568.

Zhong, Y.F., Butts, T., and Holland, P.W.H. (2008). HomeoDB: A database of homeobox gene diversity. Evol. Dev. *10*, 516–518.

Zhou, Q., and Anderson, D.J. (2002). The bHLH transcription factors OLIG2 and OLIG1 couple neuronal and glial subtype specification. Cell *109*, 61–73.

Zhu, X., Bergles, D.E., and Nishiyama, A. (2008). NG2 cells generate oligodendrocytes and gray matter astrocytes in the spinal cord. Development *135*, 145–157.

Zong, H., Espinosa, J.S., Su, H.H., Muzumdar, M.D., and Luo, L. (2005). Mosaic analysis with double markers in mice. Cell *121*, 479–492.

6. List of Publications

Stefan Zweifel, Julie Buquet, David Rousseau, Olivier Raineteau. “FlashMap” - A fast and semi-automatic tool for accurate investigation of gene expression in the SVZ’. ***in preparation***

Stefan Zweifel, Kasum Azim, Guillaume Marcy, Quentin Lo Guidice, Deqiang Li, Olivier Raineteau. ‘HOPX Defines Heterogeneity of Postnatal Subventricular Zone Neural Stem Cells’. ***under revision: Stem Cell Reports***

Vanessa Donega, Guillaume Marcy, Quentin Lo Giudice, **Stefan Zweifel**, Diane Angonin, Roberto Fiorelli, Nora Abrous, Sylvie Rival-Gervier, Muriel Koehl, Denis Jabaudon and Olivier Raineteau. ‘Transcriptional dysregulation in postnatal glutamatergic progenitor contributes to closure of the cortical neurogenic period’. **Cell Reports; 2018; 22(10); 2567-2574**

Kasum Azim, Anahi Hurtado-Chong, Bruno Fischer, Nitin Kumar, **Stefan Zweifel**, Verdon Taylor, Olivier Raineteau. ‘Transcriptional Hallmarks of Heterogeneous Neural Stem Cell Niches of the Subventricular Zone’. **Stem Cells; 2015; 33(7); 2232-2242**

Kasum Azim, **Stefan Zweifel**, Fabienne Klaus, Kazuaki Yoshikawa, Irmgard Amrein, Olivier Raineteau. ‘Early Decline in Progenitor Diversity in the Marmoset Lateral Ventricle’. **Cerebral Cortex; 2013; 23(4); 922-931**

Kasum Azim, Roberto Fiorelli, **Stefan Zweifel,** Anahi Hurtado-Chong, Kazuaki Yoshikawa, Lutz Slomianka, Olivier Raineteau. ‘3-Dimensional Examination of the Adult Mouse Subventricular Zone Reveals Lineage-Specific Microdomains’. **PLOS ONE; 2012; 7(11); e49087**

7. Acknowledgements

On this pages I would like to thank all the people who took part, professional or personal, in this journey. This would not have been possible without you!

This work was performed at the Stem Cell and Brain Research in Bron, France. First of all I would like to thank France for allowing me to perform my PhD thesis in this country. This experience did not only equip me with the chance to master a PhD thesis, I also learned to know a different culture, a different thinking and a still not satisfying understanding of the French language. I am working on the last one.

Especially, I would like to thank Olivier Raineteau for giving me the chance to be part of his newly build team at the Stem Cell and Brain Research Institute. As the French system is sometimes not very "user friendly" I almost struggled with finding my way into it. I am very thankful for the solutions you offered me. It would not have been possible without! I am grateful for your supervision, advices and patience in a challenging project. Thank you for your effort!

Next, I would like to express my thankfulness to the members of the jury, Bénédicte Durand, Nathalie Spassky and Antoine de Chevigny, who accepted my invitation and sacrificed their time to evaluate my work. I appreciate that a lot! Thank you very much!

Moreover, I would like to express my particular gratitude to my current and ancient team members. This is Dr. Elodie, who recently achieved what I am currently trying to do. I started my PhD thesis at the same time like Elodie and this gave me the chance to have somebody on the side for facing the ups and downs on this journey. We were able to share and master particular problems together. These were establishing methods, searching for contaminations, bringing sense into bureaucracy and figuring out who the largest person from the office is. Further, I would like to thank Guillaume, another founding father from the lab, who somehow manages to run a family, to execute a PhD thesis, to realize the lab orders, to understand Geranimaux and to endure my behavior every day since more than 4 years. Master G helped me a lot from the beginning on. He assisted me all the time in all small and huge problems of the daily life in France. Appreciated!!! Also I would like to thank very very much our alumni postdoc Vanessa. Together with Guillaume she was busy with achieving all the breedings for

me. Cheers! Vanessa was a little like the brain of our office. No matter what question, Vanessa knows an answer. I will never forget our outstanding discussions in Dutch: “Gezondheit!”, “Dank u wel!”, “Alsjeblieft!”. In this sense: Bedankt voor je steun! Further, I would like to send a “Cheers!” in the direction of Louis, our newest PhD student. Thanks a lot for all the time we spent so far together, in the lab and outside of the lab, discussing science or any other random subjects. Of course I would not forget to mention our students Quentin and Aymeric, who developed different tools, which I am extensively using. Thanks a lot for your work! I am really grateful for all of you for joining my journey over the past few years. To be honest, you did anyway not have a choice. I corrupted you with the best chocolates!

Further, I would like to send some “Cheers!” to Kaz, who already supervised me during my master thesis in Zurich. Thanks a lot for your energy in our ongoing collaboration and for answering all my important and less important questions! From the same “old Zurich team” I want to express my gratitude to Anahi for teaching me how to electroporate. From you I learned many details you cannot find in any paper.

Also I need thank Julie, who collaborates with me in the development of “FlashMap”. Thanks a lot for your work. Hopefully we can kick out this manuscript soon!

From the remaining SBRI I have to thank all the current and past people I learned to know during this time. I appreciated very much all the transient or permanent “late stayers” who made it possible to have some late and non-scientific chats to get the head free. I would like to thank all the “good drinkers” for all the nights I planned to go home early. I will never forget the “dark room people”, who know sun light just from the internet. Thanks for spending the dark ages with me! Further, I am also very thankful for everybody helping out on random questions or spending some time outside of the lab. Thank you very much!

I also have to thank the guy who guided my first steps I made in “school biology”, my gymnasium teacher Andreas Brunnert. Hei Andreas, has gschafft! Merci vill mal für dini unkonventionelli Art en Unterricht z’gstalte!

In my personal life, I am very thankful for the friendship to Chris. I guess we discovered Lyon quite well!

Further, I am very grateful to have such awesome friends back home. You made me feel like I was never gone, when I spent a weekend in Zurich. You are the best!

I would like to thank my lacrosse home team from Zurich for showing me a new world a long time ago. I am grateful that you allowed me to play for another 2 years despite my 0% practice attendance. I know it was also a privilege for you to have a real MVG in your team. May the Güx be with you!

I am grateful that I found a few, but motivated lacrosse players here in Lyon, for practicing, playing, celebrating and finally joining the Skunks from Fribourg for the championship.

I would like to thank all the crazy dudes from the Dreadlax crew for inaugurating me to the secrets of "Three Man". Nobody believes my when I tell them about our Boxmania weekends. Smashy is looking forward to see all of you again.

Further, I am very happy to say that I spent all my holidays with the Swiss Box and Field lacrosse team. With you guys I discovered the world, gained priceless experiences, destroyed the dreams of big nations, shocked the world and spent all my money for the sport I love. Thank you very much for all of that!

The last words I would like to address to my family. I am very happy to call Elsbeth and Jürg my parents. I am very thankful for all your support during this time, for your visits and your interested questions about complicated subjects. I would like to thank Nina and Thomas, my older and so much more adult siblings! Here I have to include their better halves Rahel and Patrick who pushed them into adulthood by extensive breeding (@Leonie, Jason and Miro: I know you are not yet interested in that anyway. Therefore I will bring you some toys when I see you next time. Then you have to thank me!;) Further, I would like to thank Mara, my younger sister, who is at least as childish and crazy as I am. Und natürlich darf ich nicht vergessen mein Grossi zu erwähnen. Du gabst mir so viel Kraft in den letzten Jahren und halfst mir mit deiner ruhigen und gemühtlichen Art gewisse Dinge leichter zu nehmen. Merci viel mal!

Last but not least I would like to thank wholeheartedly my other "Half of a Complete Idiot". You spent with me awesome and nasty times and showed me another side of life. While one journey ends now, another exciting journey just started. T'es ouf!